# Detection Strategies and Intercept Metrics for Intra-Pulse Radar-Embedded Communications

By

Justin G. Metcalf

Submitted to the graduate degree program in Electrical Engineering  Computer Science
and the Graduate Faculty of the University of Kansas School of Engineering
in partial fulfillment of the requirements for the degree of
Master of Science

Dr. Shannon Blunt, Chairperson

Committee members

Dr. Erik Perrins

Dr. Glenn Prescott

Date defended: _____

The Thesis Committee for Justin G. Metcalf certifies
that this is the approved version of the following thesis :

Detection Strategies and Intercept Metrics for Intra-Pulse Radar-Embedded Communications

_____

Dr. Shannon Blunt, Chairperson

Date approved: _____

# Abstract

This thesis presents various detection strategies and intercept metrics to evaluate and design an intra-pulse radar-embedded communication system. This system embeds covert communication symbols in masking interference provided by the reflections of a pulsed radar emission. This thesis considers the case where the communicating device is a transponder or tag present in an area that is illuminated by a radar. The radar is considered to be the communication receiver. As with any communication system, performance (as measured by reliability and data rate) should be maximized between the tag and radar. However, unlike conventional communication systems, the symbols here should also have a low-probability of intercept (LPI). This thesis examines the trade-offs associated with the design of a practical radar-embedded communication system. A diagonally-loaded decorrelating receiver is developed and enhanced with a second stage based on the Neyman-Pearson criterion. For a practical system, the communication symbols will likely encounter multipath. The tag may then use a pre-distortion strategy known as time-reversal to improve the signal-to-noise ratio at the radar receiver thereby enhancing communication performance. The development of several intercept metrics are shown and the logic behind the design evolutions are explained. A formal analysis of the processing gain by the desired receiver relative to the intercept receivers is given. Finally, simulations are shown for all cases, to validate the design metrics.

# Acknowledgment

First, I would like to thank my advisor, Dr. Blunt, for his insight, attention to detail, and patience. The guidance he has given me has been instrumental in my growth as a student and a scholar. Second, I would like to thank the Air Force Office of Scientific Research (AFOSR) for sponsoring this research. Third, I would like to thank Dr. Perrins and Dr. Prescott for agreeing to be on my thesis committee. Fourth, I would like to thank my friends and family for their support and confidence. Last, but certainly not least, I would like to thank my wife, Miranda. Her support and encouragement has been the most important component of my academic efforts.

# Contents

# List of Figures

# Chapter 1

# Introduction

Covert communications has received a great deal of attention over the last century. In this scenario, a transmitter sends information in such a way that an intended receiver can detect the transmission, but any surveillance receiver will not be able to detect the transmission. This concept is called low-probability-of-intercept (LPI) communications. A preliminary technique involving digital telephony proved quite instrumental for high-level communications by the Allies in World War II [4]. Wireless transmissions provide a more flexible framework on which to base an LPI communication system. A wireless paradigm is advantageous for positioning transmitters and receivers. However, by using wireless techniques, there are more opportunities and flexibility for an intercept receiver to detect the transmission. The foundation for LPI radio-frequency (RF) communications was laid in the 1930's and 1940's via the spread-spectrum (SS) paradigm [5].

Reproduced from [5], a modern spread-spectrum system is characterized as meeting three requirements:

1. The carrier is a pseudorandom, wideband signal.

2. The bandwidth of the carrier is much wider than the bandwidth of the data modulation.

3. Reception is accomplished by cross correlation of the received wide-band signal with a synchronously generated replica of the wide-band carrier.

Due to requirements 1 and 2, SS signals are very resistant to jamming and can be transmitted at very low power. Therefore, they provide a very effective LPI communication method. However, LPI SS communication systems suffer from the "near-far" problem. In other words, it is difficult for a transmitter and a distant receiver to communicate covertly using SS methods when an intercept receiver may be located close to the transmitter.

While SS signals are LPI by using noise to mask transmissions, further LPI gains can be produced by using interference to mask communication transmissions. The high power interference created by radar transmissions offers an attractive environment in which to embed communications. A great deal of work has been done to embed communications on an *inter*-pulse basis (*e.g.*, [6–13]) where each pulse has a phase shift modulated onto it. The communication symbol is formed from a sequence of phase shifts transmitted over the multiple pulses. However, techniques based on an inter-pulse basis suffer from very low data rates.

A novel method was proposed in [1] to embed covert communication symbols in radar reflections on an *intra*-pulse basis. In this system, a transponder or tag communicates with one or more receivers using communication symbols designed to be correlated with the ambient radar interference. Three communication symbol design methods were defined and compared using a decorrelating receiver [14]. These design methods were Eigenvectors-as-Waveforms, Weighted Combining, and Dominant Projection. The primary metric for waveform design was symbol-error-rate (SER) as a function of signal-to-interference-plus-noise ratio (SINR). In addition, a candidate metric to bound the theoretical effectiveness of intercept receivers was defined and examined. Further developments were given in [15] illustrating the superiority of the Dominant Projection method of designing REC symbols with respect to the other two design methods given in [1].

## 1.1 Motivation

The work in [1] and [15] provided a first step in the development of an LPI REC system. This thesis is motivated by the desire to improve on the previous work and provide a more formal mathematical framework for the design of a REC system. To design an effective covert communication system, the rate and reliability of transmitted data should be maximized while the capability of an intercept receiver to detect the transmissions must be minimized.

Based on the previous work, it is assumed that the Dominant Projection method of designing waveforms is the preferred method. Therefore, the receiver used by the intended recipients should be designed to maximize the data reliability while using the Dominant Projection symbols. It is also necessary to establish the capability of an intercept receiver to detect the symbols at a given SINR. Observing the SER and probability of intercept as a function of SINR illustrates the LPI nature of the Dominant Projection symbols. Also, previous work did not consider the problem of synchronization at the receiver.

This thesis develops a two-stage receiver to maximize data reliability between a transmitter and receiver in the presence of interfering radar scattering. The first stage uses a diagonally loaded decorrelating receiver to maximize detectability of the symbol with respect to SINR. The receiver forms a K-hypothesis test to detect which symbol was most likely transmitted. The null hypothesis (no symbol present) is not considered in the first stage. The second stage uses a Neyman-Pearson criterion to maximize reliability through the use of a user-defined probability of false alarm (*i.e.*, detecting a symbol when no symbol is present). In the second stage, the null hypothesis is considered against the symbol selected in thee first stage. By framing the problem as a hypothesis detection, synchronization is enabled. The first stage scans over time to provide the time instant with the highest probability of containing a symbol. The scenario when the tag is communicating with the illuminating radar is considered. In this case, it is shown that pre-distorting the symbols with a time-reversed estimate of the channel can improve the communication performance.

The intercept metric developed in [1] is re-examined and an alternate metric is proposed.

A formal analysis is derived comparing the processing gain afforded by the decorrelating receiver with the gain at the intercept metric. This derivation verifies the potential of intra-pulse REC as an LPI system. The results are considered at various SINR regimes (*e.g.*, noise dominant, clutter dominant).

## 1.2 Organization of Thesis

This thesis is organized as follows. Chapter 2 provides a thorough description of the LPI communication problem, as well as a brief background on the various processes involved. The mathematical definition of the received signal model at the radar receiver is given in Chapter 3. The Dominant Projection method of waveform generation is also given therein. Chapter 4 discusses the potential for incorporating time reversal when the tag is communicating with the illuminating radar. The design of the receiver is discussed in Chapter 5, while the prospective intercept receiver metrics are given in Chapter 6. Chapter 7 formally derives the processing gain of the diagonally loaded decorrelating receiver and the intercept metric, as well as the gain advantage of the decorrelating receiver over the intercept metric. Finally, Chapter 8 provides Monte Carlo simulation results verifying the concepts discussed in Chapters 5, 6, and 7. Conclusions and future work are given in Chapter 9.

# Chapter 2

# Background

Ever since the days of Aenas Tacticus in the 4th Century B.C., military forces have been implementing systems of secure communications [16]. The objective of a secure communication system is to reliably distribute information among the intended recipients, while denying access to the information to any individuals that might intercept the communications. Encryption has been used to great success in this area, and much research has been devoted to designing and assessing the effectiveness of encryption strategies [17].

A covert communication system is a secure system that places a further constraint on minimizing the detectability of the transmission by any unintended recipients. While it is still important that information be securely and reliably conveyed between a transmitter and desired receiver, it is of equal importance that any intercept receiver present be prevented from detecting the transmission. These systems are called low-probability-of-intercept (LPI) systems. LPI systems can take many forms. For example, steganography is the method of hiding information in objects such as images or text [18]. Of interest here is the concept of LPI communications in the radio frequency (RF) regime.

For any LPI system there must be some essential design parameter, known *a priori* to the "friendly" transmitter and receiver(s) in the system, that renders the transmission detectable. For an RF LPI system, an intercept receiver without knowledge of this key

parameter cannot distinguish between the communication symbol and the background noise and interference. In other words, the communication symbol must "hide" in interfering noise and the friendly receivers must possess a "key" to detect its presence. It is important to recognize that no signal will every be completely LPI (*i.e.* be impossible to detect) [19].

A frequency-based spread-spectrum approach can be used to form covert symbols. In direct-sequence spread-spectrum, a communication symbol is chosen from a standard constellation set (*e.g.*, phase shift keying, quadrature amplitude modulation) [20]. This symbol is then spread over a large bandwidth by multiplying it with a pseudo-random sequence that has been sampled at a much higher frequency than the communication symbol. To remain covert, the signal is transmitted at a very low SNR. Further increases in LPI may be gained from frequency hopping. Knowledge of the spreading code used to form the signal allows for a friendly receiver to coherently integrate the energy of the signal and distinguish it from the noise. Due to the wide bandwidth used, this approach also is very resistant to narrowband jamming [21]. The spread-spectrum approach depends on the noise to mask it from detection. Therefore, great care must be taken to transmit at a power low enough to prevent any nearby intercept receiver from detecting the signal. However, transmitting at lower power also reduces the reliability of the covert communication system. This trade-off between transmit power and detectability is a reoccurring problem in the covert communication paradigm.

Another approach is to use interference inherent to the RF environment. For example, existing communication systems may be exploited to allow a covert signal to be transmitted [22]. The interference will typically be of greater power than the noise, further reducing the signal-to-interference-plus-noise ratio (SINR). The reduced SINR will make a properly designed communication symbol harder to detect. Another approach is to use radar interference to mask a communication symbol.

A radar system obtains information about its environment by transmitting a pulsed or continuous wave signal and analyzing the backscattered returns. In general, the transmitter

and receiver may be located in different locations (bistatic systems), or there may be several transmitters and receivers scattered throughout a region (multistatic systems). More commonly, the radar transmitter and receiver are considered to be physically co-located (monostatic). This thesis considers a monostatic radar transmitting pulsed waveforms.

Radar systems are used for many different purposes. One such modality is moving target detection. In this scenario, the radar system must suppress unwanted interference, known as clutter, and maximize the response of a desired target. For successful detection, the reflected signal must be large enough to overcome thermal noise. For an imaging modality (*e.g.*, synthetic aperture radar, inverse synthetic aperture radar) the clutter may be considered to be the signal of interest. Regardless of modality, it is common for pulsed systems to send multiple identical pulses at some pulse repetition frequency (PRF) and coherently integrate the returns [23]. This coherent integration may be conducted in the time or frequency domains to increase the signal-to-noise power ratio (SNR). Processing in the frequency domain also improves moving target detection (*i.e.*, Doppler processing). Assuming an additive white Gaussian noise model for the thermal noise, it is easy to show that coherent integration improves the SNR by a factor equal to the number of pulses.

Radar interference offers an attractive environment within which to embed LPI communications. The pulsed, constant waveform structure may be exploited by embedding communication symbols into radar backscatter. To maximize detection, it is common for radar systems to transmit at high power. The scattering from this high power signal produces large amounts of interference, termed clutter. The high-powered clutter can be used to mask a communication symbol. Further, due to transmitter effects, radar returns often suffer from spectral spreading or bleeding [24]. This phenomenon is illustrated in Figure 2.1, which was shown in [1]. The design strategies that will be discussed in this thesis will target these regions of spectral spreading.

This thesis considers a communication system in which a tag or transponder [25] [26], hereafter called the tag, is illuminated by a radar system. If the radar waveform scatters

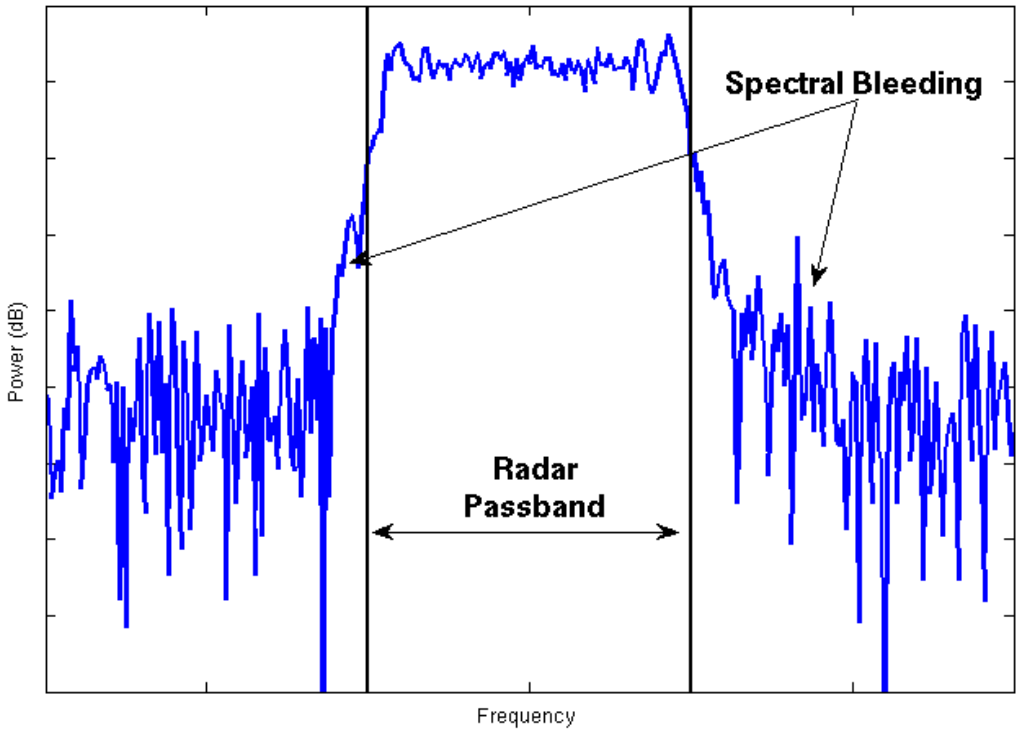


Figure 2.1: Radar spectral spreading [1]

off objects in the environment before it reaches the tag, the radiation incident on the tag is termed forward scattered-radiation. In communication literature, forward scattering is more commonly referred to as multipath. The two terms will be used interchangeably in this thesis. The radiation scattered back to the radar system is termed backscattered radiation (or simply backscatter). Previous approaches to embed a communication signal in radar backscatter operated on an *inter*-pulse basis [6]. In other words, segments of a communication symbol are embedded over multiple pulses. The earliest method employed mechanically-controlled corner reflectors to modulate the radar backscatter over the course of several pulses. Further early work can be found in [13]. More recent inter-pulse techniques involved embedding a phase shift sequence over a series of pulses [7–11]. If the phase sequence is linear, this phase shift would appear to be a Doppler signature to an intercept receiver.

The number of pulses coherently integrated by a radar is termed the coherent processing

interval (CPI). Typical CPIs are on the order of 10's-1000's of pulses. The pulse repetition frequency (PRF) of a radar is often on the order of 1-10 KHz. Due to the large number of pulses needed to form a communication symbol, inter-pulse radar embedded communications (REC) is capable of data rates on the order of 1-100 bits per second. While these data rates are low, they are sufficient to provide "identify friend" information to a synthetic aperture radar system [12]. This functionality helps to avoid "friendly fire" incidents.

For the embedding of symbols on an *intra*-pulse basis (*i.e.*, the entire communication symbol is embedded over the course of a single pulse), it is possible to achieve a communication rate on the order of the PRF of the radar system ($\sim$ Kbps). Therefore, it may be possible to achieve sufficient data rates to support audio data [27] [28] [29]. A conceptual illustration of the intra-pulse system setup is given in Figure 2.2.

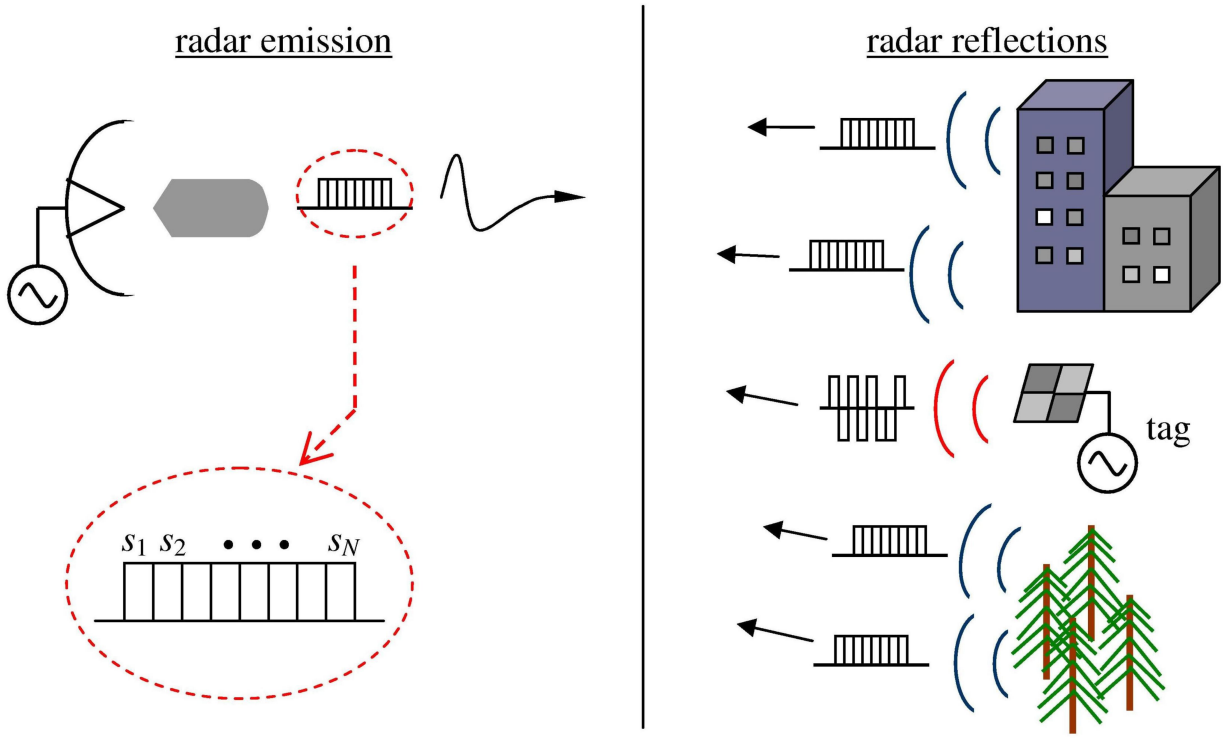


Figure 2.2: Radar embedded communication system framework [2]

Thus far, only LPI communication from tag to radar has been considered. In the framework of a two-way communication system, this is considered the "reverse-link". Also of

interest is the "forward-link" (*i.e.* radar-to-tag). Separate work has been done in the area of embedding information in the transmitted radar waveform through the use of pulse-agile radar [30].

This chapter discussed the general method of embedding a communication symbol on an intra-pulse basis. However, in order to design symbols and receivers the system model and physical model of the environment must be established. Explicit accurate modeling of the processes involved allows quantifiable design of effective LPI symbols and optimal receivers.

# Chapter 3

# Signal Model

When designing any engineering system, it is important to accurately model the system and its physical environment. This section establishes the mathematical notations used throughout the rest of the thesis and provides a clear picture of the physical environment within which the radar-embedded communication (REC) framework is intended to operate. It is important to note that all values and vectors in this thesis are considered to be complex valued, unless otherwise stated.

In the REC system, all processing is performed in the discrete domain. However, the radar waveform and communication symbols must pass through a continuous channel. Therefore, both domains must be considered. First, define the continuous time baseband representation of the radar waveform as $s(t)$. As the radar waveform is radiated, it encounters the physical environment (trees, ground, clouds, etc). Objects in the environment passively absorb and re-radiate a portion of the electromagnetic energy that impinges on them. The process of re-radiating electromagnetic energy is termed scattering. The portion scattered back to the radar is called backscatter. This process is modeled as the continuous time clutter process $x(t)$. The interaction between the radar and clutter is considered to be a linear, time-invariant (LTI) process. Therefore, this interaction is modeled as the convolution of $s(t)$ and $x(t)$. This formulation ignores the contribution of motion-induced Doppler shifts over

the pulse-width of the radar waveform. As with any system, the backscattered radiation received by the radar is corrupted by thermal noise, represented by $u(t)$. Therefore, when no communication symbol is present the signal received by the radar is given as

$$y(t) = s(t) * x(t) + u(t) \tag{3.1}$$

where $*$ denotes convolution.

If the tag is present in the illuminated area, the energy impinging on it may be scattered off of objects in the environment. The tag is then in the forward-scattering regime. Referred to in another way, the radar waveform is reflecting from scatterers in the scene, producing a multipath channel between the radar and tag. This multipath channel is denoted as $h(t)$. Using $h(t)$ to improve communication performance will be discussed further in Chapter 4. The tag will transmit one of $K$ communication symbols to one or more desired receivers. The $k^{th}$ transmitted communication symbol is defined as $c_k(t)$. The received signal when a communication symbol is present is then given as

$$y(t) = s(t) * x(t) + \alpha c_k(t) * h(t) + u(t) \tag{3.2}$$

where $\alpha$ is a complex scalar attenuation constant. A graphical representation of the REC system is shown in Figure 3.1, which appeared in [3]. A representation of (3.2) is illustrated in Figure 3.2, which was given in [2].

Conceptually, (3.2) provides the basic design space for the REC problem. The clutter term, $s(t) * x(t)$, can be thought of as interference. If the receiver in question is a desired receiver (*i.e*, a receiver the tag wishes to communicate with), the receiver structure and communication symbol should be designed to suppress the clutter and noise while maximizing the response to $c_k(t)$. However, if the receiver is an intercept receiver, the communication symbol should be designed to be indistinguishable from the clutter and noise.

The signals actually processed by the radar and tag must first be lowpass filtered and

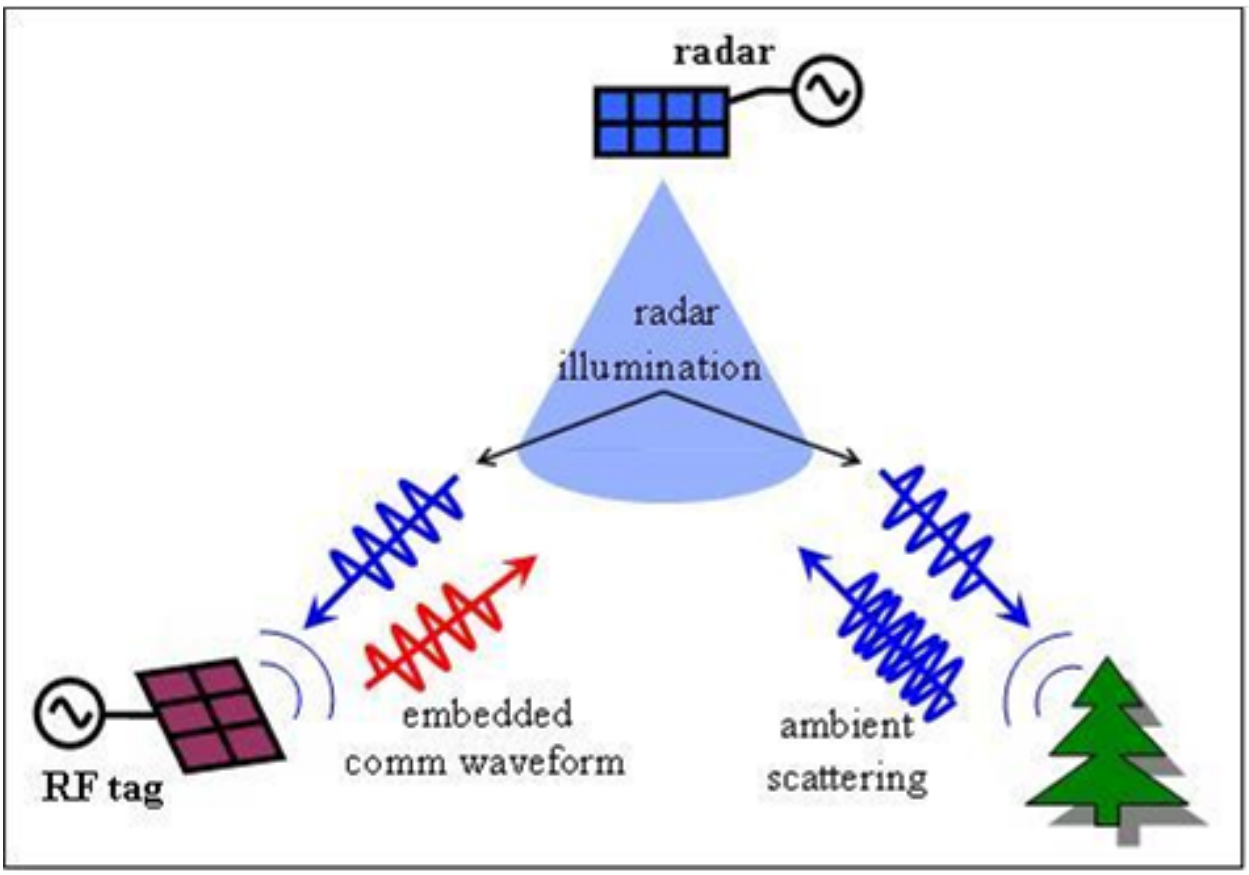


Figure 3.1: Graphical model of REC system [3]

sampled by an analog-to-digital converter. Typically, a receiver will oversample the received signal by some amount greater than the Nyquist sampling rate. Let the Nyquist sampled radar waveform have a time-bandwidth product of $N$, and be digitally sampled at a rate $M$ times the Nyquist rate. The sampled radar waveform is denoted as the length $NM$ vector $\mathbf{s}$ and the discrete clutter profile is $\mathbf{x}$. When considering the convolution of $\mathbf{s}$, notice that there are $2NM-1$ possible shifts of $\mathbf{s}$. Therefore, defining the $NM \times 2NM-1$ Toeplitz matrix $\mathbf{S}$ as

$$\mathbf{S} = \begin{bmatrix} s_{NM-1} & s_{NM-2} & \cdots & s_0 & 0 & \cdots & 0 \\ 0 & s_{NM-1} & \cdots & s_1 & s_0 & \cdots & 0 \\ \vdots & \vdots & \ddots & \vdots & \vdots & \ddots & \vdots \\ 0 & 0 & \cdots & s_{NM-1} & s_{NM-2} & \cdots & s_0 \end{bmatrix}, \tag{3.3}$$

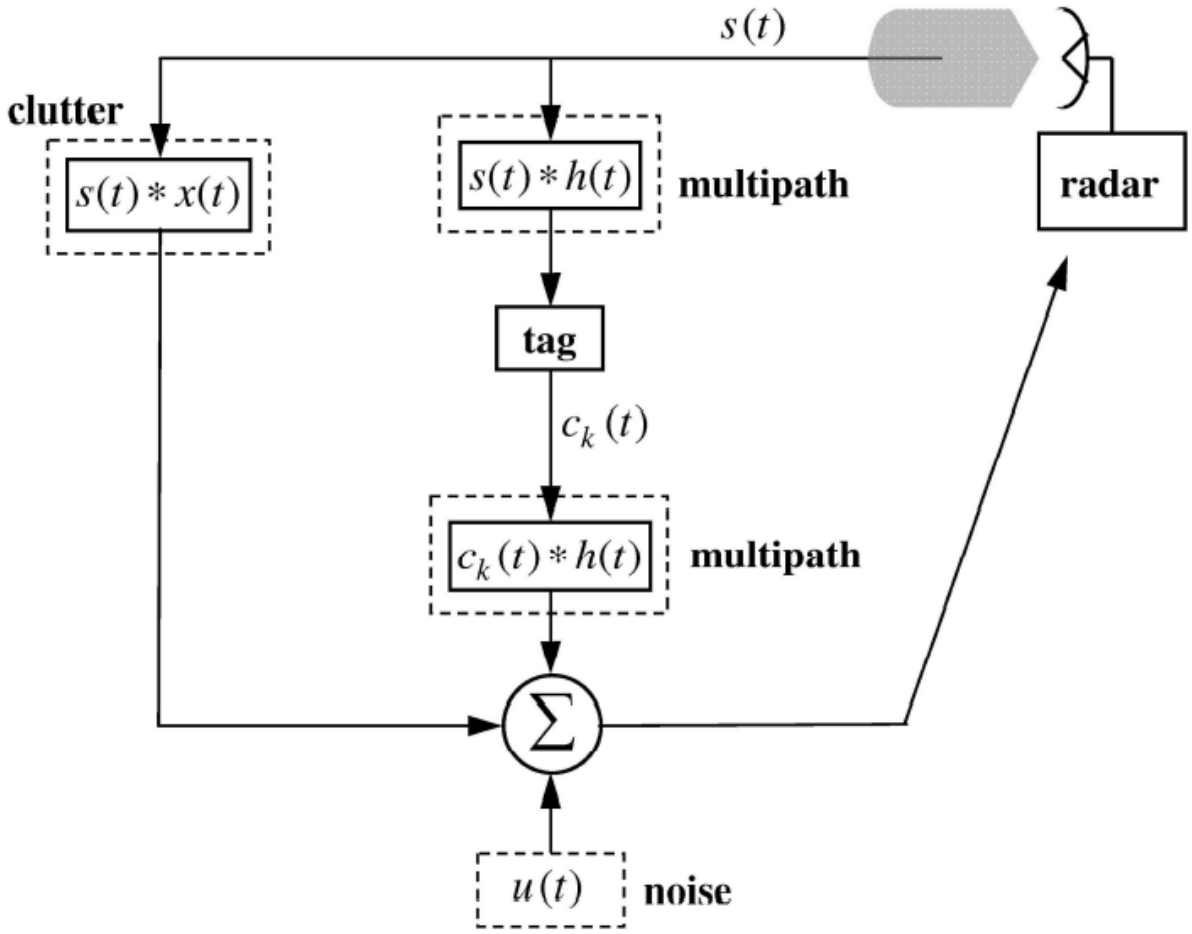


Figure 3.2: Continuous time signal model [2]

the discrete convolution of the radar waveform and clutter can be represented as

$$\mathbf{Sx} = \begin{bmatrix} s_{NM-1} & s_{NM-2} & \cdots & s_0 & 0 & \cdots & 0 \\ 0 & s_{NM-1} & \cdots & s_1 & s_0 & \cdots & 0 \\ \vdots & \vdots & \ddots & \vdots & \vdots & \ddots & \vdots \\ 0 & 0 & \cdots & s_{NM-1} & s_{NM-2} & \cdots & s_0 \end{bmatrix} \begin{bmatrix} x_1 \\ x_2 \\ \vdots \\ x_{2NM-1} \end{bmatrix}. \tag{3.4}$$

Note that the clutter process is theoretically of infinite length.

The discretely sampled received signal $\mathbf{y}$ is a vector of length $NM$. When a communica-

tion symbol is not present, $\mathbf{y}$ may be given as

$$\mathbf{y} = \mathbf{S}\mathbf{x} + \mathbf{u}. \tag{3.5}$$

Typically, thermal noise is modeled as additive white Gaussian noise (AWGN). The AWGN assumption is physically justified through use of the Central Limit Theorem (CLT) [31]. However, empirical measurements of high-resolution radars have shown that clutter distributions are not best represented by a Gaussian process. As the resolution increases, the number of discrete scatterers in a range cell may not be large enough for the CLT to apply. Clutter distributions for high resolution radars are often better approximated by the K [32], Weibull [33], or Log-normal distributions [34]. If the clutter samples are uncorrelated in range, the derivations of this work are agnostic to the clutter distribution.

The primary waveform design strategies discussed in [1, 15] use the eigenspace of the generic radar reflections to maintain correlation with the clutter. The eigenspace of the received signal may be formed as the eigendecomposition of the normalized correlation matrix

$$\begin{aligned}
\frac{1}{\sigma_x^2} E[(\mathbf{S}\mathbf{x})(\mathbf{S}\mathbf{x})^H] &= \frac{1}{\sigma_x^2} \mathbf{S} E[\mathbf{x}\mathbf{x}^H] \mathbf{S}^H \\
&= \frac{1}{\sigma_x^2} \mathbf{S} [\sigma_x^2 \mathbf{I}] \mathbf{S}^H \\
&= \mathbf{S}\mathbf{S}^H \\
&= \mathbf{V}\mathbf{\Lambda}\mathbf{V}^H
\end{aligned} \tag{3.6}$$

where $(\bullet)^H$ represents the Hermitian, or complex conjugate transpose operation on a matrix, $E[\bullet]$ is the expected value operator, and $\sigma_x^2$ is the clutter variance (power). It is assumed that the individual samples of $\mathbf{x}$ are uncorrelated. The matrix $\mathbf{V}$ contains $NM$ orthonormal vectors of length $NM$. The diagonal matrix $\mathbf{\Lambda}$ contains the corresponding eigenvalues in descending order. The $i^{th}$ eigenvalue corresponds to the power associated with the $i^{th}$ eigenvector. Assuming the radar waveform's power is normalized (*i.e.*, $||\mathbf{s}||^2 = \mathbf{s}^H\mathbf{s} = 1$), it

is easily seen that

$$\text{tr}\{\mathbf{S}\mathbf{S}^H\} = NM||\mathbf{s}||^2 = NM \tag{3.7}$$

where tr$\{\bullet\}$ represents the matrix trace operation. Therefore, using (3.6) and (3.7),

$$\begin{aligned}\text{tr}\{\mathbf{S}\mathbf{S}^H\} &= \text{tr}\{\mathbf{V}\mathbf{\Lambda}\mathbf{V}^H\} \\ &= \text{tr}\{\mathbf{\Lambda}\} \\ &= NM. \end{aligned} \tag{3.8}$$

In other words, the sum of the eigenvalues is equal to the time-bandwidth product of the radar waveform multiplied by the oversampling factor. However, the majority of the energy in correlation matrix (and therefore the eigendecomposition) comes from the radar waveform, which has dimensionality of $N$. Therefore, the first $N$ eigenvalues contain most of the energy. To illustrate this property, Figures 3.3 and 3.4 show plots of eigenvalues corresponding to a linear frequency modulated (LFM) waveform [35] at oversampling factors of $M = 2$ and $M = 4$ respectively.

The division between "large" and "small" eigenvalues leads to the concept of dominant and non-dominant subspaces. The dominant subspace consists of the eigenvectors corresponding to eigenvalues with large magnitudes. Similarly, the non-dominant subspace is made up of the eigenvectors whose eigenvalues are relatively small. Formally, the eigenvectors corresponding to the $m$ largest eigenvalues are defined to be the dominant subspace. Therefore, the non-dominant subspace is composed of the eigenvectors associated with the $NM - m$ smallest eigenvalues. Separating the eigenspace into dominant and non-dominant subspaces allows the partitioning of the eigendecomposition of (3.6) as

$$\mathbf{S}\mathbf{S}^H = \mathbf{V}\mathbf{\Lambda}\mathbf{V}^H = \left[\begin{array}{c|c} \mathbf{V}_D & \mathbf{V}_{ND} \end{array}\right] \left[\begin{array}{c|c} \mathbf{\Lambda}_D & \mathbf{0} \\ \hline \mathbf{0} & \mathbf{\Lambda}_{ND} \end{array}\right] \left[\begin{array}{c} \mathbf{V}_D^H \\ \hline \mathbf{V}_{ND}^H \end{array}\right] \tag{3.9}$$

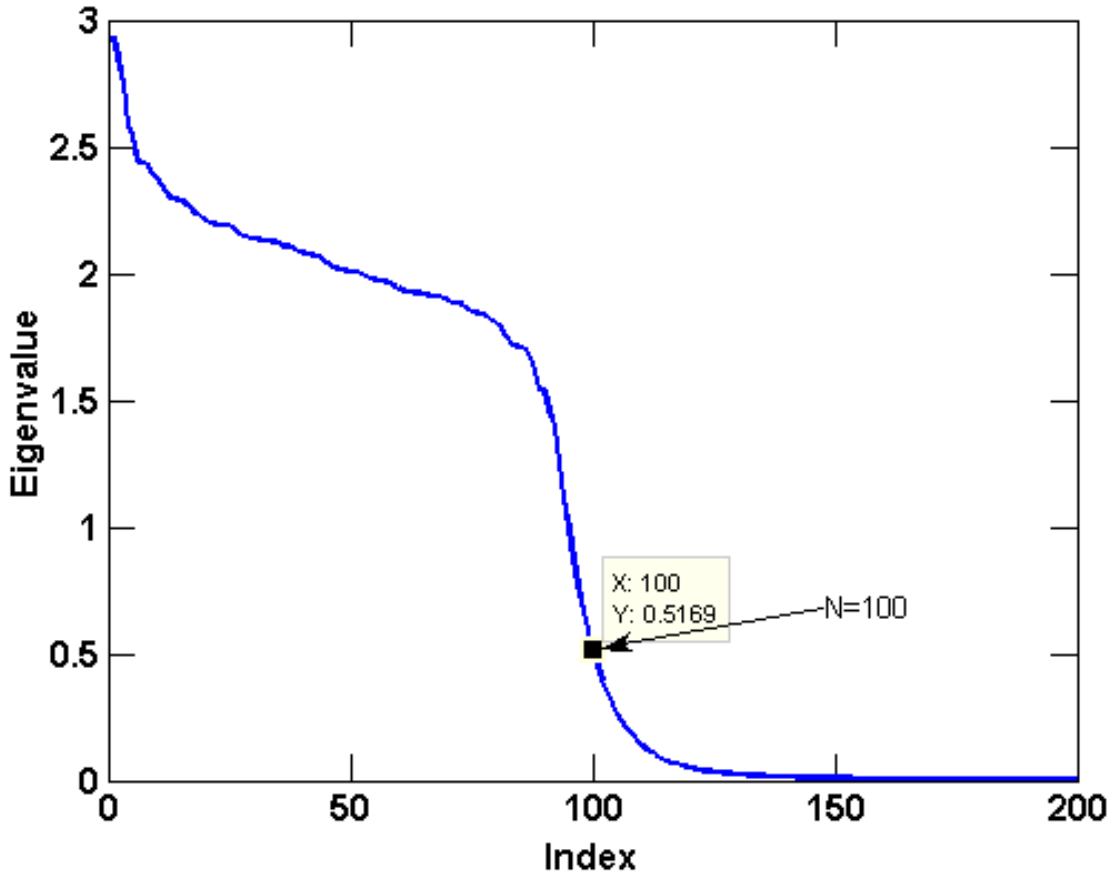


Figure 3.3: Eigenvalues of a downsampled and filtered N=100, M=2 LFM radar waveform

where $\mathbf{V}_D$ is a $NM \times m$ matrix of the $m$ dominant eigenvectors, and $\mathbf{V}_{ND}$ is of dimension $NM \times (NM - m)$ and consists of the non-dominant eigenvectors. Similarly, $\mathbf{\Lambda}_D$ is a $m \times m$ diagonal matrix of the $m$ dominant eigenvalues, and $\mathbf{\Lambda}_{ND}$ is the $(NM - m) \times (NM - m)$ diagonal matrix of non-dominant eigenvalues.

The communication symbol design methods compared in [1] take advantage of the separation between the dominant and non-dominant subspaces. Through use of the non-dominant subspace, communication symbols can be designed to be correlated with, yet separable from, the radar backscatter. For an intercept receiver, the correlation between the communication symbol and clutter makes the symbol difficult to discern. However, knowledge of the symbol allows the desired receiver to effectively cancel the clutter and retrieve the transmitted message. Previous work considered three different communication symbol design strategies.

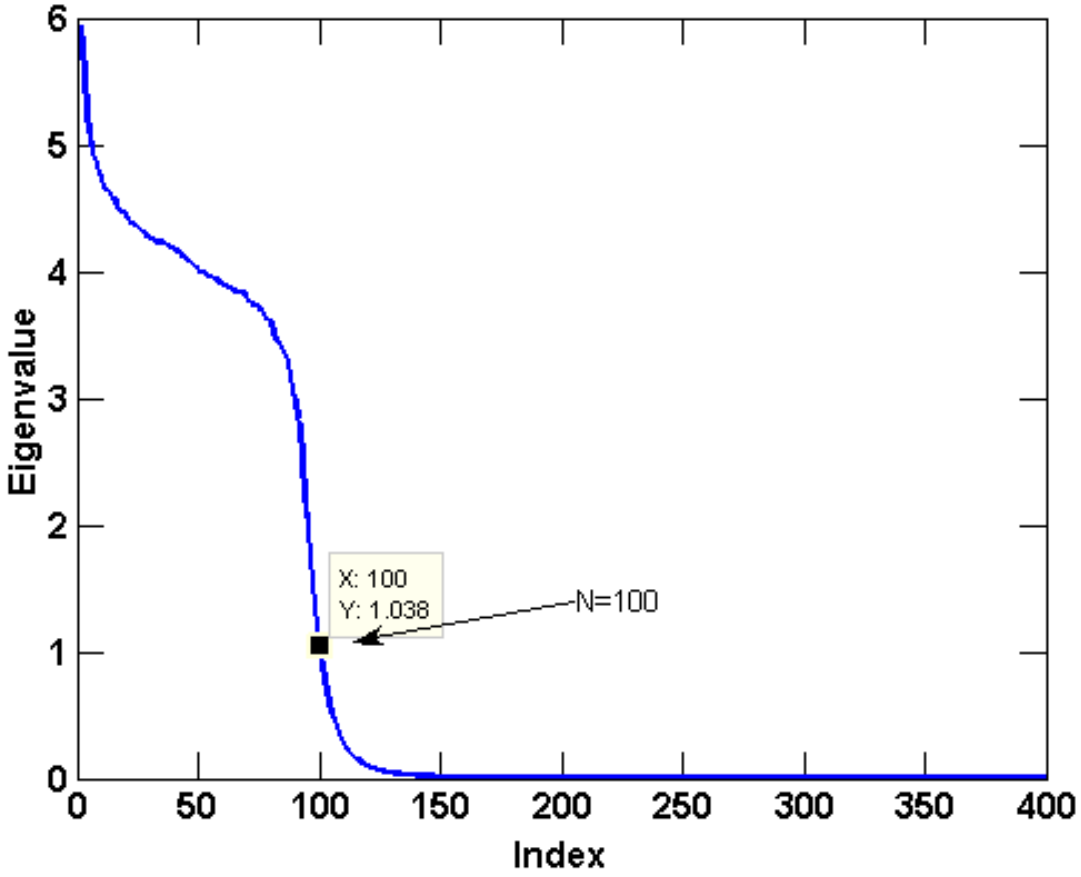


Figure 3.4: Eigenvalues of a downsampled and filtered N=100, M=4 LFM radar waveform

However, only the Dominant Projection design method has been found to be robust to multipath [1, 15]. Therefore, only the Dominant Projection approach is considered in this thesis.

The Dominant Projection method projects a seed vector (of dimensionality $NM$) away from the dominant subspace as a whole. To project away from the dominant subspace, the projection matrix

$$\mathbf{P} = \mathbf{I} - \mathbf{V}_D \mathbf{V}_D^H = \mathbf{V}_{ND} \mathbf{V}_{ND}^H \tag{3.10}$$

is used to form the $k^{th}$ communication symbol as

$$\mathbf{c}_k = \mathbf{P}\mathbf{b}_k. \tag{3.11}$$

The vector $\mathbf{b}_k$ is a pseudo-random seed that is known to both the desired receiver(s) and the tag.

When a communication symbol is present and there is no multipath (*i.e.* direct path only), the discrete received signal is

$$\mathbf{y} = \mathbf{S}\mathbf{x} + \alpha\mathbf{c}_k + \mathbf{u} \tag{3.12}$$

where $\alpha$ is a complex scalar value that accounts for any phase shift and attenuation in the channel. As the communication symbol is correlated with the radar backscatter (*i.e.*, clutter), the $\mathbf{Sx}$ term acts as interference. While the radar backscatter makes the communication harder to detect by an intercept receiver, the clutter also makes it more difficult for the desired receiver to determine the transmitted communication symbol.

Some parallels can be made between the Dominant Projection approach and traditional direct-sequence spread-spectrum communications (DSSS). In traditional DSSS the spreading vector can provide a basis for a user space (*i.e.*, orthogonal spreading vectors are uniquely assigned to a transmitter). The data symbol is then modulated on to the spreading vector. In the Dominant Projection approach, the seed vector is both a spreading vector and the data modulation. However, while a traditional spread-spectrum symbol is spread uniformly over a frequency range, the Dominant Projection symbol is shaped by the projection matrix $\mathbf{P}$. The Dominant Projection symbol is projected away from the subspace where the dominant portion of the radar signal is located, so it does not possess the degrees-of-freedom a DSSS symbol would possess.

The dominant projection technique attempts to place the communication symbol in the radar clutter. To further illustrate this phenomenon, Figure 3.5 shows the spectral content of an LFM radar waveform passed through a clutter channel and corrupted by AWGN. For the purposes of this example, the clutter is generated from a zero mean, complex Gaussian random process. The clutter-to-noise ratio (CNR) is set to 30 dB. Figure 3.6 shows a REC

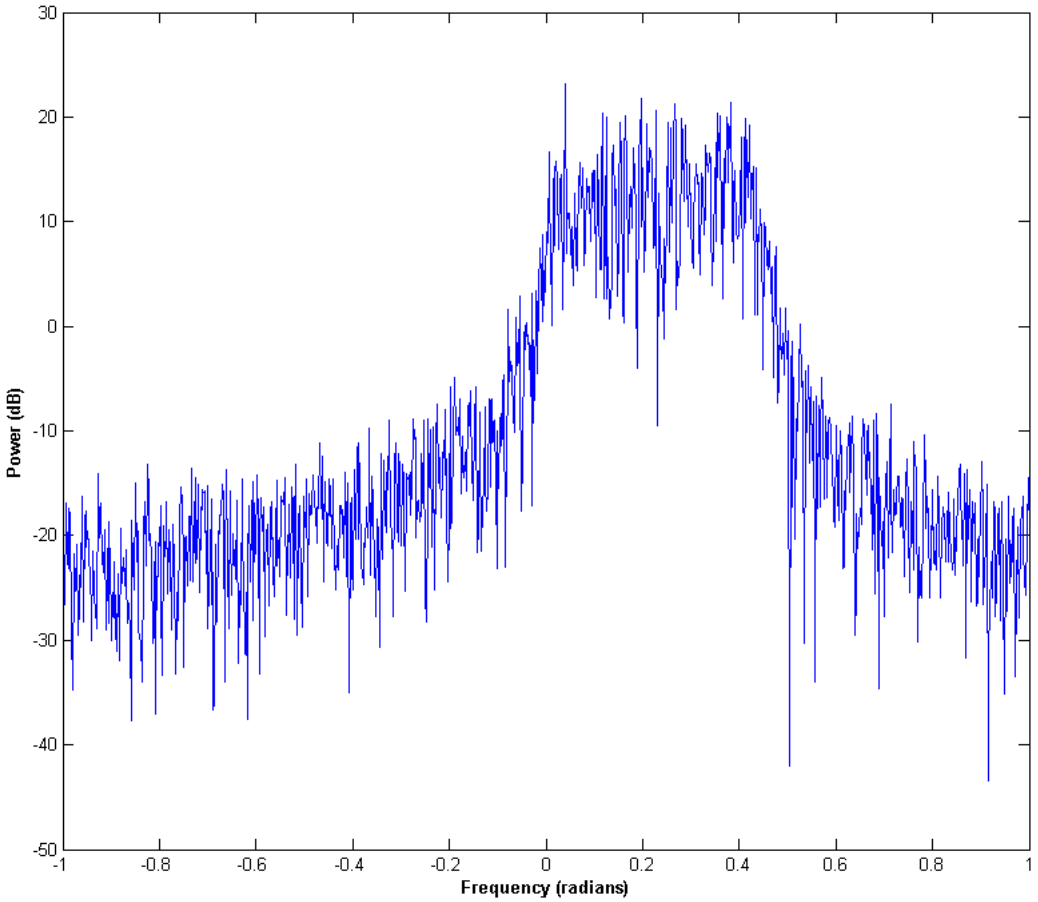


Figure 3.5: LFM radar waveform convolved with Gaussian clutter in an AWGN channel

symbol designed using the Dominant Projection method at an oversampling factor of $M = 2$. This scenario has a signal-to-noise ratio (SNR) of 0 dB and a signal-to-clutter ratio (SCR) of -30 dB. When superimposed, as in Figure 3.7, the behavior of the dominant projection technique is clear. However, it is important to maintain a low oversampling factor. The projection will attempt to place the communication symbol as "far away" from the radar signal as possible. For instance, Figure 3.8 illustrates the case when $M = 4$. The REC symbol is now embedded at frequencies with less clutter power. As a consequence, this symbol will be more easily detected than the symbol transmitted in Figure 3.7 using an oversampling factor of $M = 2$. As $M$ gets large the communication symbols cannot depend

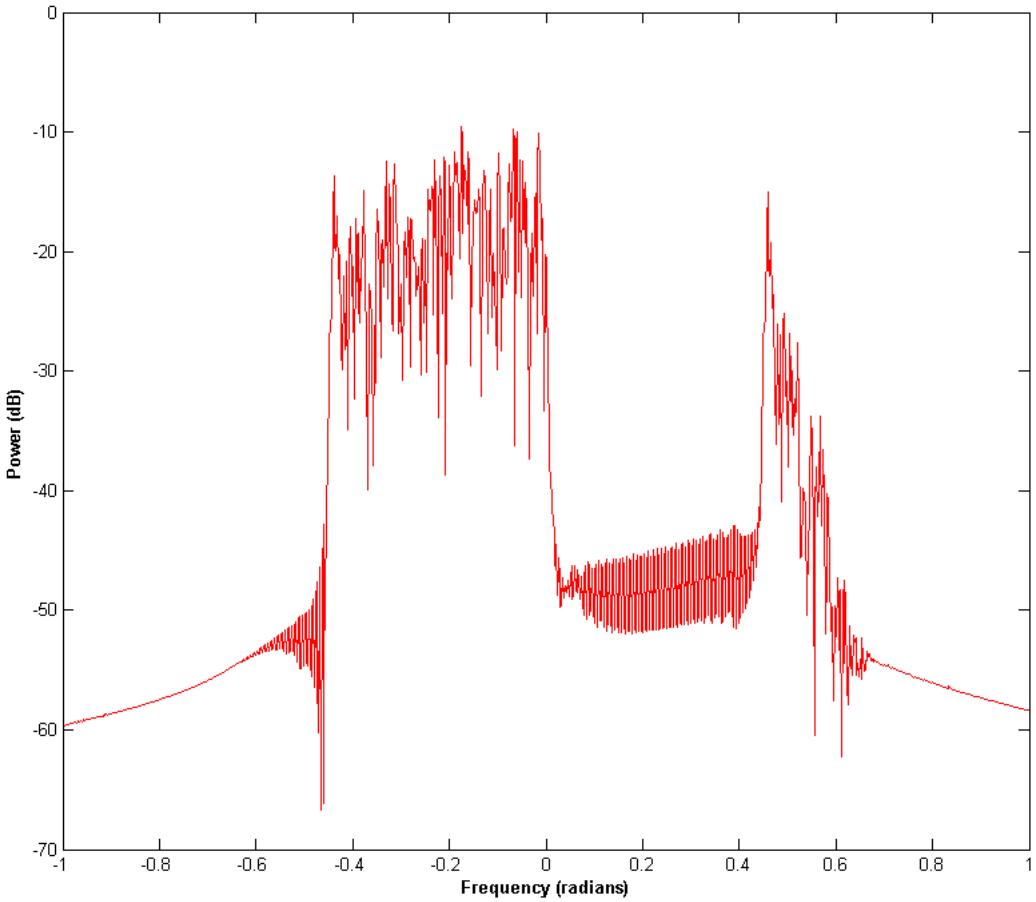


Figure 3.6: Communication symbol designed for an LFM radar waveform

on clutter to mask their presence. Therefore, in the case of large $M$ the symbols must depend on noise to mask their presence like traditional SS techniques.

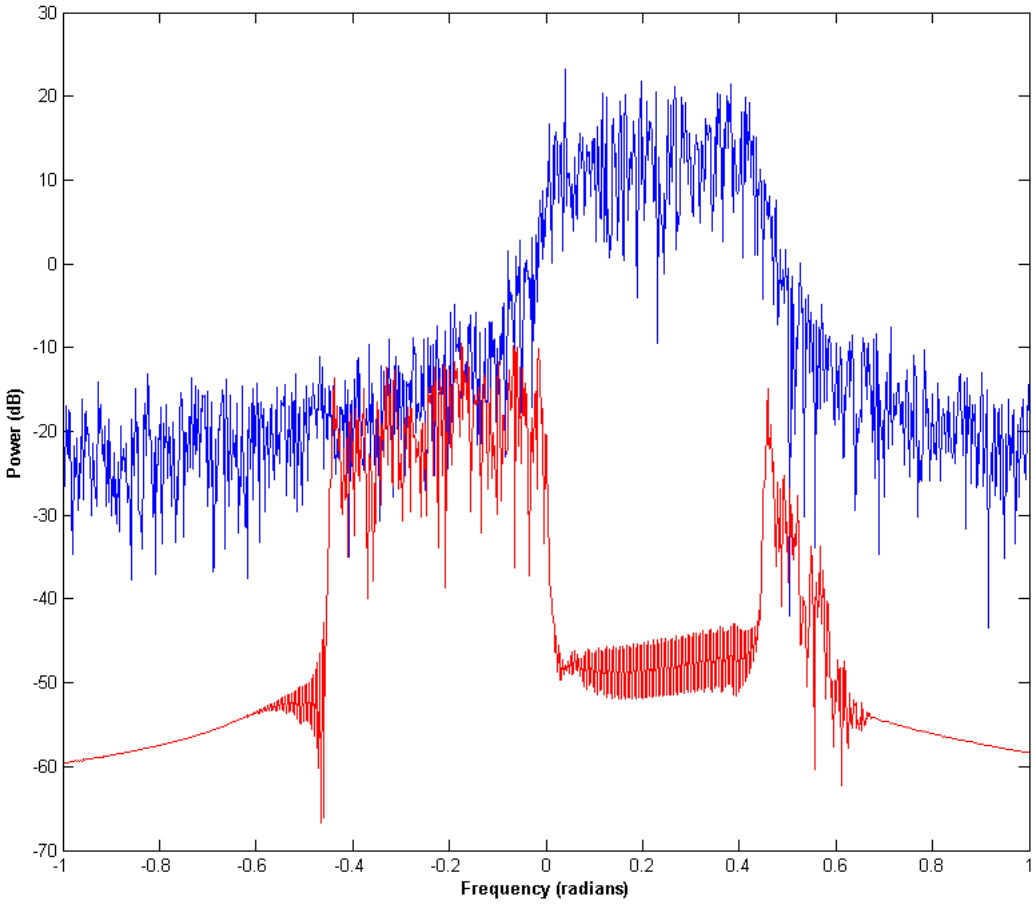


Figure 3.7: Symbol spectral content for M=2

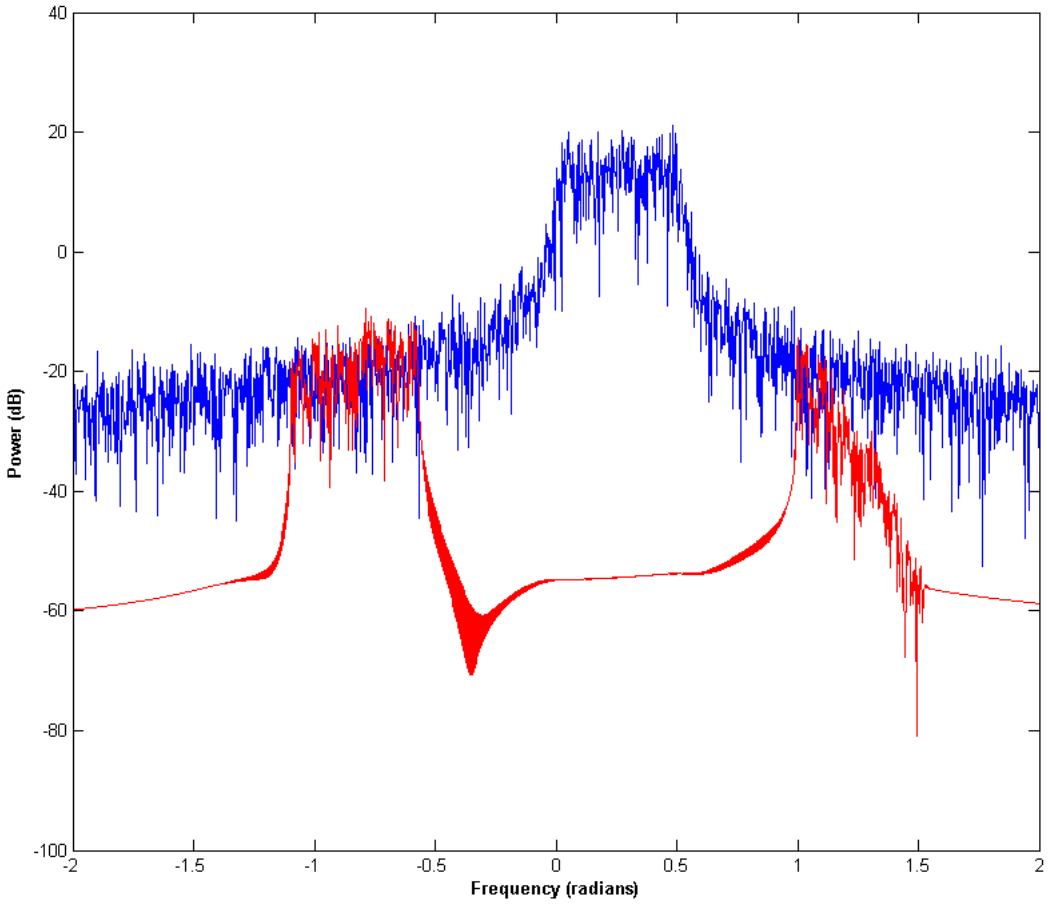


Figure 3.8: Symbol spectral content for M=4

# Chapter 4

# Environmental Considerations

## 4.1 Multipath Effects

As mentioned in Chapter 3, the radar waveform may scatter from objects outside of the direct path between the radar and tag. In the radar vernacular, this is called forward scattering while for communications this phenomenon is known as multipath. Given the presence of multipath, the received signal at the tag thus consists of the transmitted radar waveform convolved with the multipath impulse response $h(t)$ and corrupted by noise.

Convolving the radar waveform with the multipath impulse response produces multiple copies of the radar waveform that have been modulated by an amplitude and phase shift, as well as being shifted in time. The multipath-corrupted signal received at the tag may be expressed mathematically as

$$y_{\text{tag}}(t) = h(t) * s(t) + u_{\text{tag}}(t). \tag{4.1}$$

where $u_{\text{tag}}$ is the noise at the tag. In standard communication systems multipath makes symbol determination more difficult. The presence of multipath distorts the radar waveform that is incident upon the tag.

Typical communication systems transmit multiple symbols in succession. The time

delayed-copies of previously transmitted symbols can interfere with successive symbols. This is termed inter-symbol interference (ISI). The radar-embedded communication paradigm does not suffer from ISI. The time between transmitted radar waveforms provides a guard time, preventing ISI. Therefore, the multipath distortion only needs to be compensated for on a per-symbol basis.

An important result of [15] was to show that multipath has an identical mathematical structure as ambient scattering. This is due to the associative property of LTI systems where

$$\tilde{s}(t) * x(t) = s(t) * h(t) * x(t) = s(t) * \tilde{x}(t); \tag{4.2}$$

for $\tilde{x}(t)$ just another arbitrary impulse response.

## 4.2 Robustness to Multipath

It was shown in [15] and [2] that the Dominant Projection method suffers very little degradation to communication performance if forward scattering (multipath) exists. To illustrate this property, consider the correlation between the eigenvectors generated by (3.6). The eigenvectors form an orthonormal basis. Therefore, the correlation matrix of the eigenvectors is the $NM \times NM$ identity matrix. However, if the radar waveform is corrupted by multipath, the eigendecomposition in (3.6) performed by the tag will not yield the same eigenvectors as the receiver. Therefore, it is instructive to examine the correlation between the eigenvectors generated from multipath corrupted radar waveforms. For example, consider the case of an LFM radar waveform with $N = 100$, oversampled by a factor of $M = 2$. This waveform encounters two independent random multipath profiles, each consisting of a direct path and 9 multipath elements drawn from a complex Gaussian distribution. The time delays are uniformly distributed over $[0, T/2]$. Figure 4.1 shows the average correlation between the eigenvectors generated for each multipath corrupted waveform over the course of 1000 independent trials.

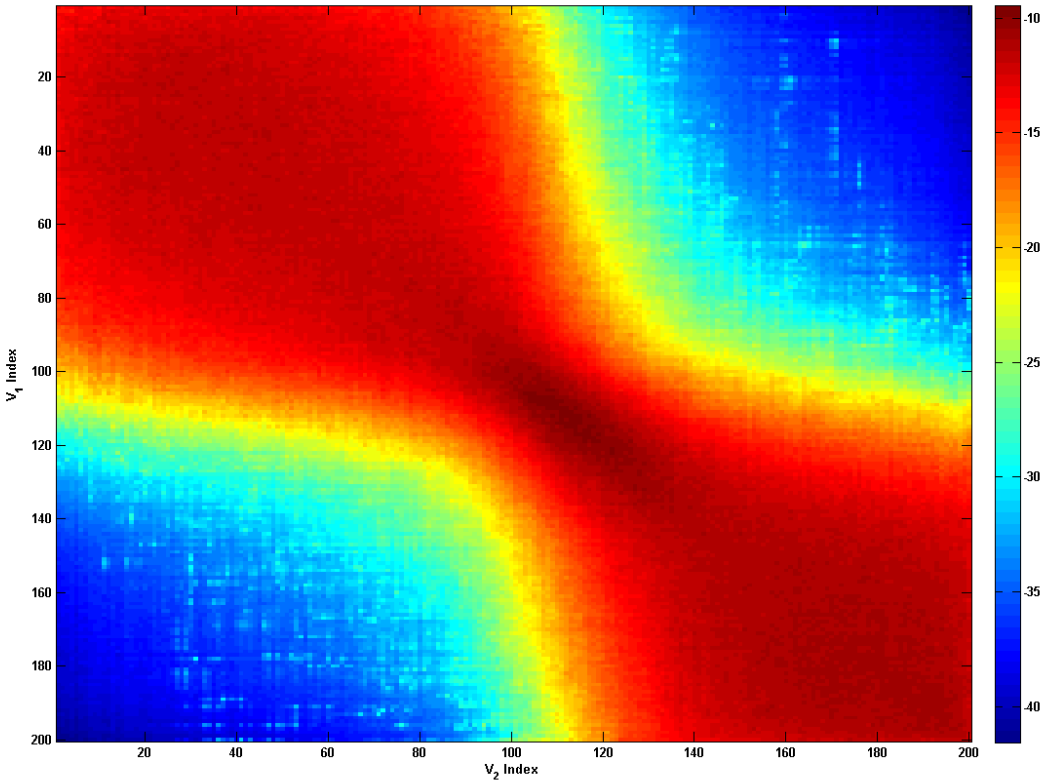


Figure 4.1: Eigenvector correlation (dB) between independent multipath-corrupted radar waveforms

Notice that the multipath causes the eigenvectors to "smear". The ideal situation (*i.e.*, no multipath) would lead to identical eigenvectors. In that case, the average correlation would be equal to one along the main diagonal and identically zero everywhere else. When the two sets of eigenvectors are generated from multipath-corrupted waveforms, the average correlation is greater than zero away from the main diagonal. Consider the dominant space to consist of the first $N$ eigenvectors. Each set of eigenvectors corresponding to the dominant subspace is highly correlated with the dominant subspace of the other set of eigenvectors (top left quadrant of Figure 4.1). This correlation also holds true for the non-dominant subspaces (bottom right quadrant of Figure 4.1). However, the subspaces as a whole are still well separated (uncorrelated). For further discussion and illustration, see [2]. It should be

noted that the tag and receiver will still be required to have knowledge of the seed vectors $\mathbf{b}_k$ from (3.11) used to create the communication symbols.

## 4.3 Time Reversal

Previous work established the robust nature of the Dominant Projection design methodology with respect to multipath [15]. If the radar is also the desired receiver, the multipath channel between the tag and radar may be approximated as being stationary and reciprocal. Therefore, it is possible to incorporate environmental knowledge into the design of the communication symbols. If the radar waveform is known *a priori* to the tag, the multipath may be estimated using matched filtering, mismatched filtering [36], least squares [37], or adaptive pulse compression (APC) [38] techniques. This estimate is denoted as $\hat{h}(t)$. Assuming the channel is approximately stationary and reciprocal, $\hat{h}(t)$ may be complex conjugated, reversed in time, and convolved with the communication symbol as a form of pre-distortion [39]. The time-reversed communication symbol is given as

$$\hat{c}_k = \hat{h}^*(-t) * c_k(t). \tag{4.3}$$

Therefore, using (4.3) the signal received by the radar is now given as

$$\begin{aligned} y(t) &= s(t) * x(t) + \alpha \hat{c}_k(t) * h(t) + u(t) \\ &= s(t) * x(t) + \alpha \hat{h}^*(-t) * c_k(t) * h(t) + u(t) \\ &= s(t) * x(t) + \alpha r(t) * c_k(t) + u(t). \end{aligned} \tag{4.4}$$

where $r(t) = \hat{h}^*(-t) * h(t)$ is the approximate autocorrelation of the multipath channel. Intuitively, it can be seen that this technique causes the multipath elements to constructively combine at the match point (*i.e.* the radar receiver). Due to the high spatial dependence of the multipath elements, it is also likely that this approach will cause destructive interference

away from the match point, such as at an intercept receiver.

Figures 4.2 and 4.3 show the effects of time reversal at the radar and intercept receivers, respectively. To construct each figure, a histogram was formed from 100,000 Monte Carlo simulations. In these simulations, the channel was constructed with impulses uniformly distributed over a channel half the length of a communication symbol (*i.e.* for $P$ multipath elements, time delay $\tau_i \sim U(0, T/2), i = 1, \ldots, P$). The complex amplitude of the multipath impulses are all initially drawn from a complex Gaussian distribution, but are then scaled by the inverse of the maximum element in the channel. Therefore, the maximum value is set to one, while the magnitude of all other elements are less than one. This ensures the existence of a direct path and constrains all indirect paths to have a smaller magnitude than the direct path. The time reversed estimate is normalized to unit energy. Therefore, the channel estimate has the same energy as a unit impulse (*i.e.* the non-time reversed case). The magnitude shown in Figures 4.2 and 4.3 is the magnitude of the maximum response at the receiver. Note that a unit energy impulse passed through the noiseless channel would always have a magnitude of one. Therefore, any response greater than one indicates a gain at the desired receiver. However, a response less than one is desired at the intercept receiver (*i.e.*, a gain less than one implies a more covert symbol at the intercept receiver).

Figure 4.2 shows the spatio-temporal focusing effect of time reversal at the desired receiver (in this scenario, the radar). It is clear that even with only two multipath components (direct path plus one additional) the time reversed symbol would outperform a non-time reversed symbol. As the number of multipath elements increases, so does the magnitude of the maximum response. The mean-shifting of the distribution of responses clearly illustrates the spatio-temporal focusing effect.

Figure 4.3 illustrates the destructive interference that an arbitrary intercept receiver experiences with respect to a time-reversed symbol. To form Figure 4.3, the time-reversed symbol was formed but convolved with an independent channel constructed using the same distribution of time delays and impulse amplitudes, and containing the same number of paths.

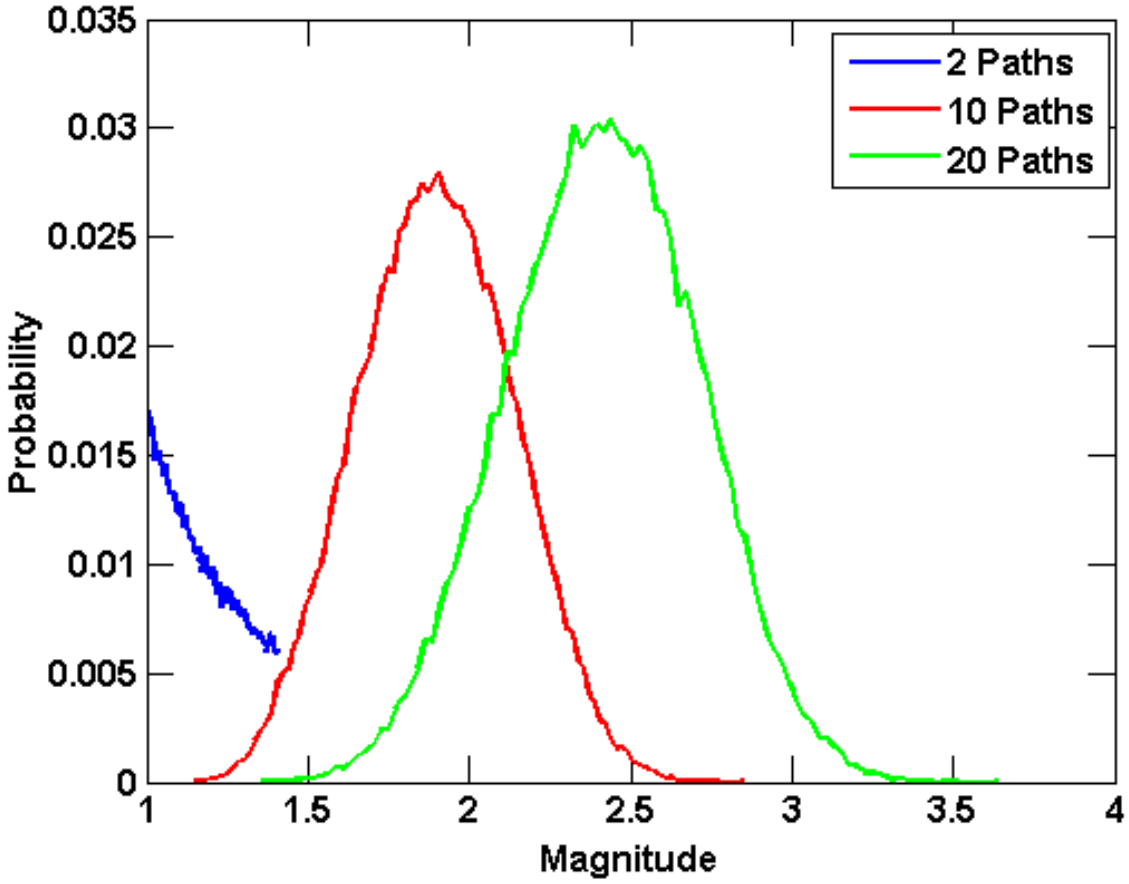


Figure 4.2: Time reversal gains at the desired receiver

The mismatch between the time reversed symbol and the independent channel illustrates the LPI improvement offered by the time-reversal processes. The received magnitude is largely less than one, indicating a negative gain at the intercept receiver. An interesting problem for future work would be to analytically examine the benefits of the time reversal.

## 4.4 Time Reversal with an Unknown Radar Waveform

If the radar waveform is not known at the tag *a priori*, the formation of the time reversed profile becomes very difficult. As mentioned in Section 4.2, the Dominant Projection symbols suffer very little degradation if a multipath-corrupted radar waveform is used at the design stage. Unfortunately, if the radar waveform is not known, estimating the multipath profile

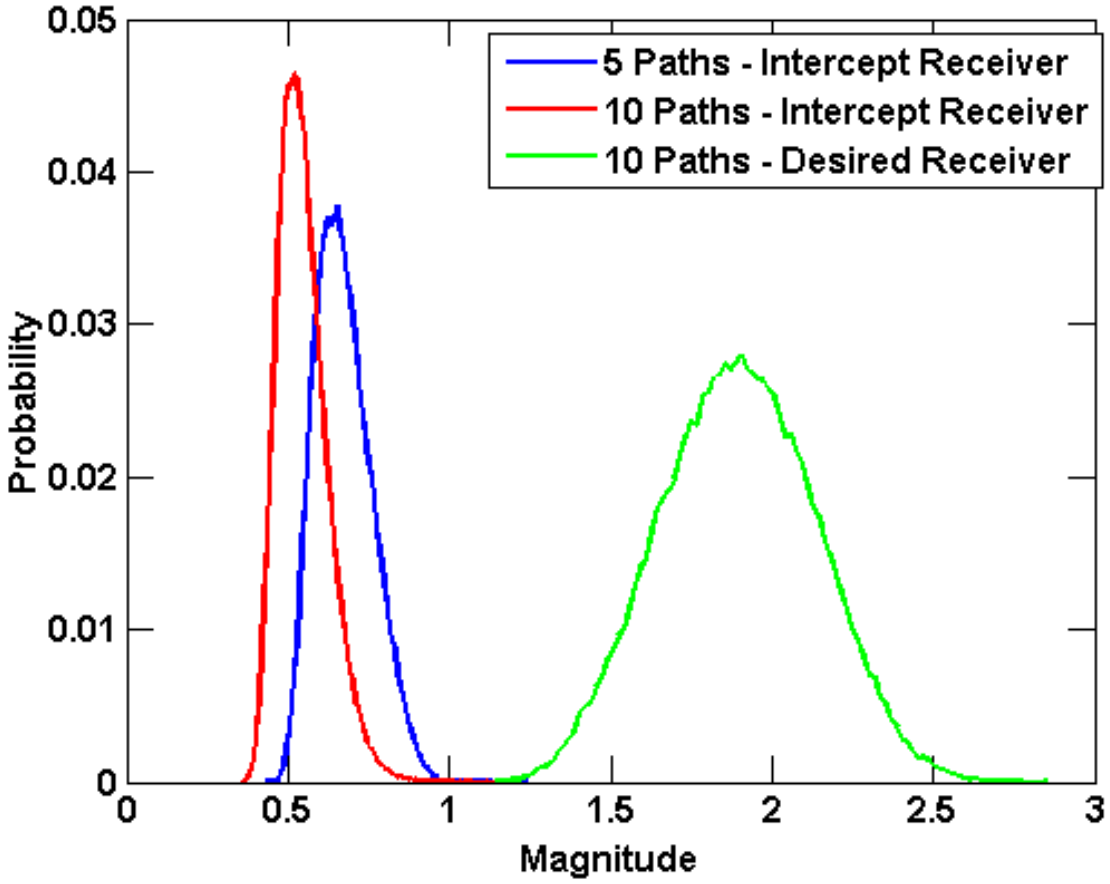


Figure 4.3: Time reversal performance for intercept receiver v. desired receiver

becomes very difficult. This estimation requires blindly deconvolving the waveform from the multipath. To solve a blind deconvolution problem, *a priori* or spatial information must be used. Assuming the individual paths correspond to different angles of arrival at the tag, direction-of-arrival (DOA) estimation may be used to distinguish the paths. If an antenna array is available at the tag, algorithms such as MUSIC [40] in conjunction with a model order selection algorithm (see [41] for a survey) can be used to isolate the direction-of arrival (DOA) of multipath components. The MUSIC algorithm can identify a number of incident signals equal to the number of antenna elements used. However, MUSIC cannot distinguish temporally correlated signals. It is possible to decorrelate the signals using sub-arrays in a spatial smoothing technique [42]. Unfortunately, spatial smoothing reduces the number of signals the algorithm is capable of isolating. Further processing would need to be done to

isolate complex amplitudes as well as relative time delays to fully reconstruct the channel. Many blind deconvolution algorithms rely on the periodic nature of a waveform. Typical waveforms used in radar and communications systems satisfy the periodic assumption. This periodic nature gives rise to cyclo-stationary statistics (see [43] [44] [45] [46] for an excellent treatment). This property can be exploited to blindly deconvolve a signal using either second order or higher order statistics (*i.e.* skew, kurtosis). However, methods based on higher order statistics require large sample sizes and many second order methods have large computational costs [46]. Another approach is to use subspace methods such as MUSIC in conjunction with cyclo-stationary statistics (*e.g.* [47]). However, correlated signals share cyclic frequencies. Just as with the time domain implementation of MUSIC, this can be rectified using spatial smoothing [48] [49].

In [3] we proposed using spatial selectivity to recover a transmitted radar waveform from a multipath corrupted channel. This approach relies on the Re-Iterative Super Resolution (RISR) [50] algorithm to isolate the transmitted radar waveform. Using the array narrow-band assumption (*i.e.* the difference between the responses to a given signal over all array elements can be modeled as a phase shift), the RISR algorithm produces a spatial filter bank corresponding to the possible spatial angles from which a signal could arrive. When applied to the temporal data collected from the antenna array, each filter isolates any signal from that angle and nulls all other signals. The RISR algorithm is robust to correlated signals. Unlike MUSIC, RISR can also be used to provide an estimate of the number of signals present. Further, it can operate on extremely low sample support and for any arbitrary array manifold (assumed known). Once the transmitted radar waveform is estimated, it can be used to estimate the multipath channel as was discussed in Section 4.3.

The simulation setup in [3] departs from that used in the rest of this thesis. Figures 4.4 and 4.5 provide an example of the possible performance of the estimation technique. A random polyphase radar code was used. Each of $N = 40$ chips $s_i$ in the code $\mathbf{s} = [s_1, s_2, \ldots, s_N]$ was constructed as $s_i = e^{j\phi_i}$, $\phi_i \sim U(0, 2\pi)$. Sampling is performed at the

Nyquist sampling frequency. The simulation uses a 10 element linear array with $\lambda/2$ spacing. The multipath channel consists of three total paths. The direct path signal arrived at an angle of $+14.48°$ from boresight with an SNR of 20 dB. The two multipath components arrive at angles of $\pm 30°$ at SNRs of 15 dB and 10 dB. Using a heuristic thresholding technique to estimate the number of signals present, the three signals were easily extracted. To evaluate the efficacy of the algorithm, the normalized amplitude and phases of the estimated signals were compared to ground truth. As Figure 4.4 illustrates, the RISR algorithm does well in

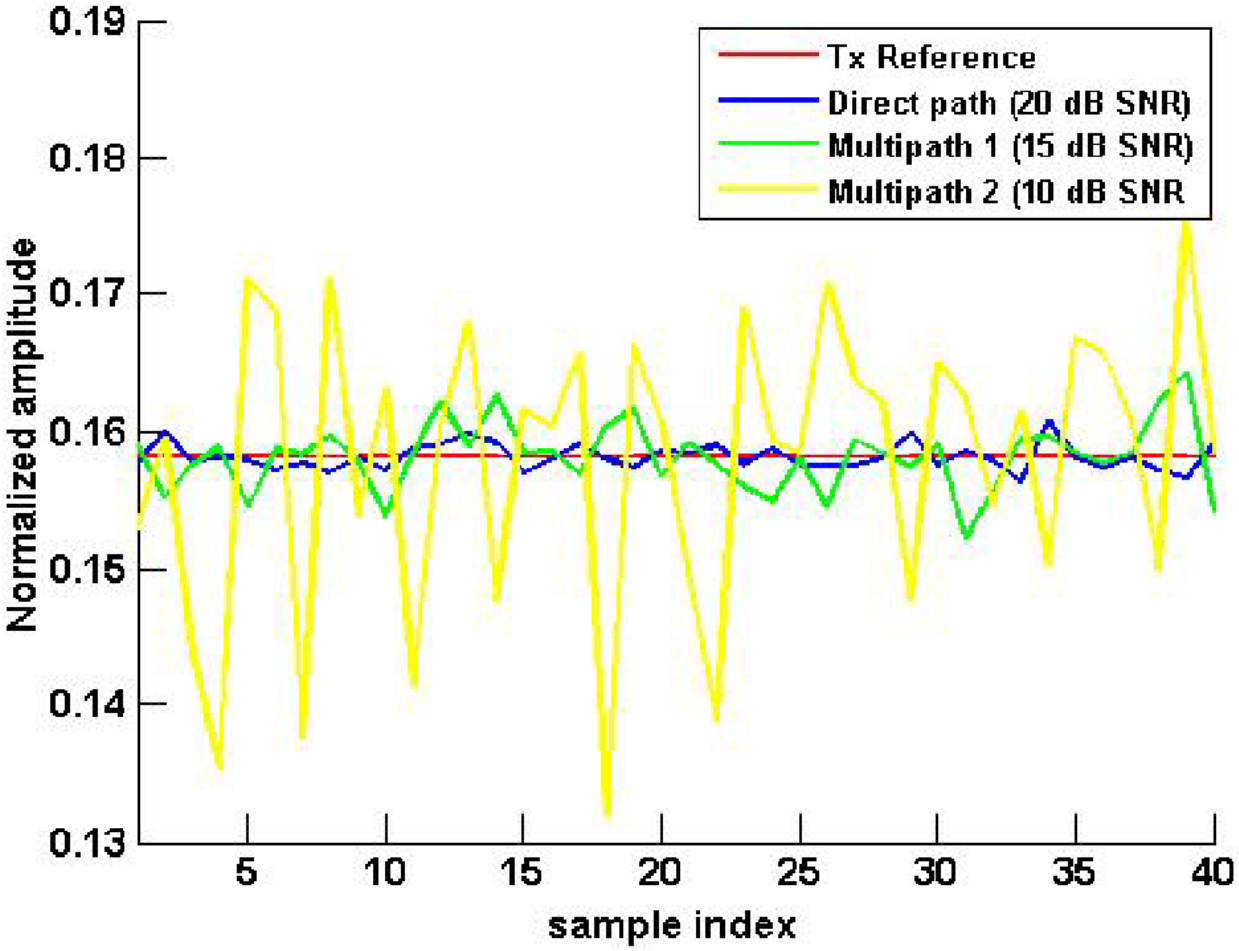


Figure 4.4: Normalized amplitudes of estimated signals, as compared to transmitted waveform

estimating the amplitudes of the transmitted waveform. It should be noted that due to the high output power and amplifier requirements practical radar waveforms are constrained to have a constant modulus. This constraint can be used to estimate the normalized amplitude.

Therefore, the wide variance of the estimate of the second multipath element should not restrict the performance of the potential system.

Of more importance is the phase estimation. Figure 4.5 shows excellent agreement between the phases of the estimated signals and the ground truth waveform. In fact, the direct path and first multipath component are visually virtually indistinguishable from the transmitted waveform. This is a very encouraging result. It is clear that RISR can be used

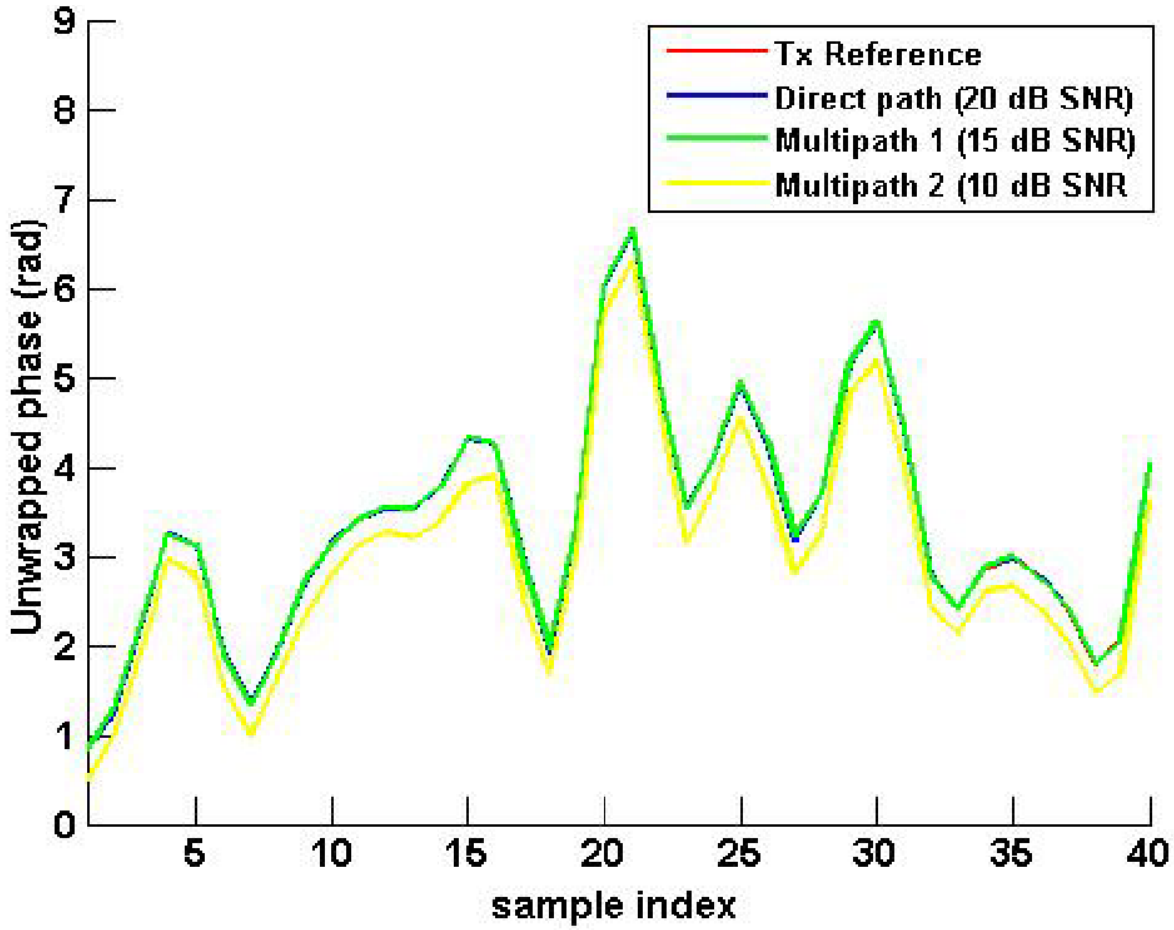


Figure 4.5: Unwrapped phases of estimated signals, as compared to transmitted waveform

to estimate the received radar waveform. In theory, this spatial selectivity can be used to estimate the transmitted radar waveform from a multipath channel. While this technique is not a strict blind deconvolution technique, the results are the same. The estimated waveform can be used to design the communication symbols and to estimate the multipath channel for the purpose of time reversal.

# Chapter 5

# Receive Processing

This chapter discusses the strategies used by a desired receiver to extract the embedded symbol from the radar clutter and noise. It is assumed that the signal has been sampled at baseband, lowpass filtered, and demodulated into in-phase and quadrature components. For an analysis of the performance of the receiver structure presented in this chapter, see Chapter 7.

The goal of a communication receiver is to minimize receive errors (*i.e.*, maximize data reliability). For the REC framework, the data rate is limited by the pulse repetition frequency (PRF) of the radar and number of bits per communication symbol. The PRF of the radar is outside the control of the tag. The optimal choice of constellation size is not discussed here, but is a topic for future work. The receive bit error rate (BER) is dependent on the signal-to-interference-plus-noise ratio (SINR) and design of the receiver. To minimize BER the receiver should be capable of suppressing the interference (*i.e.* clutter) and performing coherent integration to extract signals below the noise floor (as in traditional spread spectrum communications). As stated in Chapter 3, previous work utilized a decorrelating filter to suppress interference [15] [1]. In that formulation, the $k^{th}$ receive filter was given as

$$\mathbf{w}_k = (\mathbf{S}\mathbf{S}^H)^{-1}\mathbf{c}_k. \tag{5.1}$$

In other words, the filter consists of a whitening component (to decorrelate the interference) and a matched filter (to maximize the SNR). The symbol corresponding to the maximum residue after applying the decorrelating filterbank has been shown to be a maximum likelihood estimator [14]. Defining the size of the dominant space to be $m$, the decorrelating filter given in (5.1) can be diagonally loaded as

$$\mathbf{w}_k = (\mathbf{S}\mathbf{S}^H + \delta\mathbf{I})^{-1}\mathbf{c}_k \tag{5.2}$$

where $\mathbf{I}$ is the identity matrix and $\delta = \lambda_{m+1}$, where $\lambda_{m+1}$ is the largest non-dominant eigenvalue. Introducing the variable $m$ allows the tag to vary the size of the dominant space. Valid values for $m$ are $1 \leq m \leq NM - K$. The non-dominant space must have a rank that is greater than or equal to the number of possible communication symbols. If it does not have the degrees-of-freedom necessary, the design space is rank deficient and communication symbols will no longer be linearly independent. By varying the size of the dominant subspace, the tag may optimize the gain advantage an intended receiver enjoys over an intercept receiver. This is discussed in further detail in Chapter 7.

## 5.1 Maximum Likelihood Symbol Estimation

Previous analysis assumed that the transmitted signal is present within the observed receive interval [1]. This assumption ignores the null hypothesis (*i.e.* no symbol present), as well as the problem of synchronization. Here we propose the use of a Neyman-Pearson criterion to both determine the presence/absence of a symbol and provide a means for automatic synchronization at the receiver. This concept is further examined in Section 5.2.

In the original formulation, it was assumed that the receiver has clairvoyant knowledge that a symbol is present during a prescribed time interval that is much longer than the symbol duration. Using the signal model given in (3.12), the received sampled signal at time

sample $\ell$ (for time interval $\ell = 1, \ldots, L$ ) is the length $NM$ vector

$$\mathbf{y}_r(\ell) = \left[ \begin{array}{cccc} \mathbf{y}_r(\ell) & y_r(\ell-1) & \ldots & y_r(\ell-NM+1) \end{array} \right]^T. \tag{5.3}$$

The time interval therefore consists of the length $NM + L - 1$ collection of samples. The received signal, communication symbol, and filter structures are given in (3.11), (3.12), and (5.2). The sampled signal is then passed through a bank of $K$ filters from (5.2) corresponding to the possible symbols. The magnitude of the response of the $k^{th}$ filter at time instant $\ell$ is defined as

$$|z_y^{(k)}(\ell)| = |\mathbf{w}_k^H \mathbf{y}_r(\ell)|. \tag{5.4}$$

To select the most likely symbol, the maximum of the set of all responses is found as

$$|z_{y,max}^{(\hat{k})}| = \text{argmax}_{\ell,k} |z_y^k(\ell)| \tag{5.5}$$

where $\hat{k}$ corresponds to the selected symbol. The symbol selection given by the output of (5.5) can be considered as a $K$ hypothesis test:

$$\begin{aligned} \mathcal{H}_1: &\quad \mathbf{y}_r = \mathbf{S}\mathbf{x} + \alpha \mathbf{c}_1 + \mathbf{u} \\ \mathcal{H}_2: &\quad \mathbf{y}_r = \mathbf{S}\mathbf{x} + \alpha \mathbf{c}_2 + \mathbf{u} \\ &\quad \vdots \\ \mathcal{H}_K: &\quad \mathbf{y}_r = \mathbf{S}\mathbf{x} + \alpha \mathbf{c}_K + \mathbf{u}. \end{aligned} \tag{5.6}$$

It should be noted that this formulation ignores the null hypothesis. In this formulation, a communication symbol is always assumed to have been transmitted. In practice, the receiver does not have clairvoyant knowledge of the presence of a symbol. Therefore, it is important to establish a confidence level in the selection of a symbol.

## 5.2 Neyman Pearson Detector

When the receiver does not possess clairvoyant knowledge of the presence of a communication symbol, the problem of symbol determination may be framed as a detection problem. In this case, the receiver must not only determine which communication symbol was sent, but whether a symbol is present at all. This raises the possibility of the receiver falsely detecting a communication symbol when there is none present. Therefore, the three probabilities of interest are the probability of correctly detecting a symbol ($P_D$), the probability of not detecting a present symbol ($P_M$), and the probability of false alarm ($P_{FA}$).

The Neyman-Pearson criterion [19] is a method of maximizing the probability of detection, while holding a constant probability of false alarm. To perform a Neyman-Pearson test, the probability distribution function (PDF) of the null hypothesis must be known. In the case of detecting a single known signal, the two hypotheses are signal present and signal absent. A threshold for detection is set as the value where the integral of the right tail of the signal absent PDF is equal to the acceptable probability of false alarm. The probability of detection is then given as the integral of the right tail of the signal present PDF for all values greater than the threshold. The receiver threshold $\mathcal{T}$ is set such that the probability of a received value exceeding the threshold when a signal is not present is equal to the desired probability of false alarm, $P_{FA}$. The test statistic is then maximized when a signal is present.

As mentioned previously, the decorrelating receiver has been shown to be a maximum likelihood estimator [14] that maximizes the probability of detection (assuming a symbol is present). However, in order to express a degree of confidence in the symbol selection, we consider the idea of bounding the $P_{FA}$. First, the hypothesis test given in (5.6) is conducted via (5.5), yielding an accepted hypothesis $\hat{k}$ and $K-1$ rejected hypothesis. The rejected hypotheses may be grouped together and collectively treated as multiple realizations of the

null hypothesis:

$$\begin{aligned} \tilde{\mathcal{H}}_0 : &\quad z_y = z_x + z_u \\ \tilde{\mathcal{H}}_1 : &\quad z_y = z_x + \alpha\Delta + z_u. \end{aligned} \tag{5.7}$$

The quantities $z_x$ and $z_u$ correspond to the residues of the clutter and noise after filtering, respectively. By the Central Limit Theorem, the clutter and noise residues (resulting from the filtering operation) tend to a complex Gaussian distributions. Therefore, the magnitude of the residues tends to a Rayleigh distribution. Knowledge of the PDF allows for the generation of a threshold for a given $P_{FA}$. It can be shown that the Neyman-Pearson threshold in this case is given as [19]

$$\mathcal{T} = \sqrt{-2\ \sigma_0^2\ \ln P_{fa}} \tag{5.8}$$

where $\sigma_0^2$ is the variance of the output of the $K-1$ filters corresponding to $\tilde{\mathcal{H}}_0$. The complete receiver processing diagram is shown in Figure 5.1.

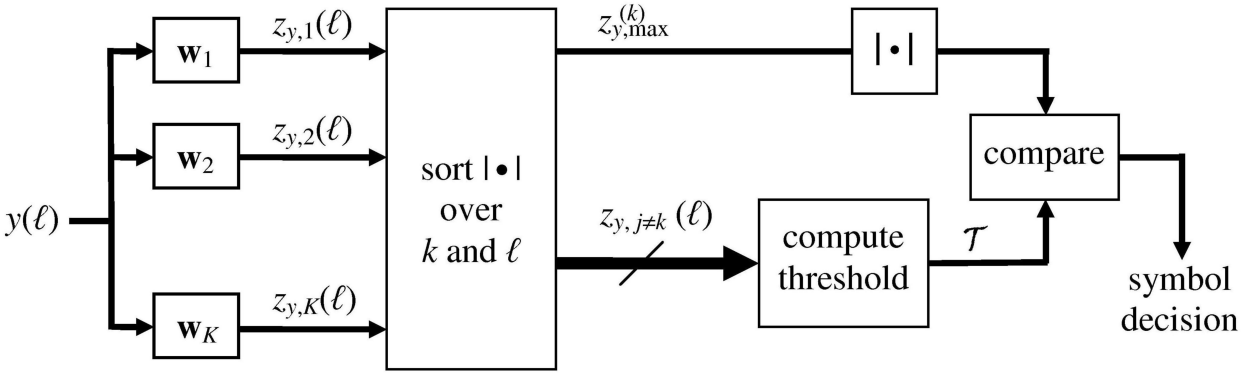


Figure 5.1: Neyman-Pearson receiver

Figure 5.2 shows the peak responses (*i.e.* magnitude of the maximum response over all time delays) from the decorrelating filter bank for both correct and incorrect responses. Numerically integrating the right tail using thresholds derived from (5.8) provided correct probabilities of false alarm. It may be possible that increasing the number of symbols improves the Rayleigh approximation.

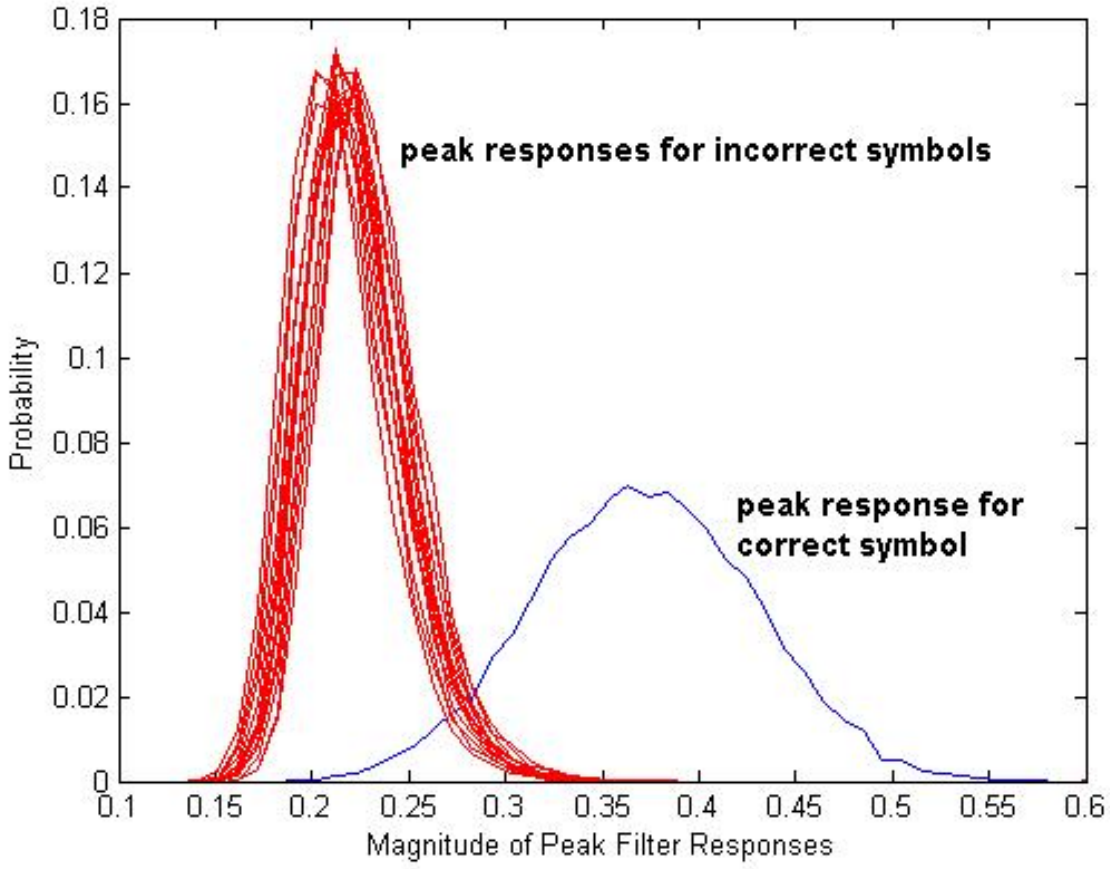


Figure 5.2: PDFs of hypothesized symbols

Note that the Neyman-Pearson formulation automatically accounts for the problem of synchronization. The maximum likelihood receiver in the first stage maximizes the probability of detection over all time samples, therefore selecting the time sample most likely to contain a communication symbol. This formulation gives two ways of examining the performance of the receiver. First, the reliability of the receiver can be examined in terms of the probability of incorrectly selecting a symbol. This is measured as the symbol-error-rate (SER) or bit-error-rate (BER). At this stage, it is still assumed that a symbol is present. Second, the receiver can be examined in terms of the detector performance. In this case, the relevant metrics of interest are $P_D$ (and conversely the probability of miss, $P_M$) and $P_{FA}$. This analysis further illuminates the capabilities of the receiver by considering the behavior of the receiver when a symbol is absent. A more formal method of analyzing the receiver

gain as a function of SINR and subspace size is given in Chapter 7.

# Chapter 6

# Probability of Intercept

The ability of an intercept receiver to detect the presence of a radar-embedded communication (REC) symbol depends on many factors. For example, the time-width and bandwidth of the communication waveform must be known to the desired receiver, but that information is not available to the intercept receiver. For all LPI metrics, the intercept receiver is assumed to have knowledge of the time-width and bandwidth used by the REC system. This knowledge provides a "worst case" scenario, and should bound the performance of an intercept receiver.

## 6.1 An Extension of Previous Work

An LPI metric was established in [1] that measures normalized correlation to quantify the covert nature of the embedded communication symbol. This metric in effect "scans" the eigenspace of the radar waveform by systematically projecting away the hypothesized dominant subspace from the received signal and examining the normalized correlation between each possible communication symbol and the residue of the projection. In other words, for $\tilde{m} = 1, 2, \ldots, NM$, define the hypothesized dominant subspace as the $NM \times \tilde{m}$ matrix $\tilde{\mathbf{V}}_{D,\tilde{m}}$ composed of the eigenvectors corresponding to the $\tilde{m}$ largest eigenvalues. Therefore,

to project away from this subspace, form a projection matrix as

$$\mathbf{P}_{\tilde{m}} = \mathbf{I} - \tilde{\mathbf{V}}_{D,\tilde{m}} \tilde{\mathbf{V}}_{D,\tilde{m}}^H = \tilde{\mathbf{V}}_{ND,\tilde{m}} \tilde{\mathbf{V}}_{ND,\tilde{m}}^H. \tag{6.1}$$

Applying $\mathbf{P}_{\tilde{m}}$ to the discretized received signal at time sample $\ell$, the $\tilde{m}^{th}$ residual is obtained as

$$\mathbf{z}_{\tilde{m}}(\ell) = \mathbf{P}_{\tilde{m}} \mathbf{y}(\ell). \tag{6.2}$$

This residue is then correlated with the $k^{th}$ communication symbol as [1]

$$\eta_{k,\tilde{m}}(\ell) = \frac{|\mathbf{c}_k^H \mathbf{z}_{\tilde{m}}(\ell)|}{\sqrt{(\mathbf{c}_k^H \mathbf{c}_k)(\mathbf{z}_{\tilde{m}}^H(\ell) \mathbf{z}_{\tilde{m}}(\ell))}}. \tag{6.3}$$

The efficacy of this metric was examined in [51]. Previous work has shown that the correct symbol produces the maximum response to this metric [1]. Therefore, only the results for the matching symbol are displayed. In all cases, the SNR at the intercept receiver is set to -5 dB, and the SIR is -35 dB. The radar signal incident at the tag (used to estimate the multipath) was corrupted by AWGN with an SNR of 30 dB. The communication symbols are designed using a dominant subspace of size 100 (*i.e.*, $N$), and 5000 Monte Carlo trials.

In Figure 6.1, the intercept receiver is placed at an identical location to the desired receiver. Therefore, the multipath channel is identical to that of the desired receiver. For each trial, time reversed and non-time reversed symbols are sent through identical channels with 5 multipath elements with random amplitudes and phases. The focusing ability of time reversal is once more observed, as the time-reversed waveform has a clearly greater magnitude.

Figure 6.2 shows the benefits of time-reversal in a more realistic situation. In this simulation, both the tag-radar channel and the tag-intercept receiver channel have 5 multipath elements. However, each channel is independently distributed in amplitude, phase, and time delay. In this scenario, the destructive interference given by time reversal in the tag-intercept

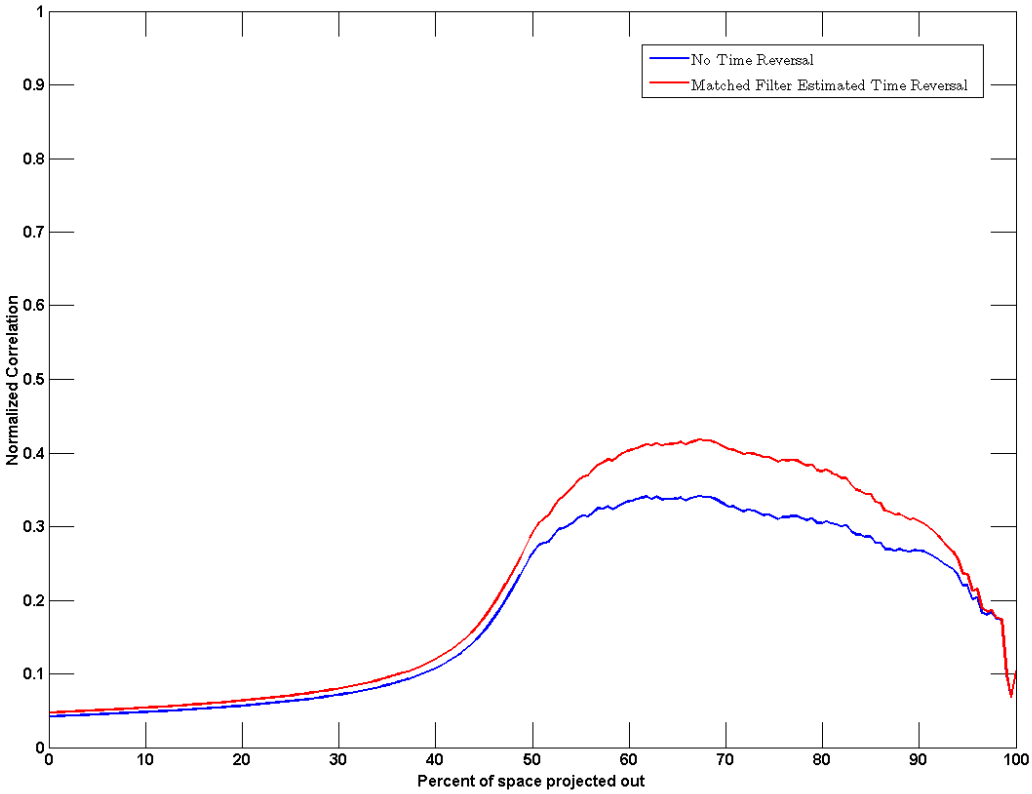


Figure 6.1: Co-located intercept receiver, 5 multipath elements

receiver channel is apparent.

Figure 6.3 provides an illuminating result. In this case, the number of multipath elements is increased to 20, but all other simulation parameters are identical to those used to produce Figure 6.2. Notice that while the time reversed symbol has a lower normalized correlation than the non-time reversed symbol for all hypothesized sizes of dominant subspace, the correlation for both types of symbols does not appear to be lower than those in Figure 6.2. One would expect that the increasing amount of multipath would have some effect on the LPI nature of the communication symbols (*i.e.*, lowered correlation), especially in the case of the time-reversed symbol. It appears that there is some clutter residue that is correlated with the symbol, providing a minimum response. It appears that there is a limit to the efficacy of this metric. Therefore, an improved metric is needed to quantify the LPI nature

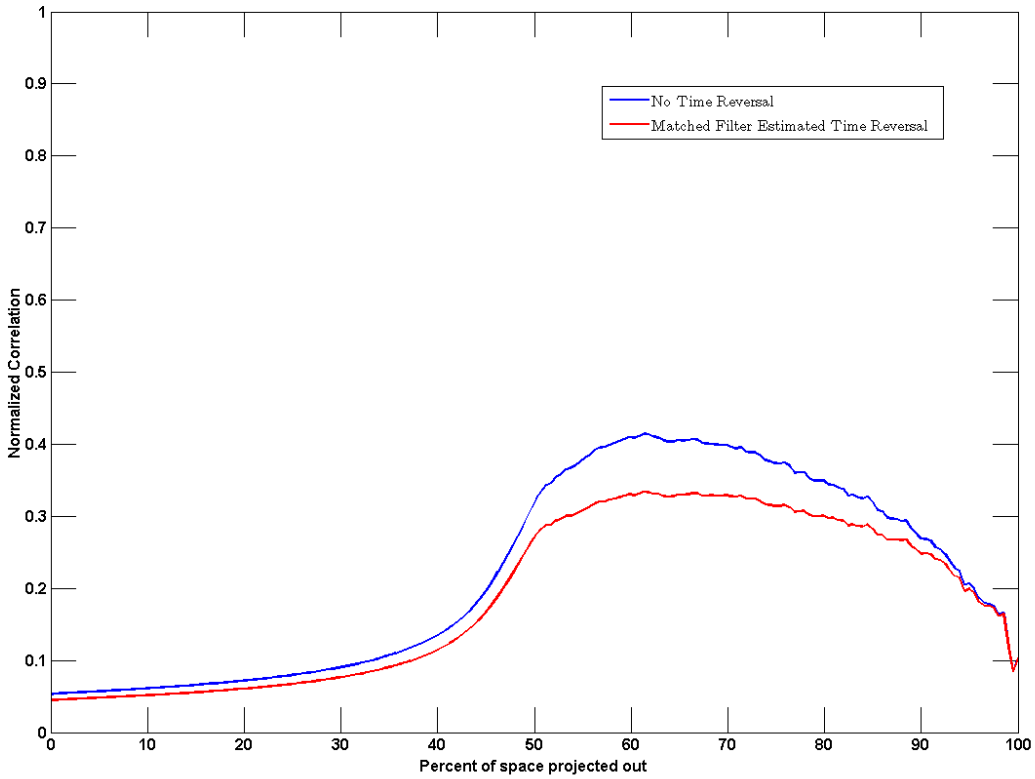


Figure 6.2: Independently located intercept receiver, 5 multipath elements

of an REC system.

## 6.2 Alternative LPI Metric I

Due to the limitations of the LPI metric in (6.3), we shall consider a new metric [2]:

$$\varepsilon_{\text{ir}}(\tilde{m}, \ell) \doteq \mathbf{y}^H(\ell)\mathbf{P}_{\tilde{m}}\mathbf{y}(\ell) \tag{6.4}$$

where $\mathbf{y}$ is the received discretized signal at the intercept receiver and the projection matrix is defined according to (6.1). This metric is indexed by time sample $\ell$ and the size of the dominant subspace $\tilde{m}$. Once more, the intercept receiver is assumed to have clairvoyant knowledge of the time-width and bandwidth of the communication symbol. Note that (6.4)

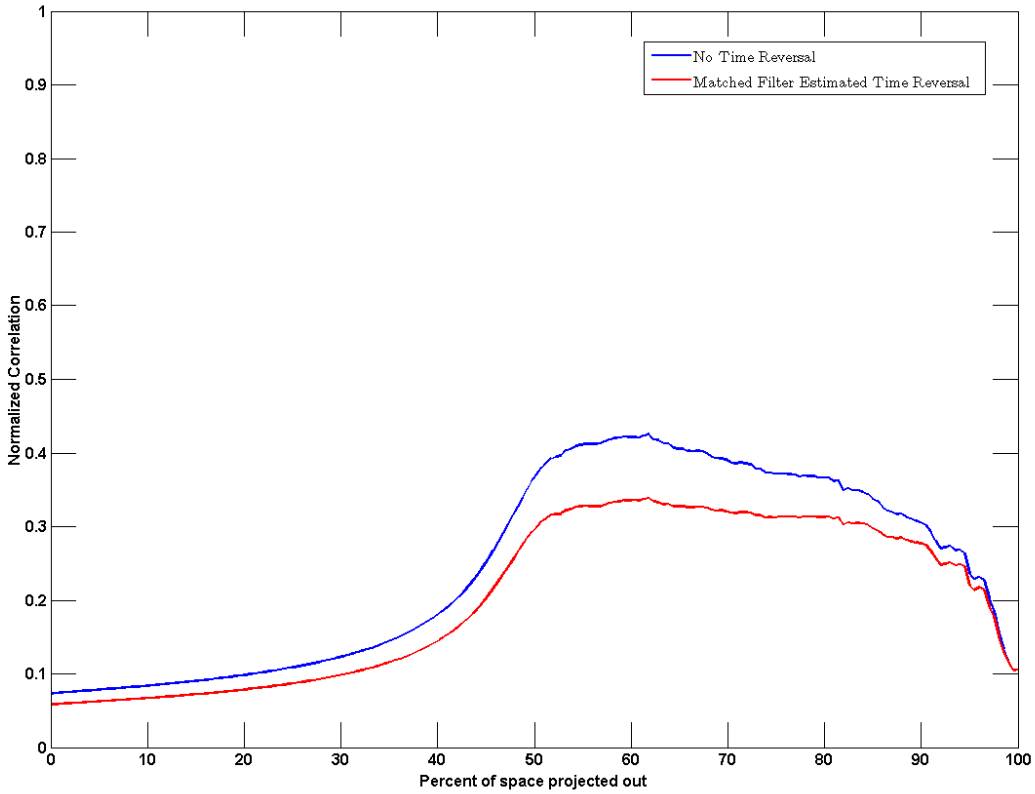


Figure 6.3: Independently located intercept receiver, 20 mulipath elements

is $\mathbf{z}_{\tilde{m}}^H(\ell)\mathbf{z}_{\tilde{m}}(\ell)$ from (6.2) by the idempotent ($\mathbf{PP} = \mathbf{P}$) and Hermitian ( $\mathbf{P}^H = \mathbf{P}$) properties of the projection matrix.

As before, this metric scans over all possible dimensionalities of the dominant subspace and projects away from the hypothesized dominant subspace to perform an energy detection on the residue. In other words, the intercept receiver attempts to determine the subspace dimensionality of the REC symbols, project away the interference, and then detect the hidden signal. This is similar to the interference canceling approach taken by the decorrelating filter for the desired receiver, though the intercept receiver does not have knowledge of the communication symbol and therefore does not benefit from the coherent integration gain.

Note that the intercept receiver still requires some method to determine the presence of a symbol. The energy given in (6.4) does not provide any way to distinguish between a present

symbol and an unusually high clutter/noise residue. Therefore, it is necessary to measure how far above the average residual noise and interference is the residue at time sample $\ell$.

We define

$$\varepsilon_{\text{ir,max}}(\tilde{m}) \doteq \max_{\ell} \{\varepsilon_{\text{ir}}(\tilde{m}, \ell)\} \tag{6.5}$$

as the maximum response over delay $\ell$ for each hypothesized dominant subspace dimensionality $\tilde{m}$. Similarly, the mean response is defined to be

$$\varepsilon_{\text{ir,mean}}(\tilde{m}) \doteq \operatorname*{mean}_{\ell} \{\varepsilon_{\text{ir}}(\tilde{m}, \ell)\} \tag{6.6}$$

over delay $\ell$ for each $\tilde{m}$. A detection statistic can then be formed as the ratio of the maximum value to the mean value for each $\tilde{m}$. The intercept receiver requires a threshold $\mathcal{T}_{\text{ir}}$ to compare the detection statistic:

$$\phi(\tilde{m}) = \frac{\varepsilon_{\text{ir,max}}(\tilde{m})}{\varepsilon_{\text{ir,mean}}(\tilde{m})} \gtrless \mathcal{T}_{\text{ir}}. \tag{6.7}$$

If the intercept receiver is matched in time to a communication symbol, the maximum values of $\varepsilon_{\text{ir}}$ should occur at the correct time sample $\ell$. All other energy residues should correspond to noise and interference. Recall that multipath causes time delayed copies to be superimposed at the receiver, which could increase the mean value of the residue as a function of time. This increase in mean value further increases the LPI nature of the communication system. Simulation analysis of this metric is discussed in Chapter 8.

It is instructive to analyze the expected value of the energy residue

$$E[\varepsilon_{\text{ir}}(\tilde{m}, \ell)] = E[\mathbf{y}^H(\ell)\mathbf{P}_{\tilde{m}}\mathbf{y}(\ell)]. \tag{6.8}$$

Redefining (6.2) as

$$\mathbf{z}_{\tilde{m}}(\ell) \doteq \mathbf{V}_{ND,\tilde{m}}^H \mathbf{y}(\ell), \tag{6.9}$$

and using the definitions of (6.1) and (6.9), the expectation in (6.8) becomes

$$\begin{aligned} E[\varepsilon_{\text{ir}}(\tilde{m},\ell)] &= E[\mathbf{y}^H(\ell)\mathbf{P}_{\tilde{m}}\mathbf{y}(\ell)] \\ &= E\left[\mathbf{z}_{\tilde{m}}^H(\ell)\mathbf{z}_{\tilde{m}}(\ell)\right] \\ &= E\left[\sum_{i=\tilde{m}+1}^{NM} |z_{i,\tilde{m}}(\ell)|^2\right]. \end{aligned} \tag{6.10}$$

If a signal is absent, the Central Limit Theorem can be applied and the individual $|z_{i,\tilde{m}}(\ell)|^2$ components can be decomposed as

$$E\left[|z_{i,\tilde{m}}(\ell)|^2\right] = (\lambda_i\sigma_x^2 + \sigma_u^2)E\left[|\tilde{z}_{i,\tilde{m}}(\ell)|^2\right] \tag{6.11}$$

where $\tilde{z}_{i,\tilde{m}}(\ell) \sim \mathcal{CN}(0,1)$. The magnitude of a complex Gaussian is Rayleigh, and a squared Rayleigh distribution has a $\chi^2$ distribution with 2 degrees of freedom. Recall that $\lambda_i$ is the $i^{th}$ eigenvalue, $\sigma_x^2$ is the clutter power, and $\sigma_u^2$ is the noise power. The details of this decomposition are provided in Chapter 7, specifically using (7.43), (7.44), and the assumption that the noise and interference are uncorrelated.

## 6.3 Alternative LPI Metric II

Upon examination of (6.11), it is noted that it may be advantageous for the intercept receiver to equalize the noise and clutter. If the intercept receiver has knowledge of the clutter and noise power, this equalization can be performed using the augmented eigenvalue matrix:

$$\tilde{\mathbf{\Lambda}}_{ND,\tilde{m}} = \sigma_x^2\mathbf{\Lambda}_{ND,\tilde{m}} + \sigma_u^2\mathbf{I}. \tag{6.12}$$

An additional intercept metric is then given by the energy residue

$$\tilde{\varepsilon_{\text{ir}}}(\tilde{m},\ell) \doteq \mathbf{y}^H(\ell)\tilde{\mathbf{P}}_{\tilde{m}}\mathbf{y}(\ell) \tag{6.13}$$

where

$$\tilde{\mathbf{P}}_{\tilde{m}} = \mathbf{V}_{ND,\tilde{m}} \tilde{\mathbf{\Lambda}}^{-1}_{ND,\tilde{m}} \mathbf{V}^{H}_{ND,\tilde{m}}. \tag{6.14}$$

It is convenient to redefine (6.9), using the decomposition of (6.14), as

$$\bar{\mathbf{z}}_{\tilde{m}}(\ell) = \tilde{\mathbf{\Lambda}}^{-\frac{1}{2}}_{ND,\tilde{m}} \mathbf{V}_{ND,\tilde{m}} \mathbf{y}(\ell). \tag{6.15}$$

Therefore, when the communication symbol is absent, the expected value of this additional intercept metric is

$$\begin{aligned} E\left[\tilde{\varepsilon_{\text{ir}}}(\tilde{m},\ell)\right] &= E\left[\mathbf{y}^{H}(\ell)\tilde{\mathbf{P}}_{\tilde{m}}\mathbf{y}(\ell)\right] \\ &= E\left[\bar{\mathbf{z}}^{H}_{\tilde{m}}(\ell)\bar{\mathbf{z}}_{\tilde{m}}(\ell)\right] \\ &= \sum_{i=\tilde{m}+1}^{NM} |\bar{z}_{i,\tilde{m}}(\ell)|^2 \\ &= \sum_{i=\tilde{m}+1}^{NM} \frac{(\lambda_i\sigma_x^2+\sigma_u^2)|\tilde{z}_{i,\tilde{m}}(\ell)|^2}{(\lambda_i\sigma_x^2+\sigma_u^2)} \\ &= \sum_{i=\tilde{m}+1}^{NM} |\tilde{z}_{i,\tilde{m}}(\ell)|^2 \end{aligned} \tag{6.16}$$

The sum of the $NM-\tilde{m}$ magnitude squared Gaussian random variables is distributed according to a $\chi^2$ distribution with $2(NM-\tilde{m})$ degrees of freedom. This allows the intercept receiver to numerically determine the threshold for its own Neyman-Pearson criterion.

The metric in threshold corresponding to the $\chi^2$ distribution could be tabulated and saved prior to system deployment. Therefore, the intercept receiver would require estimations of the noise and clutter powers to

This new formulation performs the same function as the first revision of the intercept metric (*i.e.* (6.4)). In essence, the second metric is equalized so that the final distribution of the noise and interference is known. However, the thresholds for the $\chi^2$ distribution can be predetermined for given degrees of freedom and levels of $P_{FA}$. However, this metric provides

the intercept receiver additional clairvoyant knowledge. The receiver would be required to estimate the clutter power and noise power. A more thorough analysis of (6.4) is given in Chapter 7. Chapter 8 provides simulation results and discussion of the two alternate intercept metrics.

# Chapter 7

# Theoretical Analysis

This chapter provides a formal analysis of the processing gain afforded by the diagonally loaded decorrelating receiver and the LPI metric given in (6.4). For an effective LPI system, the desired receiver should possess a distinct processing gain advantage over a hypothetical intercept receiver.

## 7.1 Processing Gain Analysis

This section analyzes the processing gain of the decorrelating filter from (5.2). The processing gain $\Delta$ is defined as the ratio of the signal-to-interference-plus-noise ratios at the input to ($SINR_i$) and output of ($SINR_o$) receive processing:

$$\Delta \doteq \frac{SINR_o}{SINR_i}. \tag{7.1}$$

The metric in (7.1) provides a performance metric for the effectiveness of the decorrelating filter. For the sake of brevity, we shall ignore the dependence on time $\ell$ for this analysis. The SINR before processing can be derived by analyzing the quantity $E[||\mathbf{y}||^2] = E[\mathbf{y}^H\mathbf{y}]$.

Recalling (3.12), this expectation can be expanded as

$$E[\mathbf{y}^H\mathbf{y}] = E[(\mathbf{S}\mathbf{x} + \alpha\mathbf{c}_k + \mathbf{u})^H(\mathbf{S}\mathbf{x} + \alpha\mathbf{c}_k + \mathbf{u})]. \tag{7.2}$$

Assuming that the clutter and noise are uncorrelated, all cross-correlation terms are zero and (7.2) becomes

$$E[\mathbf{y}^H\mathbf{y}] = E[\mathbf{x}^H\mathbf{S}^H\mathbf{S}\mathbf{x}] + |\alpha|^2 E[\mathbf{c}_k^H\mathbf{c}_k] + E[\mathbf{u}^H\mathbf{u}]. \tag{7.3}$$

The three expectations in (7.3) correspond to the clutter power, symbol power, and noise power incident at the receiver. These quantities are examined in detail in Sections 7.1.1 and 7.1.2.

The SINR after receive filtering is derived from

$$E[|\mathbf{w}_k^H\mathbf{y}|^2] = E[(\mathbf{w}_k^H\mathbf{y})^H(\mathbf{w}_k^H\mathbf{y})] = E[\mathbf{y}^H\mathbf{w}_k\mathbf{w}_k^H\mathbf{y}]. \tag{7.4}$$

The expansion of (7.4) simplifies after examining the outer product of the filter, $\mathbf{w}_k\mathbf{w}_k^H$. Using (5.2) and the orthonormal nature of eigenvectors (*i.e.* $\mathbf{V}\mathbf{V}^H = \mathbf{I}$),

$$\begin{aligned}
\mathbf{w}_k &= (\mathbf{S}\mathbf{S}^H + \delta\mathbf{I})^{-1}\mathbf{c}_k \\
&= (\mathbf{V}\mathbf{\Lambda}\mathbf{V}^H + \delta\mathbf{I})^{-1}\mathbf{c}_k \\
&= (\mathbf{V}\mathbf{\Lambda}\mathbf{V}^H + \delta\mathbf{V}\mathbf{V}^H)^{-1}\mathbf{c}_k \\
&= (\mathbf{V}[\mathbf{\Lambda} + \delta\mathbf{I}]\mathbf{V}^H)^{-1}\mathbf{c}_k \\
&= \mathbf{V}(\mathbf{\Lambda} + \delta\mathbf{I})^{-1}\mathbf{V}^H\mathbf{c}_k \\
&= \mathbf{V}(\mathbf{\Lambda} + \delta\mathbf{I})^{-1}\mathbf{V}^H\mathbf{V}_{ND}\mathbf{V}_{ND}^H\mathbf{b}_k.
\end{aligned} \tag{7.5}$$

Due to the orthonormal and unitary nature of the eigenvector matrix, and recalling that it is partitioned as $\mathbf{V} = \left[\begin{array}{c|c} \mathbf{V}_D & \mathbf{V}_{ND} \end{array}\right]$, (7.5) becomes

$$\begin{aligned}
\mathbf{w}_k &= \left[\begin{array}{c|c} \mathbf{V}_D & \mathbf{V}_{ND} \end{array}\right] \left[\begin{array}{c|c} (\mathbf{\Lambda}_D + \delta\mathbf{I})^{-1} & \mathbf{0} \\ \hline \mathbf{0} & (\mathbf{\Lambda}_{ND} + \delta\mathbf{I})^{-1} \end{array}\right] \left[\begin{array}{c} \mathbf{0} \\ \hline \mathbf{I} \end{array}\right] \mathbf{V}_{ND}^H \mathbf{b}_k \\
&= \left[\begin{array}{c|c} \mathbf{V}_D(\mathbf{\Lambda}_D + \delta\mathbf{I})^{-1} & \mathbf{0} \\ \hline \mathbf{0} & \mathbf{V}_{ND}(\mathbf{\Lambda}_{ND} + \delta\mathbf{I})^{-1} \end{array}\right] \left[\begin{array}{c} \mathbf{0} \\ \hline \mathbf{I} \end{array}\right] \mathbf{V}_{ND}^H \mathbf{b}_k \\
&= \mathbf{V}_{ND}(\mathbf{\Lambda}_{ND} + \delta\mathbf{I})^{-1} \mathbf{V}_{ND}^H \mathbf{b}_k \qquad (7.6)
\end{aligned}$$

where $\mathbf{0}$ is a matrix of all zeros and $\mathbf{V}^H\mathbf{V}_{ND} = \left[\begin{array}{c} \mathbf{0} \\ \hline \mathbf{I} \end{array}\right]$. However, as $\delta \equiv \lambda_{ND,max}$ (*i.e.*, the largest non-dominant eigenvalue), we can approximate

$$(\mathbf{\Lambda}_{ND} + \delta\mathbf{I}) \approx \delta\mathbf{I}. \qquad (7.7)$$

Combining (7.6) and (7.7) yields

$$\mathbf{w}_k \approx \delta^{-1}\mathbf{V}_{ND}\mathbf{V}_{ND}^H\mathbf{b}_k = \delta^{-1}\mathbf{c}_k. \qquad (7.8)$$

This result leads to the outer product of the filter being equal to the scaled outer product of the communication symbol

$$\mathbf{w}_k\mathbf{w}_k^H = \delta^{-2}\mathbf{c}_k\mathbf{c}_k^H. \qquad (7.9)$$

The expressions for the symbol, clutter, and noise powers after receive filtering are derived from the expected response of the filtered received signal. Using (7.9), the expected magni-

tude squared response of the filtered received signal can be obtained as

$$\begin{aligned} E[|\mathbf{w}_k^H \mathbf{y}|^2] &= E[\mathbf{y}^H \mathbf{w}_k \mathbf{w}_k^H \mathbf{y}] \\ &= \delta^{-2} E[\mathbf{y}^H \mathbf{c}_k \mathbf{c}_k^H \mathbf{y}] \\ &= E[\delta^{-2} (\mathbf{S}\mathbf{x} + \alpha \mathbf{c}_k + \mathbf{u})^H \mathbf{c}_k \mathbf{c}_k^H (\mathbf{S}\mathbf{x} + \alpha \mathbf{c}_k + \mathbf{u})]. \end{aligned} \tag{7.10}$$

Once more, as the noise and clutter are independent from each other, all cross-correlation terms are zero. The resultant filtered, received signal magnitude can be separated into symbol $S_o$, interference $R_o$, and noise $N_o$ terms as

$$E[|\mathbf{w}_k^H \mathbf{y}_r|^2] = S_o + R_o + N_o \tag{7.11}$$

$$S_o = \delta^{-2} |\alpha|^2 \mathbf{c}_k^H \mathbf{c}_k \mathbf{c}_k^H \mathbf{c}_k \tag{7.12}$$

$$R_o = \delta^{-2} E[\mathbf{x}^H \mathbf{S}^H \mathbf{c}_k \mathbf{c}_k^H \mathbf{S}\mathbf{x}] \tag{7.13}$$

$$N_o = \delta^{-2} E[\mathbf{u}^H \mathbf{c}_k \mathbf{c}_k^H \mathbf{u}]. \tag{7.14}$$

Recall that the seed vectors are assumed to be unit norm, so $\mathbf{b}_k^H \mathbf{b}_k = |\mathbf{b}_k|^2 = 1$. The symbol power is examined in Section 7.1.3, while the noise and interference terms are analyzed in Section 7.1.4.

### 7.1.1 Symbol Power Before Processing

Using (3.10) and (3.11), and observing that the symbol is purely deterministic, the symbol power before processing becomes

$$S_i = |\alpha|^2 \mathbf{c}_k^H \mathbf{c}_k = |\alpha|^2 \mathbf{b}_k^H \mathbf{V}_{ND} \mathbf{V}_{ND}^H \mathbf{V}_{ND} \mathbf{V}_{ND}^H \mathbf{b}_k. \tag{7.15}$$

Due to the orthogonal nature of eigenvectors, (7.15) is equivalent to

$$S_i = |\alpha|^2 \mathbf{b}_k^H \mathbf{V}_{ND} \mathbf{I} \mathbf{V}_{ND}^H \mathbf{b}_k = |\alpha|^2 \mathbf{b}_k^H \mathbf{V}_{ND} \mathbf{V}_{ND}^H \mathbf{b}_k. \tag{7.16}$$

For convenience, define

$$\gamma \triangleq \mathbf{V}^H \mathbf{b}_k. \tag{7.17}$$

Because an eigenvector matrix is composed of orthonormal vectors (*i.e.* it is a unitary matrix) and using the assumption that $\mathbf{b}_k$ is unit norm, it is easy to show that $|\gamma|^2 = |\mathbf{b}_k|^2 = 1$. Due to the pseudo-random nature of the seed vectors, the average magnitude of each element is

$$\begin{aligned} |\gamma_{avg}|^2 &= \frac{1}{NM} \gamma^H \gamma \\ &= \frac{1}{NM} \mathbf{b}_k^H \mathbf{V} \mathbf{V}^H \mathbf{b}_k \\ &= \frac{1}{NM} \mathbf{b}_k^H \mathbf{I} \mathbf{b}_k \\ &= \frac{1}{NM}. \end{aligned} \tag{7.18}$$

As shown in (3.9), the eigenspace can be partitioned into dominant and non-dominant subspaces. Similarly, $\gamma$ can be partitioned as

$$\gamma = \left[ \frac{\gamma_D}{\gamma_{ND}} \right] = \left[ \frac{\mathbf{V}_D^H \mathbf{b}_k}{\mathbf{V}_{ND}^H \mathbf{b}_k} \right]. \tag{7.19}$$

Using (7.18) and (7.19),

$$\begin{aligned} \gamma^H \gamma &= \left[ \begin{array}{c|c} \gamma_D^H & \gamma_{ND}^H \end{array} \right] \left[ \frac{\gamma_D}{\gamma_{ND}} \right] \\ &= \gamma_D^H \gamma_D + \gamma_{ND}^H \gamma_{ND} \\ &\cong (m) |\gamma_{avg}|^2 + (NM - m) |\gamma_{avg}|^2. \end{aligned} \tag{7.20}$$

Substituting the results for the non-dominant portion of $\gamma$ from (7.20) into (7.16), $S_i$ reduces to

$$S_i = |\alpha|^2 \mathbf{b}_k^H \mathbf{V}_{ND} \mathbf{V}_{ND}^H \mathbf{b}_k = |\alpha|^2 \gamma_{ND}^H \gamma_{ND} \cong \frac{|\alpha|^2 (NM - m)}{NM}. \tag{7.21}$$

### 7.1.2 Interference and Noise Power Before Processing

Using (7.3) and assuming all samples of the clutter are i.i.d., the interference power before processing is

$$\begin{aligned} R_i &= E[\mathbf{x}^H \mathbf{S}^H \mathbf{S} \mathbf{x}] \\ &= E[tr\{\mathbf{S} \mathbf{x} \mathbf{x}^H \mathbf{S}^H\}] \\ &= tr\{\mathbf{S} E[\mathbf{x} \mathbf{x}^H] \mathbf{S}^H\} \\ &= \sigma_x^2 tr\{\mathbf{S} \mathbf{S}^H\}. \end{aligned} \tag{7.22}$$

It is interesting to note that $tr\{\mathbf{S}\mathbf{S}^H\} = tr\{\mathbf{V}\mathbf{\Lambda}\mathbf{V}^H\} = tr\{\mathbf{\Lambda}\}$ due to the orthonormal nature of the eigenvector matrix (*i.e.*, $\mathbf{V}^H\mathbf{V} = \mathbf{I} \Rightarrow \mathbf{V}^H = \mathbf{V}^{-1}$) and the commutative property of the trace operation. Therefore, the interference power is given as

$$R_i = \sigma_x^2 tr\{\mathbf{\Lambda}\}. \tag{7.23}$$

Assuming the radar waveform is constant modulus and $||\mathbf{s}||^2 = 1$, it is found that $tr\{\mathbf{S}\mathbf{S}^H\} = NM$. In this case, the interference power is

$$R_i = \sigma_x^2 tr\{\mathbf{\Lambda}\} = \sigma_x^2 NM. \tag{7.24}$$

Assuming that the noise is additive white Gaussian, the noise power before receive filtering is given as

$$N_i = E[\mathbf{u}^H \mathbf{u}] = \sigma_u^2 NM. \tag{7.25}$$

### 7.1.3 Symbol Power After Processing

Using (7.21) and (7.12), the symbol power after receive filtering becomes

$$\begin{aligned} S_o &= \delta^{-2}|\alpha|^2 \mathbf{c}_k^H \mathbf{c}_k \mathbf{c}_k^H \mathbf{c}_k \\ &= \delta^{-2}|\alpha|^2 \frac{NM-m}{NM} \frac{NM-m}{NM} \\ &= \frac{|\alpha|^2 (NM-m)^2}{(\delta NM)^2}. \end{aligned} \tag{7.26}$$

### 7.1.4 Interference and Noise Power After Processing

Using (7.13) and the identity $E[\mathbf{a}^H\mathbf{a}] = E[tr\{\mathbf{a}\mathbf{a}^H\}]$ for $\mathbf{a}$ some arbitrary vector, the interference power after receive filtering can be given as

$$\begin{aligned} R_o &= \delta^{-2} E[\mathbf{x}^H \mathbf{S}^H \mathbf{c}_k \mathbf{c}_k^H \mathbf{S}\mathbf{x}] \\ &= \delta^{-2} E[tr\{\mathbf{c}_k^H \mathbf{S}\mathbf{x}\mathbf{x}^H \mathbf{S}^H \mathbf{c}_k\}] \\ &= \delta^{-2} tr\{\mathbf{c}_k^H \mathbf{S} E[\mathbf{x}\mathbf{x}^H] \mathbf{S}^H \mathbf{c}_k\} \\ &= \delta^{-2} \sigma_x^2 tr\{\mathbf{c}_k^H \mathbf{S}\mathbf{S}^H \mathbf{c}_k\} \\ &= \delta^{-2} \sigma_x^2 tr\{\mathbf{b}_k^H \mathbf{V}_{ND} \mathbf{V}_{ND}^H \mathbf{V} \mathbf{\Lambda} \mathbf{V}^H \mathbf{V}_{ND} \mathbf{V}_{ND}^H \mathbf{b}_k\}. \end{aligned} \tag{7.27}$$

Note that $\mathbf{V}_{ND}^H \mathbf{V} \mathbf{\Lambda} \mathbf{V}^H \mathbf{V}_{ND}$ simplifies to

$$\begin{aligned}
\mathbf{V}_{ND}^H \mathbf{V} \mathbf{\Lambda} \mathbf{V}^H \mathbf{V}_{ND} &= \mathbf{V}_{ND}^H \left[\begin{array}{c|c} \mathbf{V}_D & \mathbf{V}_{ND} \end{array}\right] \left[\begin{array}{c|c} \mathbf{\Lambda}_D & \mathbf{0} \\ \hline \mathbf{0} & \mathbf{\Lambda}_{ND} \end{array}\right] \left[\begin{array}{c} \mathbf{V}_D^H \\ \hline \mathbf{V}_{ND}^H \end{array}\right] \mathbf{V}_{ND} \\
&= \left[\begin{array}{c|c} \mathbf{0} & \mathbf{I} \end{array}\right] \left[\begin{array}{c|c} \mathbf{\Lambda}_D & \mathbf{0} \\ \hline \mathbf{0} & \mathbf{\Lambda}_{ND} \end{array}\right] \left[\begin{array}{c} \mathbf{0} \\ \hline \mathbf{I} \end{array}\right] \\
&= \left[\begin{array}{c|c} \mathbf{0} & \mathbf{\Lambda}_{ND} \end{array}\right] \left[\begin{array}{c} \mathbf{0} \\ \hline \mathbf{I} \end{array}\right] \\
&= \mathbf{\Lambda}_{ND}. \qquad (7.28)
\end{aligned}$$

Substituting (7.17), (7.18), and (7.28) into (7.27), the interference power is shown to be equivalent to

$$\begin{aligned}
R_o &= \delta^{-2} \sigma_x^2 tr\{\mathbf{b}_k^H \mathbf{V}_{ND} \mathbf{V}_{ND}^H \mathbf{V} \mathbf{\Lambda} \mathbf{V}^H \mathbf{V}_{ND} \mathbf{V}_{ND}^H \mathbf{b}_k\} \\
&= \delta^{-2} \sigma_x^2 tr\{\gamma_{ND}^H \mathbf{\Lambda}_{ND} \gamma_{ND}\} \\
&\cong \delta^{-2} \sigma_x^2 tr\{\mathbf{\Lambda}_{ND}\} \frac{1}{NM} \\
&= \frac{\sigma_x^2 tr\{\mathbf{\Lambda}_{ND}\}}{\delta^2 NM}. \qquad (7.29)
\end{aligned}$$

The residual noise power after receive filtering as given in (7.14) can be simplified using the uncorrelated nature of additive white Gaussian noise and (7.17) and (7.18) as

$$
\begin{aligned}
N_o &= \delta^{-2} E[\mathbf{u}^H \mathbf{c}_k \mathbf{c}_k^H \mathbf{u}] \\
&= \delta^{-2} E[tr\{\mathbf{c}_k^H \mathbf{u}\mathbf{u}^H \mathbf{c}_k\}] \\
&= \delta^{-2} tr\{\mathbf{c}_k^H E[\mathbf{u}\mathbf{u}^H] \mathbf{c}_k\} \\
&= \delta^{-2} \sigma_u^2 tr\{\mathbf{c}_k^H \mathbf{c}_k\} \\
&= \delta^{-2} \sigma_u^2 \mathbf{b}_k^H \mathbf{V}_{ND} \mathbf{V}_{ND}^H \mathbf{V}_{ND} \mathbf{V}_{ND}^H \mathbf{b}_k \\
&= \delta^{-2} \sigma_u^2 \gamma_{ND}^H \gamma_{ND} \\
&\cong \frac{\sigma_u^2 (NM - m)}{\delta^2 NM}
\end{aligned} \tag{7.30}
$$

where $\sigma_u^2$ is the noise power.

### 7.1.5 SINR and Processing Gain

For an arbitrary radar waveform and using (7.21), (7.23), and (7.25), the SINR before receive processing is

$$
SINR_i = \frac{S_i}{R_i + N_i} = \frac{|\alpha|^2 (NM - m)}{(NM)(\sigma_x^2 tr\{\mathbf{\Lambda}\} + \sigma_u^2 (NM))}. \tag{7.31}
$$

Using (7.26), (7.29), and (7.30), the SINR after receive processing with the decorrelating filter from (5.2) is

$$
\begin{aligned}
SINR_o &= \frac{S_o}{R_o + N_o} \\
&= \frac{|\alpha|^2 \delta^2 (NM - m)^2 NM}{\delta^2 (NM)^2 (\sigma_x^2 tr\{\mathbf{\Lambda}_{ND}\} + \sigma_u^2 (NM - m))} \\
&= \frac{|\alpha|^2 (NM - m)^2}{NM(\sigma_x^2 tr\{\mathbf{\Lambda}_{ND}\} + \sigma_u^2 (NM - m))}.
\end{aligned} \tag{7.32}
$$

Using the definition for processing gain given in (7.1), and substituting in (7.31) and (7.32), the processing gain paramaterized by the dominant subspace dimensionality $m$ is

$$\Delta(m) = \frac{SINR_o}{SINR_i} = \frac{(NM-m)(\sigma_x^2 \text{tr}\left\{\mathbf{\Lambda}\right\} + \sigma_u^2 NM)}{\sigma_x^2 \text{tr}\left\{\mathbf{\Lambda}_{ND}\right\} + \sigma_u^2(NM-m)}. \tag{7.33}$$

If the radar waveform is constant modulus, (7.33) simplifies to

$$\Delta(m) = \frac{(NM)(NM-m)(\sigma_x^2+\sigma_u^2)}{\sigma_x^2 \text{tr}\{\mathbf{\Lambda}_{ND}\} + \sigma_u^2(NM-m)}. \tag{7.34}$$

Notice that with $\lambda_{m+1}$ the largest non-dominant eigenvalue,

$$\text{tr}\{\mathbf{\Lambda}_{ND}\} \leq \lambda_{m+1}(NM-m). \tag{7.35}$$

Using (7.35) in (7.34) results in a lower bound of

$$\Delta(m) \geq NM \frac{\sigma_x^2+\sigma_u^2}{\sigma_x^2\lambda_{m+1}+\sigma_u^2}. \tag{7.36}$$

This bound proves useful in visualizing the behavior of processing gain as a function of the noise and interference. If $\sigma_u^2 \gg \sigma_x^2$ (*i.e.* the noise power is much greater than the clutter power), then (7.36) results in $\Delta(m) \approx NM$. This is the expected gain from coherently integrating the symbol energy. However, if $\sigma_x^2 \gg \sigma_u^2$ (*i.e.* the clutter power is much greater than the noise power), then (7.36) simplifies to $\Delta(m) \approx NM\lambda_{m+1}^{-1}$. It can be observed that the majority of the clutter power is concentrated in the first $N$ eigenvalues, as shown in Figure 3.3. Therefore, assuming that $m > N$, the eigenvalues in the non-dominant space are typically small. When optimizing (7.36) over values of $m$, it may be assumed that $\lambda_{m+1} \ll 1$. This inequality is due to the redundancy caused by oversampling the radar waveform. Small values of $\lambda_{m+1}$ ensure the processing gain becomes much greater than the coherent integration gain ($NM$). These concepts are explored in detail in Chapter 8.

## 7.2 SINR at the Intercept Receiver

In order to analyze the processing gain of the LPI metric in (6.4), the SINR at the intercept receiver after processing must be derived. Expanding (6.4) yields

$$\varepsilon_{\text{ir}}(\tilde{m}) = E[(\mathbf{S}\mathbf{x} + \alpha\mathbf{c}_k + \mathbf{u})^H \mathbf{P}_{\tilde{m}}(\mathbf{S}\mathbf{x} + \alpha\mathbf{c}_k + \mathbf{u})]. \tag{7.37}$$

Due to the uncorrelated nature of the noise and interference, all cross-correlation terms go to zero. Therefore,

$$\begin{aligned}\varepsilon_{\text{ir}}(\tilde{m}) &= E[\mathbf{x}^H\mathbf{S}^H\mathbf{P}_{\tilde{m}}\mathbf{S}\mathbf{x}] + |\alpha|^2\mathbf{c}_k^H\mathbf{P}_{\tilde{m}}\mathbf{c}_k + E[\mathbf{u}^H\mathbf{P}_{\tilde{m}}\mathbf{u}] \\ &= S_{\text{ir}} + R_{\text{ir}} + N_{\text{ir}}\end{aligned} \tag{7.38}$$

where the signal term $S_{\text{ir}}$, interference term $R_{\text{ir}}$, and noise term $N_{\text{ir}}$ of the received signal are given by

$$S_{\text{ir}} = |\alpha|^2\mathbf{c}_k^H\mathbf{P}_{\tilde{m}}\mathbf{c}_k \tag{7.39}$$

$$R_{\text{ir}} = E[\mathbf{x}^H\mathbf{S}^H\mathbf{P}_{\tilde{m}}\mathbf{S}\mathbf{x}] \tag{7.40}$$

$$N_{\text{ir}} = E[\mathbf{u}^H\mathbf{P}_{\tilde{m}}\mathbf{u}]. \tag{7.41}$$

The SINR at the intercept receiver is then

$$\text{SINR}_{\text{ir}} = \frac{S_{\text{ir}}}{R_{\text{ir}} + N_{\text{ir}}} \tag{7.42}$$

Using (6.1), $R_{\text{ir}}$ in (7.42) can be simplified as

$$\begin{aligned}
R_{\text{ir}} &= E[\mathbf{x}^H\mathbf{S}^H\mathbf{P}_{\tilde{m}}\mathbf{S}\mathbf{x}] \\
&= E[\mathbf{x}^H\mathbf{S}^H\tilde{\mathbf{V}}_{ND,\tilde{m}}\tilde{\mathbf{V}}_{ND,\tilde{m}}^H\mathbf{S}\mathbf{x}] \\
&= E[\text{tr}\left\{\tilde{\mathbf{V}}_{ND,\tilde{m}}^H\mathbf{S}\mathbf{x}\mathbf{x}^H\mathbf{S}^H\tilde{\mathbf{V}}_{ND,\tilde{m}}\right\}] \\
&= \sigma_x^2\text{tr}\left\{\tilde{\mathbf{V}}_{ND,\tilde{m}}^H\mathbf{V}\mathbf{\Lambda}\mathbf{V}^H\tilde{\mathbf{V}}_{ND,\tilde{m}}\right\} \\
&= \sigma_x^2\text{tr}\left\{\tilde{\mathbf{V}}_{ND,\tilde{m}}^H\left[\begin{array}{c|c} \mathbf{V}_{D,\tilde{m}} & \mathbf{V}_{ND,\tilde{m}} \end{array}\right]\left[\begin{array}{c|c} \mathbf{\Lambda}_{D,\tilde{m}} & \mathbf{0} \\ \hline \mathbf{0} & \mathbf{\Lambda}_{ND,\tilde{m}} \end{array}\right]\left[\begin{array}{c} \mathbf{V}_{D,\tilde{m}}^H \\ \hline \mathbf{V}_{ND,\tilde{m}}^H \end{array}\right]\mathbf{V}_{ND,\tilde{m}}\right\} \\
&= \sigma_x^2\text{tr}\left\{\left[\begin{array}{c|c} \mathbf{0} & \mathbf{I} \end{array}\right]\left[\begin{array}{c|c} \mathbf{\Lambda}_{D,\tilde{m}} & \mathbf{0} \\ \hline \mathbf{0} & \mathbf{\Lambda}_{ND,\tilde{m}} \end{array}\right]\left[\begin{array}{c} \mathbf{0} \\ \hline \mathbf{I} \end{array}\right]\right\} \\
&= \sigma_x^2\text{tr}\left\{\mathbf{\Lambda}_{ND,\tilde{m}}\right\}. \qquad (7.43)
\end{aligned}$$

Similarly, the noise at the intercept receiver can be decomposed as

$$\begin{aligned}
N_{\text{ir}} &= E\left[\mathbf{u}^H\mathbf{P}_{\tilde{m}}\mathbf{u}\right] \\
&= E\left[\mathbf{u}^H\tilde{\mathbf{V}}_{ND,\tilde{m}}\tilde{\mathbf{V}}_{ND,\tilde{m}}^H\mathbf{u}\right] \\
&= E\left[\text{tr}\left\{\tilde{\mathbf{V}}_{ND,\tilde{m}}^H\mathbf{u}\mathbf{u}^H\tilde{\mathbf{V}}_{ND,\tilde{m}}\right\}\right] \\
&= \sigma_u^2\text{tr}\left\{\tilde{\mathbf{V}}_{ND,\tilde{m}}^H\tilde{\mathbf{V}}_{ND,\tilde{m}}\right\} \\
&= \sigma_u^2(NM-\tilde{m}). \qquad (7.44)
\end{aligned}$$

Using (7.43) and (7.44) in (7.42), the SINR at the intercept receiver becomes

$$\text{SINR}_{\text{ir}} = \frac{|\alpha|^2\mathbf{c}_k^H\mathbf{P}_{\tilde{m}}\mathbf{c}_k}{\sigma_x^2\text{tr}\left\{\mathbf{\Lambda}_{ND,\tilde{m}}\right\}+\sigma_u^2(NM-\tilde{m})}. \qquad (7.45)$$

Recall that the intercept receiver does not have knowledge of the true dimensionality of the dominant subspace. Therefore, all possible values of $\tilde{m}$ must be considered by the

intercept receiver. If $\tilde{m} \leq m$, then $m-\tilde{m}$ eigenvectors will be added to the true non-dominant subspace. Let the $NM \times (m - \tilde{m})$ matrix of extra eigenvectors be given as

$$\mathbf{V}_r = \left[ \begin{array}{cccc} \mathbf{v}_{D,\tilde{m}} & \mathbf{v}_{D,\tilde{m}+1} & \dots & \mathbf{v}_{D,m} \end{array} \right] \tag{7.46}$$

where $\mathbf{v}_{D,m}$ is the eigenvector corresponding to smallest eigenvalue in the dominant subspace. Note that in the case of $\tilde{m} = m$, $\mathbf{V}_r$ is simply an empty matrix. Therefore, the hypothesized non-dominant subspace can be expressed as

$$\mathbf{V}_{ND,\tilde{m}} = \left[ \begin{array}{c|c} \mathbf{V}_r & \mathbf{V}_{ND} \end{array} \right]. \tag{7.47}$$

Using (3.10), (3.11), and (7.47) in (7.39), and recalling the orthonormal nature of eigenvectors, the signal power incident on the intercept receiver when $\tilde{m} \leq m$ becomes

$$\begin{aligned} S_{\text{ir}} &= |\alpha|^2 \mathbf{b}_k^H \mathbf{V}_{ND,m} \mathbf{V}_{ND,m}^H \mathbf{V}_{ND,\tilde{m}} \mathbf{V}_{ND,\tilde{m}}^H \mathbf{V}_{ND,m} \mathbf{V}_{ND,m}^H \mathbf{b}_k \\ &= |\alpha|^2 \mathbf{b}_k^H \mathbf{V}_{ND,m} \mathbf{V}_{ND,m}^H \left[ \begin{array}{c|c} \mathbf{V}_r & \mathbf{V}_{ND,m} \end{array} \right] \left[ \begin{array}{c} \mathbf{V}_r^H \\ \hline \mathbf{V}_{ND,m}^H \end{array} \right] \mathbf{V}_{ND,m} \mathbf{V}_{ND,m}^H \mathbf{b}_k \\ &= |\alpha|^2 \mathbf{b}_k^H \mathbf{V}_{ND,m} \left[ \begin{array}{c|c} \mathbf{0} & \mathbf{I} \end{array} \right] \left[ \begin{array}{c} \mathbf{0} \\ \hline \mathbf{I} \end{array} \right] \mathbf{V}_{ND,m}^H \mathbf{b}_k \\ &= |\alpha|^2 \mathbf{b}_k^H \mathbf{V}_{ND,m} \mathbf{V}_{ND,m}^H \mathbf{b}_k \\ &= |\alpha|^2 \gamma_{ND}^H \gamma_{ND}. \end{aligned} \tag{7.48}$$

From (7.21) and (7.48), the symbol power at the intercept receiver when the hypothesized dominant subspace is less than or equal to the true dominant subspace is

$$S_{\text{ir}} \cong \frac{|\alpha|^2 (NM - m)}{NM}. \tag{7.49}$$

It is interesting to note that the symbol power is not affected by underestimating the size

of the dominant subspace. Only the size of the dominant subspace chosen by the radar-embedded communication (REC) system has any effect on the symbol power at the intercept receiver.

Now consider the case where $\tilde{m} > m$. Here it is convenient to define the $NM \times (\tilde{m} - m)$ matrix

$$\mathbf{V}_p \doteq \left[ \begin{array}{cccc} \mathbf{v}_{ND,m+1} & \mathbf{v}_{ND,m+2} & \cdots & \mathbf{v}_{ND,\tilde{m}} \end{array} \right] \tag{7.50}$$

which can be used to partition the true non-dominant subspace as

$$\mathbf{V}_{ND,m} = \left[ \begin{array}{c|c} \mathbf{V}_P & \mathbf{V}_{ND,\tilde{m}} \end{array} \right]. \tag{7.51}$$

Notice that

$$\begin{aligned} S_{\text{ir}} &= |\alpha|^2 \mathbf{b}_k^H \mathbf{V}_{ND,m} \mathbf{V}_{ND,m}^H \mathbf{V}_{ND,\tilde{m}} \mathbf{V}_{ND,\tilde{m}}^H \mathbf{V}_{ND,m} \mathbf{V}_{ND,m}^H \mathbf{b}_k \\ &= |\alpha|^2 \mathbf{b}_k^H \mathbf{P} \mathbf{P}_{\tilde{m}} \mathbf{P} \mathbf{b}_k. \end{aligned} \tag{7.52}$$

Examining the quantity $\mathbf{P}\mathbf{P}_{\tilde{m}}\mathbf{P}$, and using (7.51),

$$\begin{aligned} \mathbf{P}\mathbf{P}_{\tilde{m}}\mathbf{P} &= \left[ \begin{array}{c|c} \mathbf{V}_P & \mathbf{V}_{ND,\tilde{m}} \end{array} \right] \left[ \begin{array}{c} \mathbf{V}_P^H \\ \hline \mathbf{V}_{ND,\tilde{m}}^H \end{array} \right] \mathbf{V}_{ND,\tilde{m}} \mathbf{V}_{ND,\tilde{m}}^H \left[ \begin{array}{c|c} \mathbf{V}_P & \mathbf{V}_{ND,\tilde{m}} \end{array} \right] \left[ \begin{array}{c} \mathbf{V}_P^H \\ \hline \mathbf{V}_{ND,\tilde{m}}^H \end{array} \right] \\ &= \left[ \begin{array}{c|c} \mathbf{V}_P & \mathbf{V}_{ND,\tilde{m}} \end{array} \right] \left[ \begin{array}{c} \mathbf{0} \\ \hline \mathbf{I} \end{array} \right] \left[ \begin{array}{c|c} \mathbf{0} & \mathbf{I} \end{array} \right] \left[ \begin{array}{c} \mathbf{V}_P^H \\ \hline \mathbf{V}_{ND,\tilde{m}}^H \end{array} \right] \\ &= \mathbf{V}_{ND,\tilde{m}} \mathbf{V}_{ND,\tilde{m}}^H. \end{aligned} \tag{7.53}$$

Substituting (7.53) into (7.52), and recalling that eigenvectors preserve the length of the unit normed seed vectors $\mathbf{b}_k$, the signal power at the intercept receiver when the size of the

dominant subspace is *overestimated* is

$$\begin{aligned} S_{\text{ir}} &= |\alpha|^2 \mathbf{b}_k^H \mathbf{V}_{ND,\tilde{m}} \mathbf{V}_{ND,\tilde{m}}^H \mathbf{b}_k \\ &= |\alpha|^2 \gamma_{ND,\tilde{m}}^H \gamma_{ND,\tilde{m}} \\ &\cong |\alpha|^2 \frac{NM - \tilde{m}}{NM}. \end{aligned} \tag{7.54}$$

Using the results of (7.49) and (7.54), it becomes apparent that the signal power at the intercept receiver is expressed as

$$S_{\text{ir}} = |\alpha|^2 \frac{NM - \max(m, \tilde{m})}{NM}. \tag{7.55}$$

Using (7.55) in (7.45), the SINR at the intercept receiver is then

$$\text{SINR}_{\text{ir}} = \frac{|\alpha|^2 (NM - \max(m, \tilde{m}))}{(NM)\left(\sigma_x^2 \text{tr}\left\{\mathbf{\Lambda}_{ND,\tilde{m}}\right\} + \sigma_u^2 (NM - \tilde{m})\right)}. \tag{7.56}$$

## 7.3 Analysis of the LPI Metric

Recall that the SINR before processing was derived in Section 7.1, yielding the expression in (7.31). Therefore, we define the processing gain of the intercept receiver as

$$\Delta_{\text{ir}} \doteq \frac{SINR_{\text{ir}}}{SINR_{\text{i}}}. \tag{7.57}$$

This processing gain can be simplified as

$$\begin{aligned} \Delta_{\text{ir}} &= \frac{|\alpha|^2 (NM - \max(m, \tilde{m}))}{(NM)\left(\sigma_x^2 \text{tr}\left\{\mathbf{\Lambda}_{ND,\tilde{m}}\right\} + \sigma_u^2 (NM - \tilde{m})\right)} \frac{NM\left(\sigma_x^2 \text{tr}\left\{\mathbf{\Lambda}\right\} + NM\sigma_u^2\right)}{|\alpha|^2 (NM - m)} \\ &= \frac{(NM - \max(m, \tilde{m}))(\sigma_x^2 \text{tr}\left\{\mathbf{\Lambda}\right\} + NM\sigma_u^2)}{(NM - m)\left(\sigma_x^2 \text{tr}\left\{\mathbf{\Lambda}_{ND,\tilde{m}}\right\} + \sigma_u^2 (NM - \tilde{m})\right)}. \end{aligned} \tag{7.58}$$

Consider the ratio of the processing gains afforded by the diagonally loaded decorrelating receiver and the new intercept receiver, defined as

$$\Psi(m,\tilde{m}) \doteq \frac{\Delta}{\Delta_{\text{ir}}}. \tag{7.59}$$

This definition provides a criterion with which to optimize the "gain advantage" via a Maxi-Min approach. Using (7.33) and (7.58), this gain advantage can be expressed as

$$\begin{aligned}\Psi(m,\tilde{m}) &= \frac{\Delta}{\Delta_{\text{ir}}} \\ &= \frac{(NM-m)(\sigma_x^2\text{tr}\left\{\mathbf{\Lambda}\right\}+\sigma_u^2 NM)}{\sigma_x^2\text{tr}\left\{\mathbf{\Lambda}_{ND,m}\right\}+\sigma_u^2(NM-m)}\frac{(NM-m)\left(\sigma_x^2\text{tr}\left\{\mathbf{\Lambda}_{ND,\tilde{m}}\right\}+\sigma_u^2(NM-\tilde{m})\right)}{(NM-\max(m,\tilde{m}))(\sigma_x^2\text{tr}\left\{\mathbf{\Lambda}\right\}+NM\sigma_u^2)} \\ &= \frac{(NM-m)^2(\sigma_x^2\text{tr}\left\{\mathbf{\Lambda}_{ND,\tilde{m}}\right\}+\sigma_u^2(NM-\tilde{m}))}{(NM-\max(m,\tilde{m}))(\sigma_x^2\text{tr}\left\{\mathbf{\Lambda}_{ND,m}\right\}+\sigma_u^2(NM-m))}.\end{aligned} \tag{7.60}$$

The gain advantage of the decorrelating receiver can be divided into three different cases.

**Case 1: Intercept Receiver Underestimates Size of Dominant Subspace**

If the size of the dominant subspace is underestimated, then $m > \tilde{m}$. For this case, (7.60) reduces to

$$\Psi(m,\tilde{m}) = \frac{(NM-m)(\sigma_x^2\text{tr}\left\{\mathbf{\Lambda}_{ND,\tilde{m}}\right\}+\sigma_u^2(NM-\tilde{m}))}{\sigma_x^2\text{tr}\left\{\mathbf{\Lambda}_{ND}\right\}+\sigma_u^2(NM-m)}. \tag{7.61}$$

Notice that for $m > \tilde{m}$, $\text{tr}\left\{\mathbf{\Lambda}_{ND,\tilde{m}}\right\} > \text{tr}\left\{\mathbf{\Lambda}_{ND}\right\}$ and $(NM-\tilde{m}) > (NM-m)$. It is clear that

$$\frac{\sigma_x^2\text{tr}\left\{\mathbf{\Lambda}_{ND,\tilde{m}}\right\}+\sigma_u^2(NM-\tilde{m})}{\sigma_x^2\text{tr}\left\{\mathbf{\Lambda}_{ND}\right\}+\sigma_u^2(NM-m)} > 1 \tag{7.62}$$

so $\Psi(m,\tilde{m}) > (NM-m)$. Therefore, when the intercept receiver underestimates the size of the dominant subspace, the desired receiver always has a gain advantage.

**Case 2: Intercept Receiver Matches Size of Dominant Subspace**

If the size of the dominant subspace is estimated correctly, then $m = \tilde{m}$. For this case,

(7.60) reduces to

$$\begin{aligned}\Psi(m,\tilde{m}) &= \frac{(NM-m)(\sigma_x^2 \mathrm{tr}\left\{\mathbf{\Lambda}_{ND,m}\right\} + \sigma_u^2(NM-m))}{\sigma_x^2 \mathrm{tr}\left\{\mathbf{\Lambda}_{ND,m}\right\} + \sigma_u^2(NM-m)} \\ &= NM - m. \end{aligned} \tag{7.63}$$

In this case, the desired receiver once more has a clear advantage.

**Case 3: Intercept Receiver Overestimates Size of Dominant Subspace**

If the size of the dominant subspace is overestimated, then $m < \tilde{m}$. For this case, (7.60) reduces to

$$\Psi(m,\tilde{m}) = \frac{(NM-m)^2(\sigma_x^2 \mathrm{tr}\left\{\mathbf{\Lambda}_{ND,\tilde{m}}\right\} + \sigma_u^2(NM-\tilde{m}))}{(NM-\tilde{m})(\sigma_x^2 \mathrm{tr}\left\{\mathbf{\Lambda}_{ND,m}\right\} + \sigma_u^2(NM-m))}. \tag{7.64}$$

Unfortunately, when $m < \tilde{m}$ the two portions of (7.64) provide conflicting results. Clearly,

$$\frac{(NM-m)^2}{NM-\tilde{m}} > 1. \tag{7.65}$$

However, $\mathrm{tr}\left\{\mathbf{\Lambda}_{ND,\tilde{m}}\right\} < \mathrm{tr}\left\{\mathbf{\Lambda}_{ND}\right\}$ and $(NM-\tilde{m}) < (NM-m)$. Therefore,

$$\frac{\sigma_x^2 \mathrm{tr}\left\{\mathbf{\Lambda}_{ND,\tilde{m}}\right\} + \sigma_u^2(NM-\tilde{m})}{\sigma_x^2 \mathrm{tr}\left\{\mathbf{\Lambda}_{ND}\right\} + \sigma_u^2(NM-m)} < 1. \tag{7.66}$$

Recall that the fundamental problem in the REC framework is to maximize the performance of the desired receivers and to minimize the performance of any intercept receiver. Therefore, optimizing (7.59) is a maxi-min problem. Formally, the optimization is given as

$$\max_{m} \min_{\tilde{m}} \Psi(m,\tilde{m}) \tag{7.67}$$

under the constraint $NM - m \geq K$. Fortunately, the search space for optimization is of dimension $(NM)(NM-K)$. Recall that $M$ is constrained to be small, to maintain the LPI nature of the system. Also, the optimization does not need to be performed in real time. Therefore, this function can be optimized through a brute force search. Results of this brute

force search are shown in Chapter 8.

# Chapter 8

# Simulation Results

## 8.1 High Fidelity Modeling

For the purpose of this thesis, the simulation setup used in previous work was modified to include a more realistic scenario. The only exception occurs in Section 4.4, and the differences are explained there. First, all processing undertaken by the radar, tag, or intercept receiver employ an oversampling rate of $M = 2$. This sampling rate is twice that required by the Nyquist criterion. However, in a real system, the radar waveform and communication symbol pass through a continuous channel. To simulate continuous time, all signals entering the channel (*e.g.* communication symbol transmitted from the tag, radar waveform transmitted from the radar system) are upsampled to a rate 14 times Nyquist. All channel phenomenon, such as multipath, interference, and additive noise operations are simulated at this higher sampling rate. The AWGN is filtered at this sampling rate to bandlimit it to the same bandwidth as the signal.

All SNR, signal-to-interference (SIR), and signal-to-interference-plus-noise (SINR) calculations are obtained at the higher sampling rate. Unless otherwise noted, the interference-to-noise ratio (INR) is 30 dB. The clutter (interference) was modeled as a Gaussian random process for all simulations.

All signals incident on a receiver (*e.g.* communication waveform impinging on radar receiver, radar waveform incident on tag) are low pass filtered and downsampled to the discrete sampling rate. The transmitted radar waveform used in all simulations is an LFM radar waveform [35] with a time-bandwidth product of $N = 100$. In all simulations, there are $K = 16$ possible communication symbols.

## 8.2 Simulation Plots

Figure 8.1 shows the BER for the decorrelating receiver given in (5.2). For Figures 8.1, 8.2, 8.3, and 8.5, the dominant subspace was chosen to be of size $m = 160$. This size was chosen from a brute force optimization of (7.60) using the approximation (7.35) [2]. Notice the multipath corrupted communication system performs similar to the case of no multipath. However, the advantage of time reversal is clearly shown.

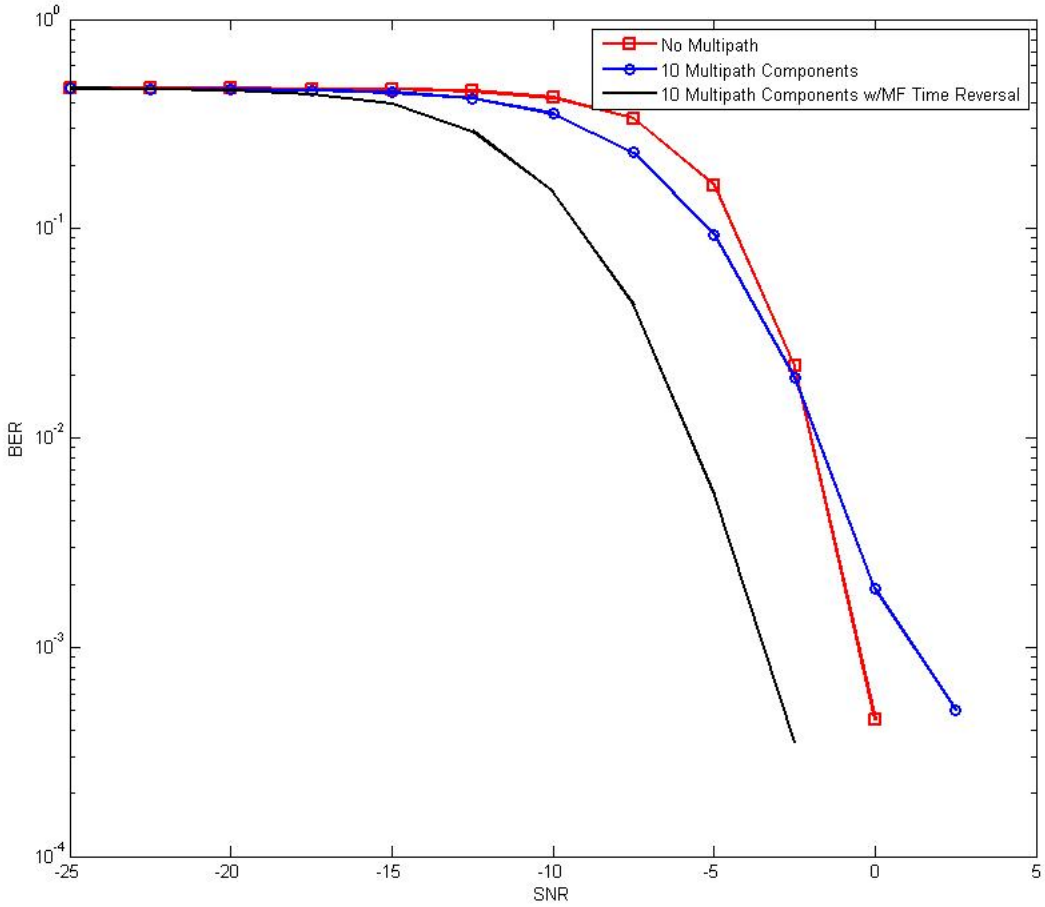


Figure 8.1: BER before Neyman-Pearson processing

Figure 8.2 shows the effectiveness of the Neyman-Pearson two stage receiver. The simulation setup is the same as used in Figure 8.1. The Neyman-Pearson criterion was set with a $P_{fa}$ of $10^{-5}$. As a worst case, the BER after the Neyman-Pearson detector is only $\sim 10^{-2}$, implying very few incorrect symbols pass the detector.

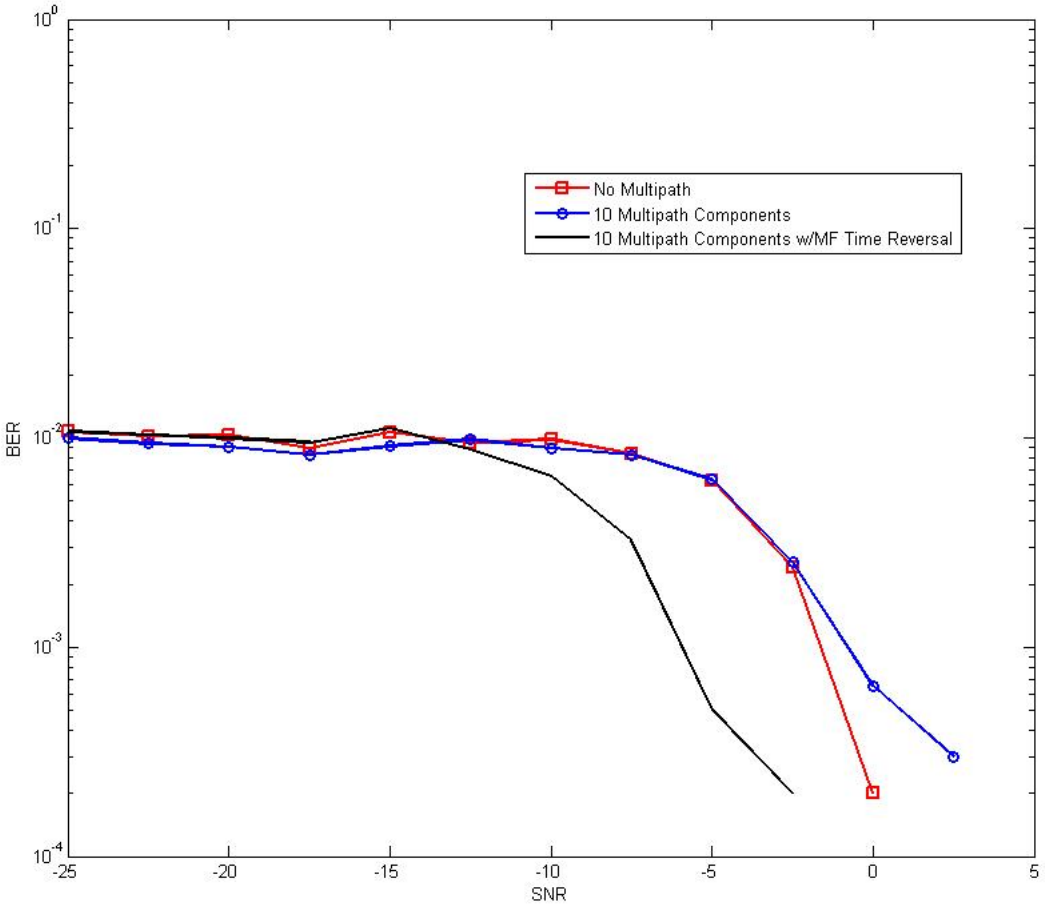


Figure 8.2: BER after Neyman-Pearson processing

If the Neyman-Pearson detector is used, then the performance of the receiver may be analyzed in terms of the probability of detection, $P_d$, and the probability of miss, $P_m$. Define

$$P_d = \frac{\text{number of correct symbols detected}}{\text{total number of symbols transmitted}} \tag{8.1}$$

and

$$P_m = \frac{\text{number of correct symbols not detected}}{\text{total number of correct symbols}}. \tag{8.2}$$

In other words, (8.2) represents the number of correct symbols rejected between the two stages. The results of the simulation of these two metrics are shown in Figures 8.3 and 8.4.

Figure 8.3 also shows the probability of an intercept receiver detecting the communication symbol. The intercept receiver has the same conditions as the multipath corrupted symbol. It uses the equalized receiver given in (6.16) and has clairvoyant knowledge of the noise and clutter powers. The threshold was found numerically using a $P_{fa} = 10^{-5}$.

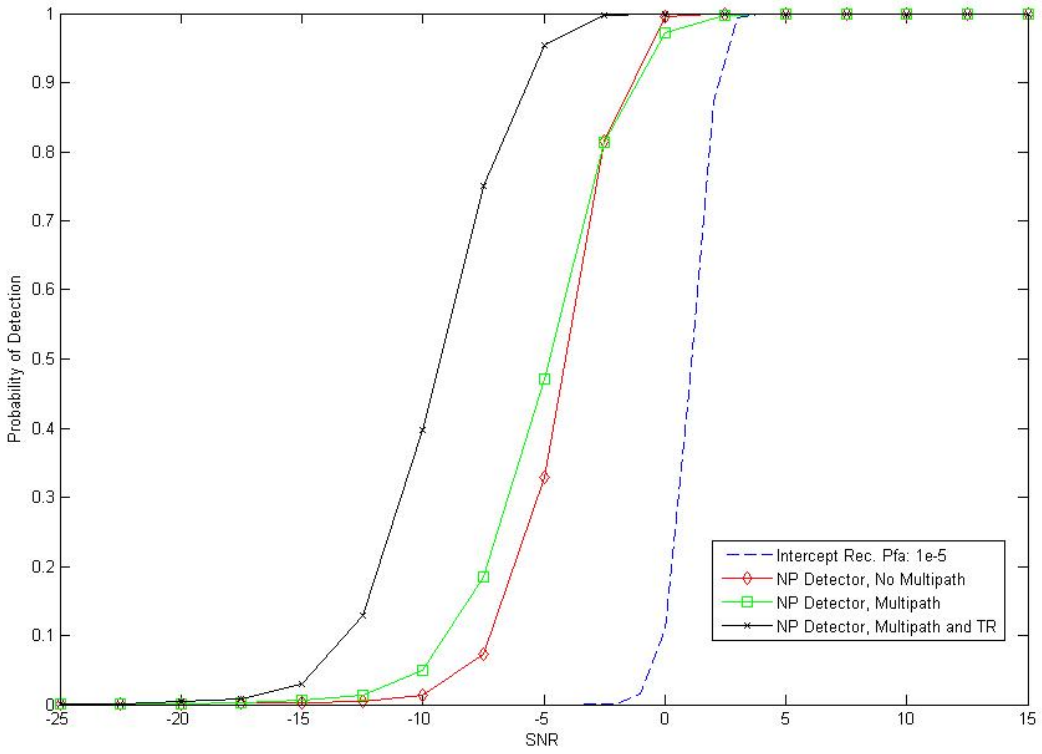


Figure 8.3: Probability of detection with equalization

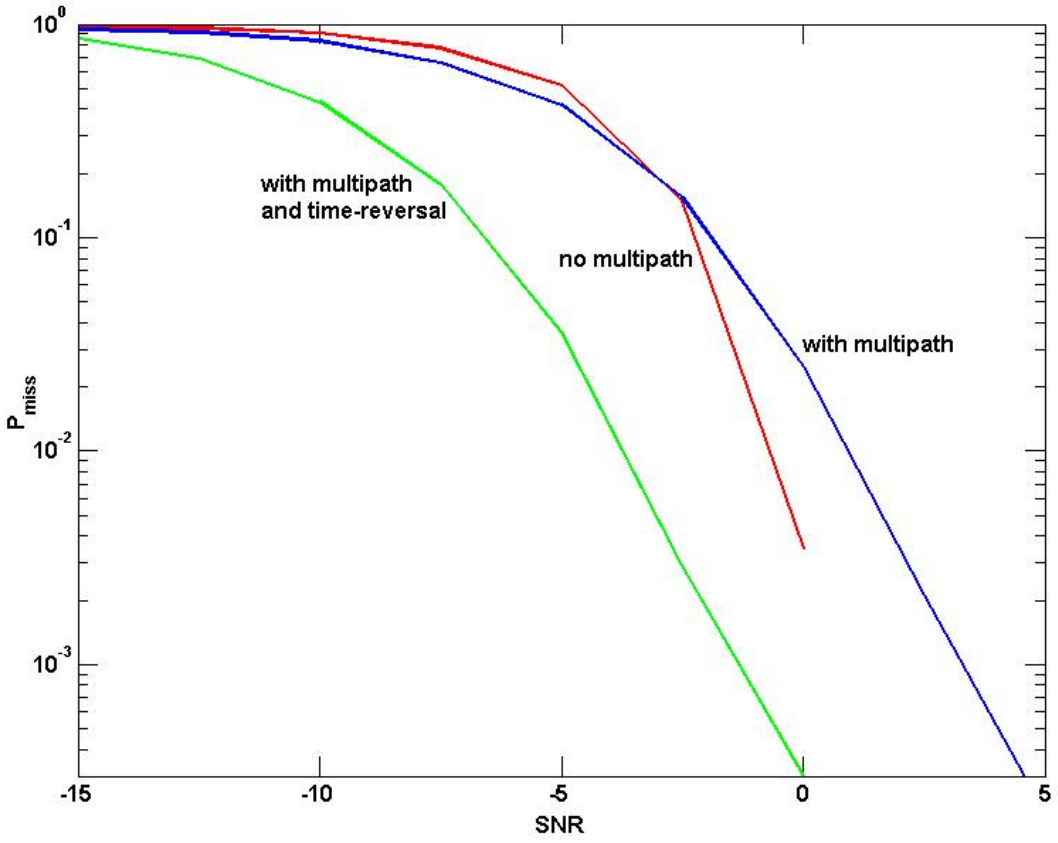


Figure 8.4: Probability of miss after Neyman-Pearson processing

Figure 8.5 shows the probabilities of detection for an intercept receiver using the non-equalized metric given in (6.7) and the equalized metric given in (6.13). Curves for $P_{fa} = 10^{-4}$and $10^{-5}$ are shown. The metrics produce similar results. As the intercept receiver is given clairvoyant knowledge in these metrics, it is expected that these metrics closely bound the performance of an intercept receiver.

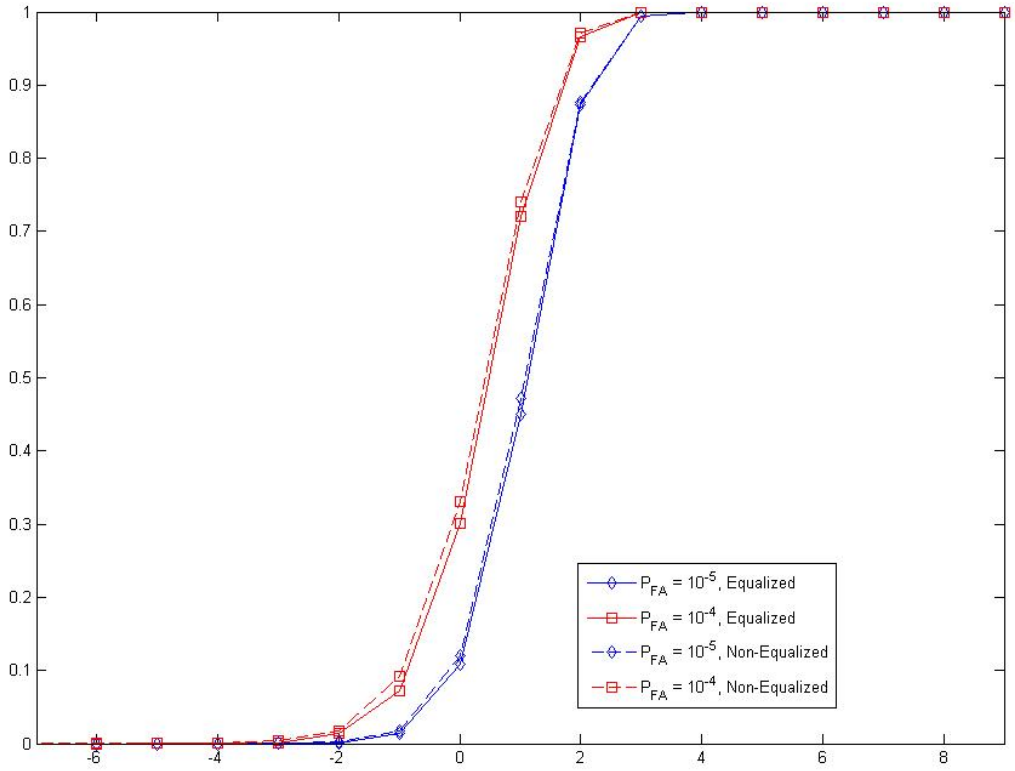


Figure 8.5: Probability of detection with and without equalization

As mentioned in Section 7.1 the processing gain at the decorrelating receiver is dependent on the INR of the scenario. Figure 8.6 shows the case where the clutter is dominant. In this case, the INR is set to 30 dB. Notice that the clutter cancellation allows for a much greater gain than would be the case of simple coherent integration.

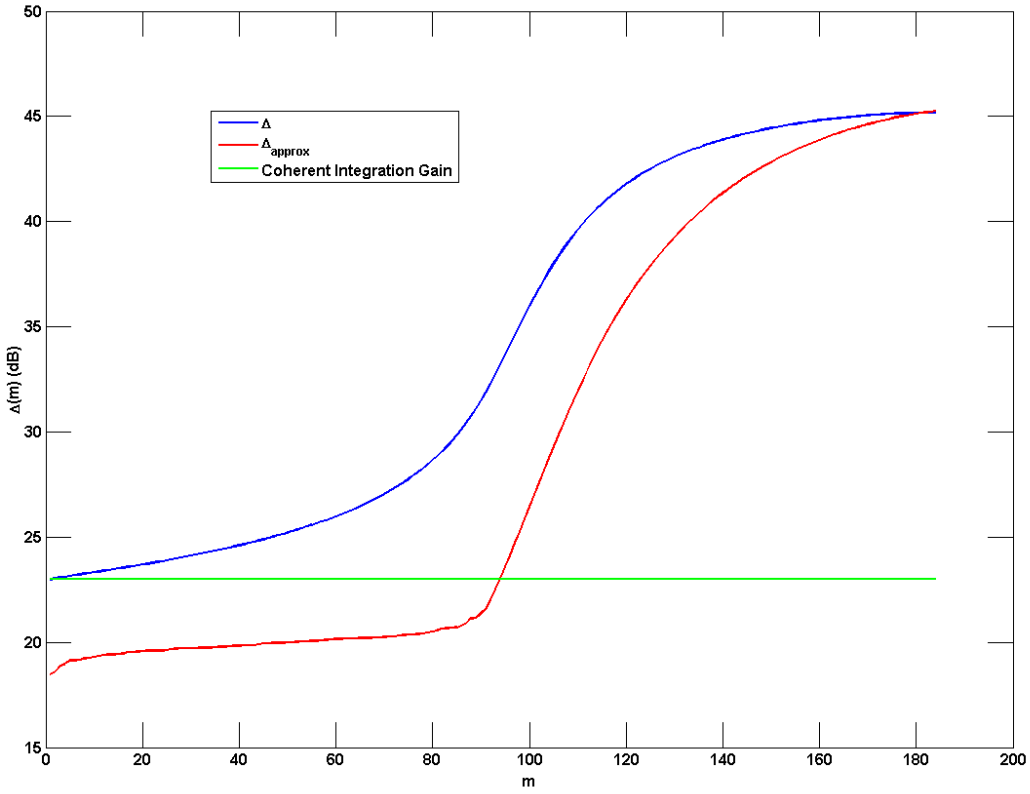


Figure 8.6: Processing gain - clutter dominant

However, in the case when the noise is dominant, the clutter cancellation provides no further gain. In Figure 8.7, the INR is set to -30 dB.

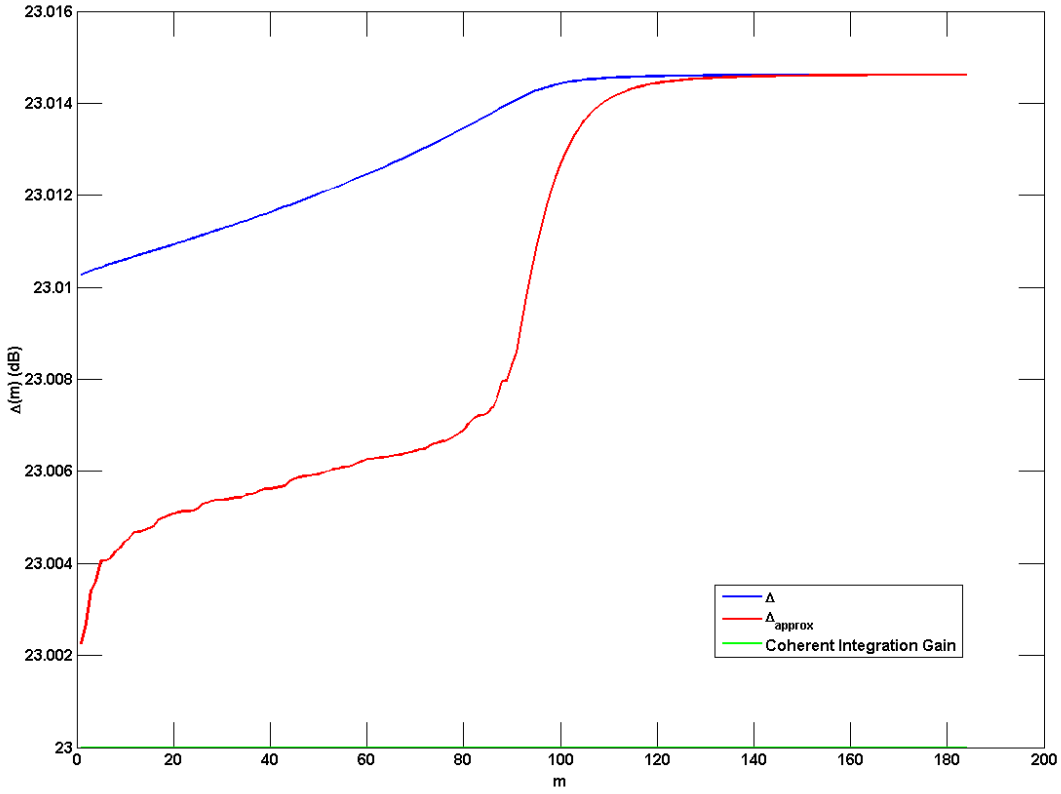


Figure 8.7: Processing gain - noise dominant

Figure 8.8 shows the surface of $\Psi(m, \tilde{m})$ with $K = 16$ possible symbols. Therefore, $1 \leq m \leq 184$ and $1 \leq \tilde{m} \leq 199$. It is informative to take cuts of this surface.

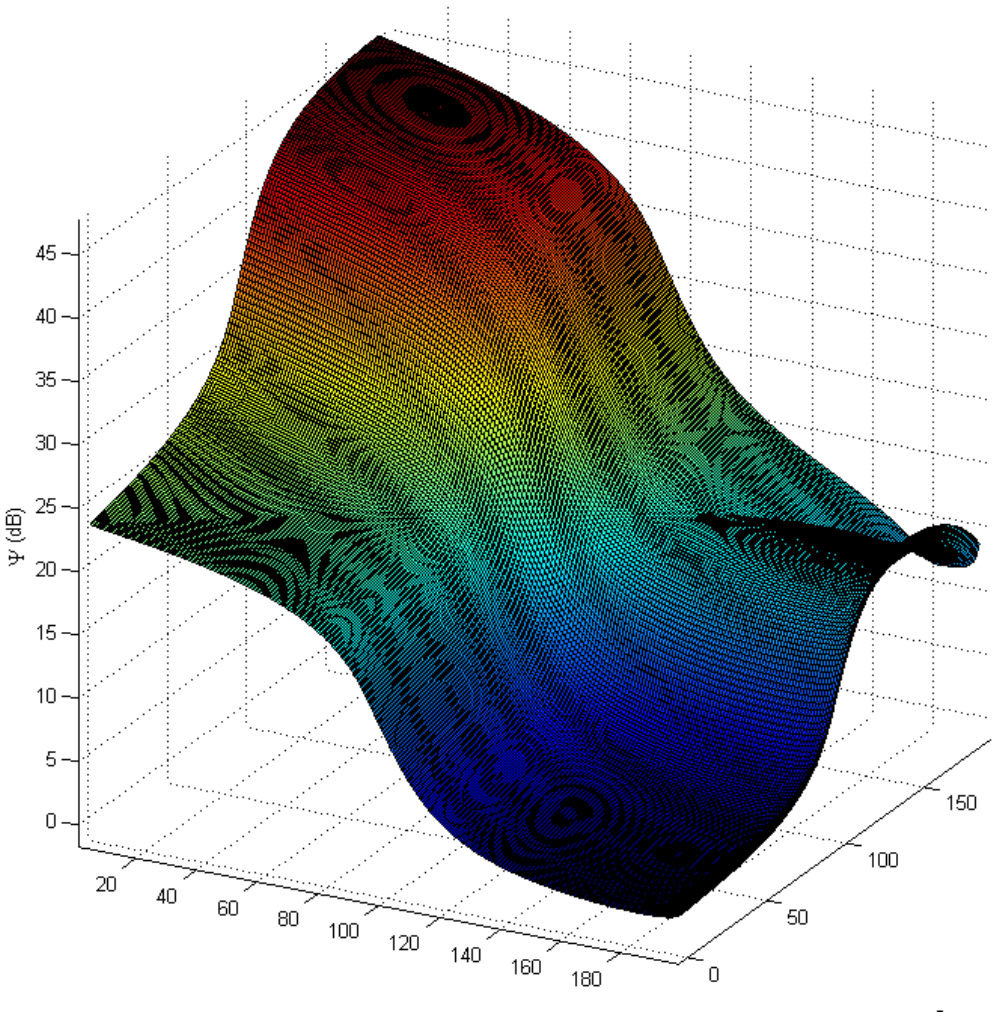


Figure 8.8: $\Psi(m, \tilde{m})$

Figure 8.9 shows three interesting cuts of $\Psi(m, \tilde{m})$. The cases of $m = 100, m = 160,$ and $m = 184$ are considered. It is interesting to see the advantage gained by using $m = 160$ versus using $m = 100$. The size of the dominant subspace in previous work was set at $m = 100$, though the diagonally loaded receiver was not used. Notice that the gain advantage is very similar for the cases of $m = 160$ and $m = 184$ when $\tilde{m}$ is relatively small. However, when the size of the hypothesized dominant subspace gets very large, the behavior is different. In the case of $m = 184$, the communication symbols lie in a very small subspace. They are of the same rank as the subspace available. Therefore, their energy is concentrated in that

subspace. When everything else is projected out, the communication symbols will dominate over what noise remains. However, if the dominant subspace is smaller, the waveforms are more "spread out". The intercept receiver projects away signal energy in addition to noise and interference as the hypothesized dominant subspace is increased.

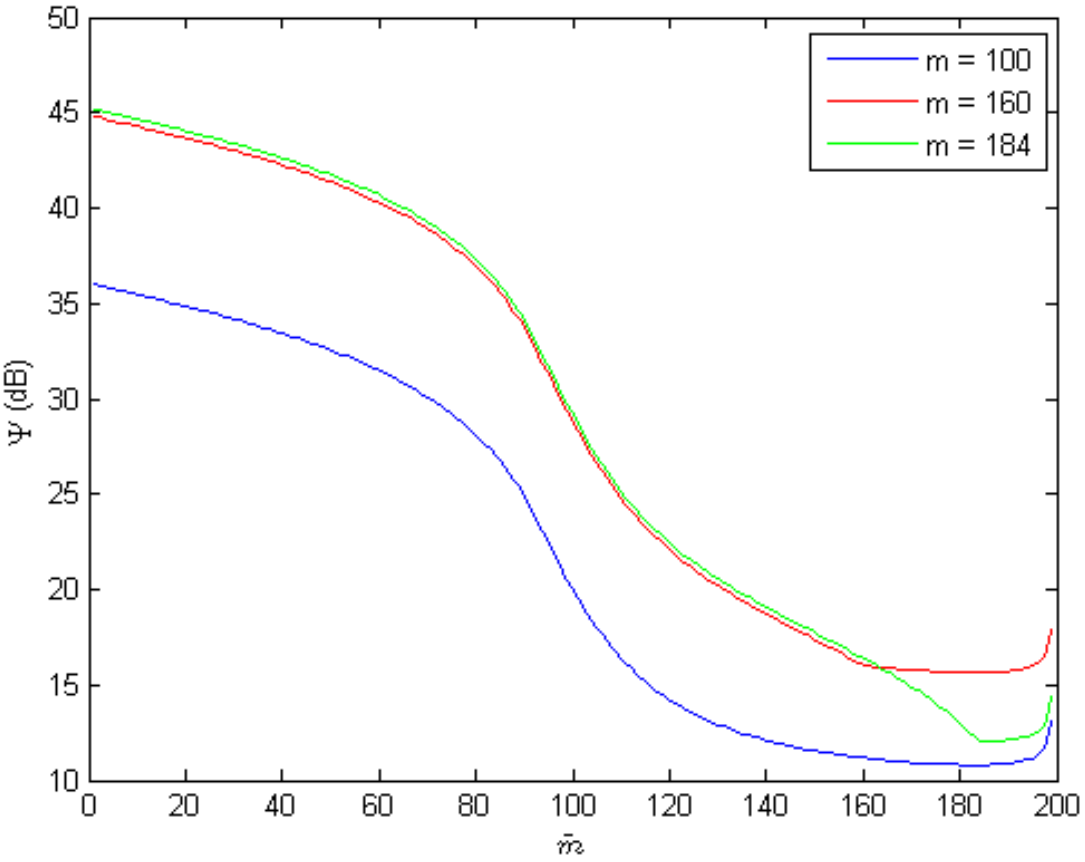


Figure 8.9: $\Psi(m, \tilde{m})$ for 3 values of $m$

The progression of this effect is shown in Figure 8.10, where 34 cuts of $\Psi(m, \tilde{m})$ are shown as a function of $\tilde{m}$. These cuts correspond to $150 \leq m \leq 184$. There is very little variance between these cuts at relatively large non-dominant subspaces (*i.e.* close to dominant subspace size of 150), but the spreading is apparent at relatively small non-dominant subspaces (*i.e.* close to dominant subspace size of $NM - K = 184$).

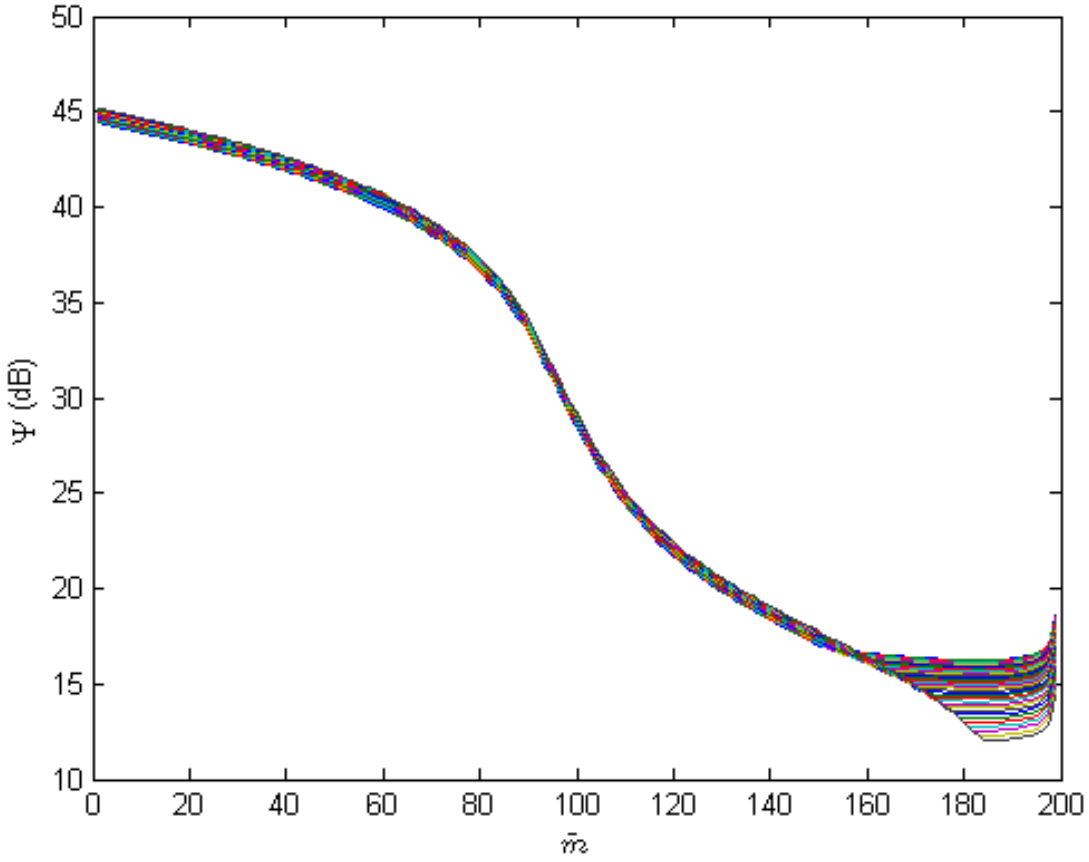


Figure 8.10: $\Psi(m, \tilde{m})$ for 34 values of $m$

Figure 8.11 is a slightly different optimization. In this case, for each possible value of $m$, the minimum value of $\Psi(m, \tilde{m})$ was selected. In other words, for each $m$,

$$\min_{\tilde{m}} \Psi(m, \tilde{m}) \tag{8.3}$$

was evaluated. This gives the "worst" processing gain point for every dimensionality of non-dominant subspace. Notice that there is a wide choice of values that give similar results. Using the approximation in (7.35), it was numerically determined in [2] that selecting the dominant subspace to be $m = 160$ maximized the function shown in Figure 8.11. This is the "maximum" stage of the maxi-min criterion. However, for the exact surface (*i.e.* using (7.60), the maximum is identically reached at values of $m = 138, 139, 140$.

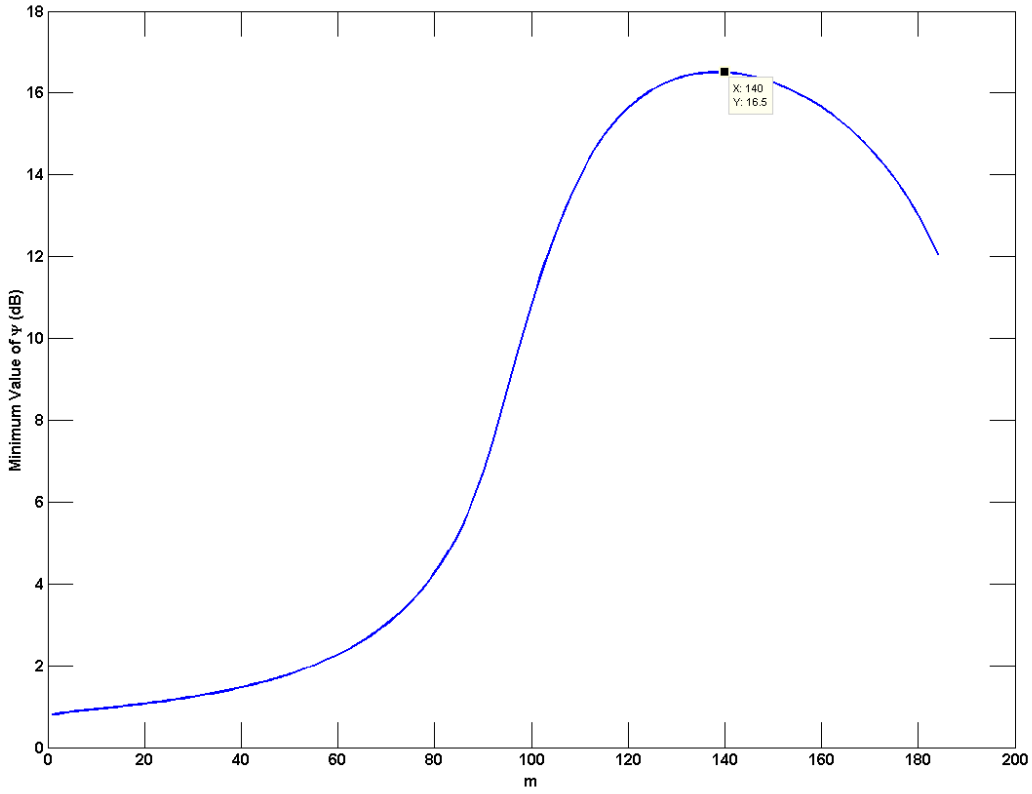


Figure 8.11: Minimum values of $\Psi(m, \tilde{m})$ as a function of $m$

The masking power of the interference is made clear in Figure 8.12. In this case, the INR is set to -30. Notice that as the size of the dominant space increased, the decorrelating receiver enjoys a much smaller advantage over the intercept receiver. In this case, the REC system is essentially a standard spread-spectrum LPI communications system. It depends only on the noise to mask the communication symbols.

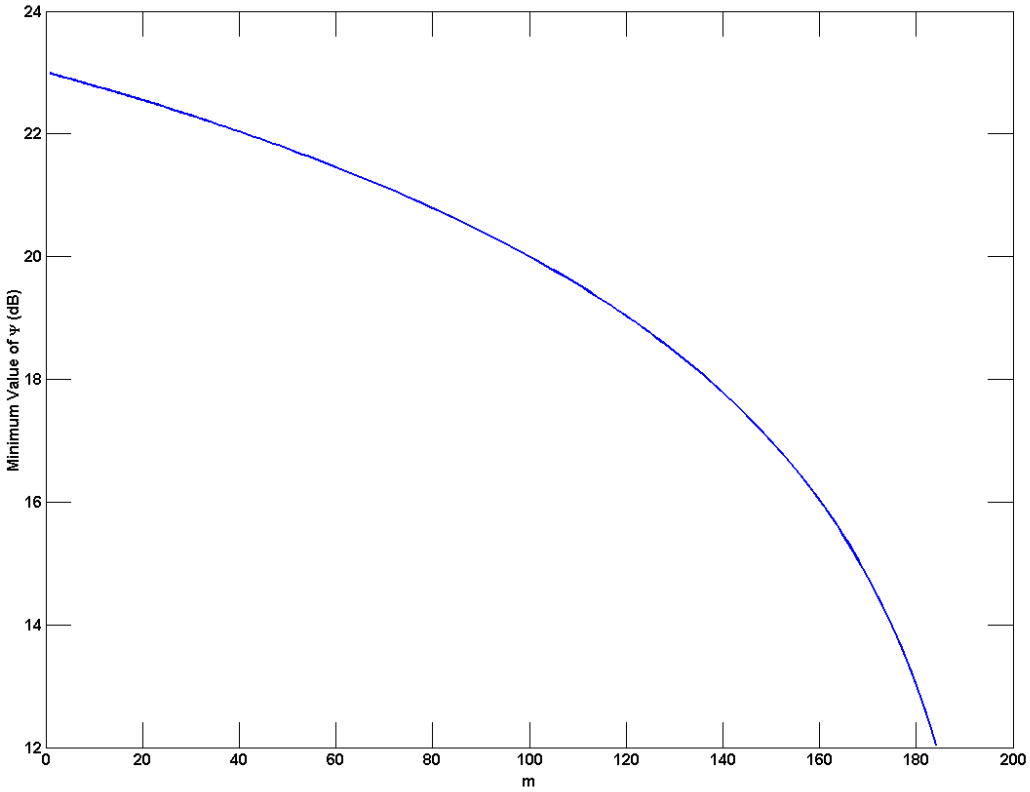


Figure 8.12: Minimum values of $\Psi(m, \tilde{m})$ as a function of $m$, noise dominant case

# Chapter 9

# Conclusion

This thesis examined a method of covert wireless communications which used ambient radar scattering to mask communication symbols from a transponder/tag. The Dominant Projection method of symbol design is effective at forming symbols that can be embedded on an intra-pulse basis, allowing for data rates on the order of the PRF of a pulsed radar system.

Multipath distortion was shown to have little effect on symbols designed via the Dominant Projection method. Furthermore, if the desired receiver is the illuminating radar, time reversal may be used to improve performance in two ways. First, the spatio-temporal focusing afforded by time reversal improves the probability of correctly detecting a symbol. Second, the spatial dependence of multipath causes destructive interference with respect to a time reversed symbol at an intercept receiver. This destructive interference decreases the probability that an intercept receiver can detect a communication symbol. Time reversal results were shown for the case when the radar waveform is known at the tag. A method of estimating the radar waveform using spatial degrees of freedom was shown for the case when the radar waveform is not known at the tag.

A two-stage Neyman-Pearson receiver was developed. The first stage of the receiver consists of a maximum likelihood receiver that maximizes the probability of detecting a

symbol. This stage selects the most likely symbol sent over a given time interval. The second stage uses the residues of the filters corresponding to the symbols not selected by the first stage to form a null hypothesis. Due to the Central Limit Theorem the magnitude of these residues is Rayleigh distributed. A threshold can then be determined to give an acceptable probability of false alarm.

An LPI communication system must consider both maximizing data reliability and minimizing probability of intercept. Therefore, this thesis examined several intercept metrics to provide a bound on the probability of intercept. A previous metric was shown to require improvement. An alternate metric was shown which systematically projected away hypothesized dimensionalities of dominant subspace and performed an energy detection on the residues. This metric used the ratio of the maximum to the minimum values of the residues over a time period to establish the probability of a symbol being present. However, the thresholds for determining a symbol while maintaining an acceptable rate of false alarm where determined numerically. An equalized metric was then shown that, given clairvoyant knowledge of clutter and noise powers, yielded a $\chi^2$ distributed null hypothesis. This development allows for offline determination of thresholds.

Previous work had assumed the dimension of the dominant subspace to be equal to the time-bandwidth product of the radar waveform. This thesis provided a formal analysis of the processing gain given by the diagonally loaded decorrelating receiver and the alternative intercept metric. The ratio of the processing gain of the decorrelating receiver to the intercept metric provides the gain advantage of the desired receiver over an intercept receiver. This gain advantage can then be optimized over possible dimensionalities of the dominant subspace.

Finally, simulation results were shown to verify and explore the concepts discussed in this thesis. The various properties of the Neyman-Pearson receiver were examined. In addition, the gain advantage of the desired receiver over the intercept metric was shown in terms of the probability of detection. The equivalence of the alternate intercept metric to the equalized

alternate intercept metric was determined. Finally, the gain advantage surface was explored in detail.

## 9.1 Future Work

There are several promising areas for future work. First, the analysis on time reversal depended on simulation results to show the effectiveness of the pre-distortion. A rigorous mathematical analysis would be beneficial.

Second, the impact of the REC symbols on the radar performance has not been analyzed. Due to the radar receiver having exact knowledge of the waveforms, it is assumed that they may be nulled with little effect on the radar detection. However, due to the correlation of the radar waveform with the communication symbol, this may result in some loss of sensitivity and/or dynamic range. A thorough analysis of this effect should be explored.

A third avenue of questioning arises from the assumptions on the clutter distribution. For the purposes of the derivations in this thesis, it is assumed that the clutter is uncorrelated in range. If this were not the case, what would be the impact on the performance? How much error would this introduce into the formal analysis conducted in this thesis?

The simulations in this thesis assumed a constellation size of 16 symbols. This selection of constellation size impacted the numerical optimization of the dominant subspace size. It would be useful to optimize the design of the REC over possible constellation sizes as well as subspace sizes.

# References


[1] S. D. Blunt, P. Yatham, and J. Stiles, "Intrapulse radar-embedded communications," *Aerospace and Electronic Systems, IEEE Transactions on*, vol. 46, no. 3, pp. 1185 –1200, Jul. 2010.

[2] S. D. Blunt, J. Metcalf, C. Biggs, and E. Perrins, "Performance characteristics and metrics for intra-pulse radar-embedded communications," *Journal of Selected Areas of Communications*, Dec. 2011.

[3] S. Blunt and J. Metcalf, "Estimating temporal multipath via spatial selectivity: Building environmental knowledge into waveform design for radar-embedded communications," in *Electromagnetics in Advanced Applications, 2009. ICEAA '09. International Conference on*, Sep. 2009, pp. 513 –516.

[4] W. Bennett, "Secret telephony as a historical example of spread-spectrum communication," *Communications, IEEE Transactions on*, vol. 31, no. 1, pp. 98 – 104, jan 1983.

[5] R. Scholtz, "The origins of spread-spectrum communications," *Communications, IEEE Transactions on*, vol. 30, no. 5, pp. 822 – 854, may 1982.

[6] H. Stockman, "Communication by means of reflected power," *Proceedings of the IRE*, vol. 36, no. 10, pp. 1196 – 1204, oct. 1948.

[7] R. Axline, G. Sloan, and R. Spalding, "Radar transponder apparatus and signal processing technique," U.S. Patent 5,486,830, Jan 23, 1996.

[8] ——, "Transponder data processing methods and systems," U.S. Patent 6 577 266, Jun 10, 2003.

[9] D. Hounam and K.-H. Wagel, "A technique for the identification and localization of sar targets using encoding transponders," *Geoscience and Remote Sensing, IEEE Transactions on*, vol. 39, no. 1, pp. 3 –7, jan 2001.

[10] D. Richardson, S. Stratmoen, G. Bendor, H. Lee, and M. Decker, "Tag communication protocol and system," U.S. Patent 6,329,944, Dec 11, 2001.

[11] R. Ormesher and R. Axline, "Methods and system suppressing clutter in a gain-block, radar-responsive tag system," U.S. Patent 7,030,805, Apr 18, 2006.

[12] M. Padilla, "Sandia demonstrates athena tag for preventing tragic battlefield 'friendly fire' incidents," *Sandia Lab News*, nov. 2005.

[13] B. Cantrell, J. O. Coleman, and G. Trunk, "Radar communications," Naval Research Laboratory, Tech. Rep. 8515, 1991.

[14] S. Verdu, *Multiuser Detection.* Cambridge University Press, 2003.

[15] S. Blunt and C. Biggs, "Practical considerations for intra-pulse radar-embedded communications," in *Waveform Diversity and Design Conference, 2009 International*, Feb. 2009, pp. 244 –248.

[16] A. Tacticus, *How to Survive Under Siege/Aineias the Tactician.* Oxford, U.K.: Clarendon, 1990.

[17] B. Kaliski, "A survey of encryption standards," *Micro, IEEE*, vol. 13, no. 6, pp. 74 –81, dec 1993.

[18] F. Petitcolas, R. Anderson, and M. Kuhn, "Information hiding-a survey," *Proceedings of the IEEE*, vol. 87, no. 7, pp. 1062 –1078, jul 1999.

[19] S. M. Kay, *Fundamentals of Statistical Signal Processing: Detection Theory.* Prentice Hall PTR, 1998.

[20] J. Proakis and M. Salehi, *Digital Communications.* McGraw-Hill, 2007.

[21] D. Nicholson, *Spread Spectrum Signal Design: Low Probability of Exploitation and Anti-Jam Systems.* San Francisco: Freeman, 1988.

[22] Z. Hijaz and V. Frost, "Exploiting ofdm systems for covert communication," in *MILITARY COMMUNICATIONS CONFERENCE, 2010 - MILCOM 2010*, 31 2010-nov. 3 2010, pp. 2149 –2155.

[23] S. Kingsley and S. Quegan, *Understanding Radar Systems.* SciTech Publishing Inc., 1999.

[24] J. de Graaf, H. Faust, J. Alatishe, and S. Talapatra, "Generation of spectrally confined transmitted radar waveforms: experimental results," in *Radar, 2006 IEEE Conference on*, april 2006, p. 8 pp.

[25] B. Kaliski, "Microwave tag identification systems," *RCA Review*, vol. 44, no. 4, pp. 589 –610, dec 1983.

[26] A. Koelle, S. Depp, and R. Freyman, "Short-range radio-telemetry for electronic identification, using modulated rf backscatter," *Proceedings of the IEEE*, vol. 63, no. 8, pp. 1260 – 1261, aug. 1975.

[27] L. Supplee, R. Cohn, J. Collura, and A. McCree, "Melp: the new federal standard at 2400 bps," in *Acoustics, Speech, and Signal Processing, 1997. ICASSP-97., 1997 IEEE International Conference on*, vol. 2, apr 1997, pp. 1591 –1594 vol.2.

[28] T. Wang, K. Koishida, V. Cuperman, A. Gersho, and J. Collura, "A 1200 bps speech coder based on melp," in *Acoustics, Speech, and Signal Processing, 2000. ICASSP '00. Proceedings. 2000 IEEE International Conference on*, vol. 3, 2000, pp. 1375 –1378 vol.3.

[29] M. Chamberlain, "A 600 bps melp vocoder for use on hf channels," in *Military Communications Conference, 2001. MILCOM 2001. Communications for Network-Centric Operations: Creating the Information Force. IEEE*, vol. 1, 2001, pp. 447 – 453 vol.1.

[30] S. Blunt, M. Cook, and J. Stiles, "Embedding information into radar emissions via waveform implementation," in *Waveform Diversity and Design Conference (WDD), 2010 International*, Aug. 2010, pp. 000 195 –000 199.

[31] K. S. Shanmugan and A. Breipohl, *Random Signals: Detection, Estimation and Data Analysis*. John Wiley & Sons, 1988.

[32] S. Watts and K. Ward, "Spatial correlation in k-distributed sea clutter," *Communications, Radar and Signal Processing, IEE Proceedings F*, vol. 134, no. 6, pp. 526 –532, october 1987.

[33] M. Sekine, T. Musha, Y. Tomita, T. Hagisawa, T. Irabu, and E. Kiuchi, "On weibull-distributed weather clutter," *Aerospace and Electronic Systems, IEEE Transactions on*, vol. AES-15, no. 6, pp. 824 –830, nov. 1979.

[34] E. Jakeman and P. Pusey, "A model for non-rayleigh sea echo," *Antennas and Propagation, IEEE Transactions on*, vol. 24, no. 6, pp. 806 – 814, nov 1976.

[35] B. Lewis and F. Kretschmer, "Linear frequency modulation derived polyphase pulse compression codes," *Aerospace and Electronic Systems, IEEE Transactions on*, vol. AES-18, no. 5, pp. 637 –641, Sep. 1982.

[36] M. Ackroyd and F. Ghani, "Optimum mismatched filters for sidelobe suppression," *Aerospace and Electronic Systems, IEEE Transactions on*, vol. AES-9, no. 2, pp. 214 –218, march 1973.

[37] T. Felhauer, "Digital signal processing for optimum wideband channel estimation in the presence of noise," *Radar and Signal Processing, IEE Proceedings F*, vol. 140, no. 3, pp. 179 –186, jun 1993.

[38] S. Blunt and K. Gerlach, "Adaptive pulse compression via mmse estimation," *Aerospace and Electronic Systems, IEEE Transactions on*, vol. 42, no. 2, pp. 572 – 584, april 2006.

[39] A. Derode, A. Tourin, J. de Rosny, M. Tanter, S. Yon, and M. Fink, "Taking advantage of multiple scattering to communicate with time-reversal antennas," *Phys. Rev. Lett.*, vol. 90, no. 1, p. 014301, jan 2003.

[40] R. Schmidt, "Multiple emitter location and signal parameter estimation," *Antennas and Propagation, IEEE Transactions on*, vol. 34, no. 3, pp. 276 – 280, mar 1986.

[41] P. Chen, T.-J. Wu, and J. Yang, "A comparative study of model selection criteria for the number of signals," *Radar, Sonar Navigation, IET*, vol. 2, no. 3, pp. 180 –188, june 2008.

[42] J. Thompson, P. Grant, and B. Mulgrew, "Performance of spatial smoothing algorithms for correlated sources," *Signal Processing, IEEE Transactions on*, vol. 44, no. 4, pp. 1040 –1046, apr 1996.

[43] W. Gardner and C. Spooner, "The cumulant theory of cyclostationary time-series. i. foundation," *Signal Processing, IEEE Transactions on*, vol. 42, no. 12, pp. 3387 –3408, dec 1994.

[44] C. Spooner and W. Gardner, "The cumulant theory of cyclostationary time-series. ii. development and applications," *Signal Processing, IEEE Transactions on*, vol. 42, no. 12, pp. 3409 –3429, dec 1994.

[45] W. Gardner, "Exploitation of spectral redundancy in cyclostationary signals," *Signal Processing Magazine, IEEE*, vol. 8, no. 2, pp. 14 –36, apr 1991.

[46] S. Haykin, *Adaptive Filter Theory.* Prentice Hall, 2002.

[47] G. Xu and T. Kailath, "Direction-of-arrival estimation via exploitation of cyclostationary-a combination of temporal and spatial processing," *Signal Processing, IEEE Transactions on*, vol. 40, no. 7, pp. 1775 –1786, jul 1992.

[48] Y.-T. Lee and J.-H. Lee, "Direction-finding methods for cyclostationary signals in the presence of coherent sources," *Antennas and Propagation, IEEE Transactions on*, vol. 49, no. 12, pp. 1821 –1826, dec 2001.

[49] L. Xue-liang, G. Yan, L. Ning, and W. Jin-long, "Doa estimation of cyclostationary signals in the presence of coherent sources," in *Signal Processing, 2008. ICSP 2008. 9th International Conference on*, oct. 2008, pp. 341 –344.

[50] S. Blunt, T. Chan, and K. Gerlach, "Robust doa estimation: The reiterative super-resolution (risr) algorithm," *Aerospace and Electronic Systems, IEEE Transactions on*, vol. 47, no. 1, pp. 332 –346, janu 2011.

[51] S. Blunt and J. Metcalf, "Using time reversal of multipath for intra-pulse radar-embedded communications," in *Waveform Diversity and Design Conference (WDD), 2010 International*, Aug. 2010, pp. 000 155 –000 158.